PRESUPERNOVA MODELS AND SUPERNOVAE

DAIICHIRO SUGIMOTO

Department of Earth Science and Astronomy, College of General Education, University of Tokyo, Meguro-ku, Tokyo 153, Japan

and

KEN'ICHI NOMOTO*

Department of Physics, Ibaraki University, Mito 310, Japan

(Received 3 October, 1979)

Abstract. Present status of the theories for presupernova evolution and triggering mechanisms of supernova explosions are summarized and discussed from the standpoint of the theory of stellar structure and evolution. It is not intended to collect every detail of numerical results thus far obtained, but to extract physically clear-cut understanding from complexities of the numerical stellar models. For this purpose the evolution of stellar cores is discussed in a generalized fashion. The following types of the supernova explosions are discussed. The carbon deflagration supernova of intermediate mass star which results in the total disruption of the star. Massive star evolves into a supernova triggered by photo-dissociation of iron nuclei which results in a formation of a neutron star or a black hole depending on its mass. These two are typical types of the sueprnovae. Between them there remains a range of mass for which collapse of the stellar core is triggered by electron captures, which has been recently shown to leave a neutron star despite oxygen deflagration competing with the electron captures. Also discussed are combustion and detonation of helium or carbon which take place in accreting white dwarfs, and the collapse which is triggered by electron-pair creation in very massive stars.

Contents

Those who are interested only in the general picture and observational accounts are suggested to read Sections 1 and 12 only. Those who are not interested in logical accounts in the theory of stellar structure may skip Sections 2 and 3.

* Present address: NASA, Goddard Space Flight Center, Greenbelt, MD 20771, U.S.A.

Space Science Reviews **25** (1980) 155–227. 0038–6308/80/0252–0155 $10.95.

1. Introduction

It has been about twenty years since Hoyle and Fowler (1960) advanced an excellent theory explaining the causes of supernova explosion. They assigned the supernova explosions triggered by nuclear flash in electron-degenerate core to type I supernovae, and those triggered by photodissociation of iron nuclei to type II. Even in the present days the basic ideas for the triggering mechanisms are considered to be essentially the same, though the difference in the types are attributed to the difference in the envelopes of presupernovae rather than the triggering mechanism itself.

Since then a great progress has been accomplished. In the observational side many neutron stars have been discovered as pulsars. Of particular importance is the discovery of a neutron star in the Crab nebula. It gave a strong evidence that a neutron star should be left after some supernova explosions as imagined by Oppenheimer and Volkoff (1939) many years ago. Moreover, a black hole has also been discovered as Cyg X−1. It gave also an evidence that a black hole should be formed in a gravitational collapse of massive object as discussed also by Oppenheimer and Snyder (1939) long time ago.

The aim of theories for supernova explosion has been to explain these processes by using appropriate models which cover the evolution of the star to presupernova stage through the dynamical collapse and explosion.

During these fifteen years, many models for the evolution of the stars have been computed up to the presupernova stage. As a result of such effort, we have the following picture concerning the final fate of evolution. In what follows, we will denote the mass of a star at its zero-age main-sequence by M_{ms}. It is, in general, different from the current mass of the star M in a later phase of evolution, because the star may have suffered from mass loss or mass accretion by itself or in binary system. According to *common sense* of the picture, the star of $M_{ms} \leqslant 4M_{\odot}$ loses its mass in its red giant phase and its mass is reduced down to the Chandrasekhar limit as was first discussed by Paczyński and Ziołkowski (1968). Its final fate is a white dwarf composed mainly of helium or carbon plus oxygen, depending upon its M_{ms}.

In the stars of mass $4 \leqslant M/M_{\odot} \leqslant 8$, the mass of the carbon–oxygen (C–O) core is smaller than the Chandrasekhar limit and thus electrons are degenerate in it. The core mass grows as the hydrogen- and helium-shell burnings process matter into carbon and oxygen. When the core mass becomes very close to the Chandrasekhar limit and when the density of matter at the center of the star reaches $\rho_c = 2 \times 10^9$ g cm^{-3}, carbon bigins to burn. The carbon burning runs away and the energy generation becomes explosive as first suggested by Arnett (1968). The carbon burning releases nuclear energy more than the gravitational binding energy of the stellar core, and after all the core is totally disrupted and no remnant is left behind. This phenomenon is called as carbon deflagration (or detonation) supernova.

This total disruption of the star raised problems of the shortage of pulsar progenitors and over-production of iron group elements. Though much effort has been done to suppress the explosive nuclear burning anticipating to leave a neutron star, it has been unsuccessful.

For the mass range of $8 \leqslant M/M_{\odot} \leqslant 12$ electrons are non-degenerate in the C–O core but become degenerate in the succeeding phase of oxygen core. Little is known about this mass range, because the evolution of the core is very complicated after the carbon burning phase and because electron captures complicate the transition stages from the presupernova through the core collapse. Such stars will be discussed in Sections 8 and 9 as a supernova triggered by electron captures.

The star of mass in the range of $10^2 \geqslant M_{ms}/M_{\odot} \geqslant 12$ evolves until an iron core is formed in its central region. After Colgate and White (1966), and Arnett (1967) a

great many numerical experiments have been done for the purpose of simulating the collapse of iron core. However, such simulations did not yield any clear-cut results, and did not seem to succeed in leaving an neutron star either. After Colgate and White (1966), input physics became much more elaborate. However, weak interaction processes, effect of general relativity, and more plausible equation of state had not helped the situation, but, contrary, the bounce of the collapsing core and the mass ejection therefrom had seemed more difficult.

In 1973 experiments gave evidence for the existence of neutral currents in the weak interaction of the elementary particles (Hasert *et al.*, 1973; Benvenuti *et al.*, 1974). As its result and according to Weinberg (1967) and Salam's (1968) unified theory of weak and electromagnetic interactions, neutrinos were shown to be scattered coherently by atomic nucleus (Freedman, 1974), which yields a cross section per nucleon of about $A/4$ times the scattering by an electron. This lit a hope that the neutrinos emitted from the core should be scattered in outer layers, where the nuclei of large mass number A still exist, and should deposit energy there. However, such neutrino deposition does not seem strong enough to expel the outer mantle of the core, as far as the plausible value for the Weinberg's angle is concerned (e.g. Bruenn *et al.*, 1977).

Another effect of the increased scattering cross section of neutrino is that the neutrinos should be trapped within the stellar core. Recently many investigations have been done concerning the effects of the neutrino trapping and of revision in the equation of state at high densities. The core bounce and the associated mass ejection seem hopeful as will be discussed in Section 11.

In the stars of masses $M_{ms} \gtrsim 100 M_{\odot}$, electron-pair creation becomes appreciable in the phase of oxygen core (Arnett, 1973a). It reduces the ratios of specific heats γ below $\frac{4}{3}$, and the star becomes dynamically unstable. Then the star explodes by oxygen burning (Barkat *et al.*, 1967; Fraley, 1968), or collapses into a black hole (Wheeler, 1977).

The above are a historical summary and a present-day picture of matter. They are neither complete nor fine enough. One of the most difficult points is that we have no detailed model in which neutron stars can be formed consistently. This difficulty may be related with the fact that almost all of our quantitative studies have been confined within the regime of spherical stars. Of course, such difficulty might be lifted if we considered effects of rotation, magnetic field etc. However, only under simplifying assumptions we can study such effects quantitatively, and the results of such studies are in many cases difficult to evaluate. Therefore, it is important to make clear how far we can conclude quantitatively within the frame-work of spherical stars. Throughout the present article we assume that the star is spherical and that there is neither rotation of the star nor magnetic field in the star.

Even under such restrictions the problems of presupernova and supernova explosion are too diversified yet too complicated to be treated in a single article. As for selected topics, some excellent review articles are available. For carbon detonation supernova, the process of detonation was extensively discussed by Bruenn

(1972a) and by Buchler *et al.* (1974). For the collapses of iron cores Arnett (1978a, b, 1979a) discussed them in great detail. Beside them many review talks have been given in relevant symposia and workshops (Schramm, 1977; Giacconi and Ruffini, 1978; Danziger and Renzini, 1978), though they are not for ordinary audience but rather for specialists. We need not duplicate such review articles.

When we read such excellent articles and recent papers, we personally have the following impressions. The physical elementary processes are well described and then they suddenly jump into a huge pile of numerical results. Moreover, such pile is described too much in every detail to make a bold assessment among known facts. It is rather difficult to understand the physics involved in stellar structure and stellar hydrodynamics, i.e., the mechanism through which such elementary processes lead to such numerical behavior of models. Such tendency seems to become stronger and stronger as numerical models take more details into accounts. By means of such modelling we can know some specific results but they hardly extend our understanding of logics governing stellar evolution. Rather than more detailed modelling we need more numerical experiments to extract intentionally the physics through bold interpretations and assessments of numerical results.

In the present article, therefore, we will try to extract such accounts and to construct overall and clear-cut picture and summary of problems. Moreover, we will concentrate more to the presupernova evolution than the supernova explosions themselves, because the latter have been discussed in more numbers of review articles.

Recently, supernova explosions in binary system are also paid attention to. They consist of three topics. In the first place, evolution of the stars and mass exchange in binary system may affect the presupernova model. Secondly, mass accretion from a companion star induces supernova explosions in different conditions. Thirdly, observations of X-ray binaries give information restricting the theory of presupernova evolution and supernova explosion. The second topics will be discussed in Section 7. However, the first and the third topics will be left to somewhere else. (Notations are summarized in Appendix.)

2. Validity of Single Star Approximation for the Evolution of Stellar Core

Recently, studies of stellar evolution are presented only by their numerical results. Moreover, they become too complex because everything from the stellar core through the hydrogen-rich envelope is put into one melting pot. However, the following simple considerations, which will be discussed in this and the next section, give understanding and insight to their numerical results. It is the usual way in physics to divide a complex system into sub-systems among which the interactions are relatively weak but within each of which the internal coupling is strong. Those who may be interested only in specific results and not in their logical connection may skip Sections 2 and 3.

2.1. HYDROSTATIC EQUILIBRIUM OF THE STARS

The hydrostatic equilibrium of a spherical star is described by

$$U \equiv \frac{\mathrm{d} \ln M_r}{\mathrm{d} \ln r} = \frac{4\pi r^3 \rho}{M_r}, \tag{2.1}$$

$$V \equiv -\frac{\mathrm{d} \ln P}{\mathrm{d} \ln r} = \frac{GM_r \rho}{rP}, \tag{2.2}$$

where r is the radial distance of a shell from the center of the star, and M_r is the mass contained interior to its shell. The density ρ and the pressure P are related by the polytropic index as

$$\frac{\mathrm{d} \ln \rho}{\mathrm{d} \ln P} = \frac{N}{N+1}. \tag{2.3}$$

Differentiating Equations (2.1) and (2.2) we obtain

$$\mathrm{d} \ln r = -\frac{1}{\Delta} (\mathrm{d} \ln U - \mathrm{d} \ln V), \tag{2.4}$$

$$\Delta \equiv 2U + V - 4, \tag{2.5}$$

$$\mathrm{d} \ln \theta = -\frac{U-1}{\Delta} (\mathrm{d} \ln U - \mathrm{d} \ln V) - \mathrm{d} \ln V, \tag{2.6}$$

$$\theta \equiv P/\rho. \tag{2.7}$$

We shall compare two core solutions each other as illustrated in Figure 2.1. The center of the star corresponds to the point c, at which $U = 3$ and $V = 0$ according to boundary conditions. Two core solutions extend as $c - a - 2$, and $c - b - 3$, respectively. For the purpose of comparison and of the following discussions, segments of $U - V$ curves are also shown in this figure for polytropes of $N = 0$ ($c - b_0$), $N = 1.5$ ($c - b_{1.5}$) and $N = \infty$ ($c - a_\infty$).

Integrating Equation (2.6) along a closed path of $L(c - b - 3 - 2 - a - c)$ and using Stokes' theorem we obtain

$$\oint_L \mathrm{d} \log \theta = I(S_A) + I(S_B), \tag{2.8}$$

$$I(S) \equiv (\log e) \int_S \frac{V - 2U}{\Delta^2} \frac{\mathrm{d}U}{U} \frac{\mathrm{d}V}{V}, \tag{2.9}$$

where S_A is the area enclosed by $b - 3 - 2 - a - b$ and S_B is one by $c - b - a - c$. Here, we assume that these curves do not cross the locus of $\Delta = 0$, and the segment $2 - 3$ and $a_\infty - a - b - b_{1.5} - b_0$ are taken along which $V/U = \text{constant}$ and, in particular,

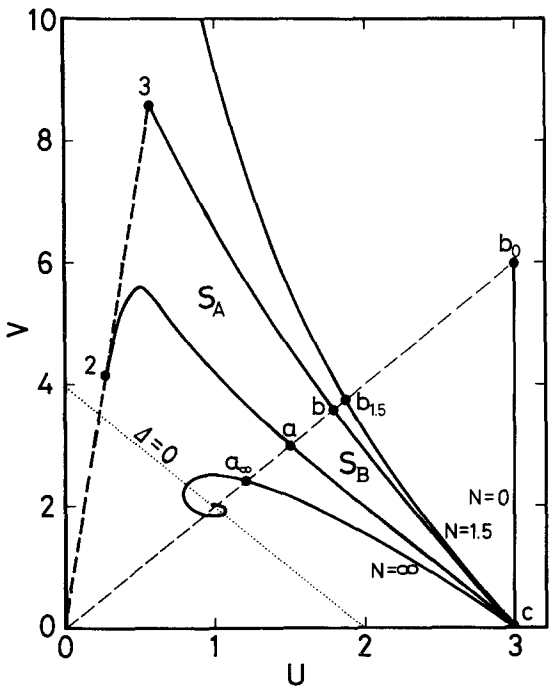

Fig. 2.1. Solutions for stellar structure illustrated in U–V plane.

$V = 2U$ for the latter. Therefore, the integrand of Equation (2.9) is always positive in S_A and negative in S_B. We can estimate the upper bound of the absolute value of $I(S_B)$ as follows

$$I(c-b_0-a_\infty-c) = -0.21 < I(c-b_{1.5}-a_\infty-c) = -0.12 < I(S_B) \leqq 0\,. \tag{2.10}$$

Unless the central region is superadiabatic, $-0.12 \leqq I(S_B) \leqq 0$ are the strict bounds.

The difference in θ between the two $U-V$ curves $c-b-3$ and $c-a-2$ are obtained from Equations (2.6) and (2.8) as

$$\log(\theta_c/\theta_2) = \log V_2 + I(S_A) + \log J_3 + I(S_B)\,, \tag{2.11}$$

$$\log J \equiv \log(\theta_c/\theta) - \log V. \tag{2.12}$$

As seen from Equations (2.4) and (2.6), J_3 is increasing toward the stellar surface in the region of $U < 1$. For Emden solution it tends to a certain limiting value when the point 3 approaches to the stellar surface ($V_3 \to \infty$ and thus $U_3 \to 0$). Its limiting value is $\log J_3 \to -0.27$ for the polytrope of $N = 1.5$ and $\log J_3 \to -0.07$ for $N = 3$.

Therefore a large value of $\log(\theta_c/\theta_2)$ can be realized when the following conditions are satisfied: (i) V_2 is large; (ii) $I(S_A)$ is large; and/or (iii) the $U-V$ curve runs close to the locus of $\Delta = 0$.

2.2. Definition of the Core and the Mass Contained in the Envelope

Examples of U–V curves for the presupernova stages are shown in Figure 2.2 for the supernova triggered by the photo-dissociation of iron core (Model A; Sugimoto and Nomoto, 1974) and in Figure 2.3 for the carbon deflagration supernova (Model B; Sugimoto and Nomoto, 1975). In Figure 2.4, their θ-distributions are also shown against log (U/V).

As seen in these figures and from Equation (2.4), the value of U/V is decreasing as we go outward from the center of the star where Δ is positive. When a point of $\Delta = 0$ is reached, the value of U/V takes a local minimum there, and then turns to increase.

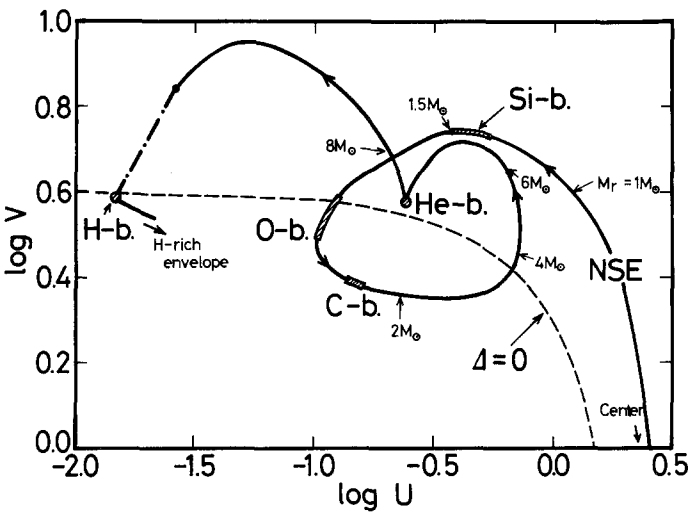

Fig. 2.2. Structure of $30M_\odot$ star at the presupernova stage. The hydrogen-rich envelope is omitted. Regions of shell burnings are indicated by H-b (hydrogen-burning) etc. Lagrangian mass coordinates M_r are shown at some points along the U–V curve. Dashed line is the locus of $\Delta = 2U + V - 4 = 0$ which defines the core edge. (Computed by Sugimoto and Nomoto (1974), and Nomoto *et al.* (1979a), but was not published therein.)

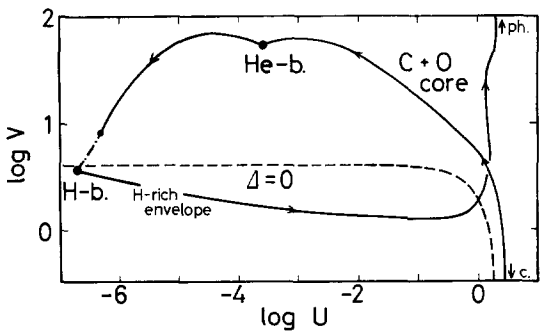

Fig. 2.3. The same as Figure 2.2, but for the core of an intermediate mass star at a stage just preceding the carbon deflagration supernova. (Computed by Sugimoto and Nomoto (1975), but was not published therein.) Also shown is the U–V curve for the hydrogen-rich envelope of $7M_\odot$ star (Nomoto and Sugimoto, 1972), which is fitted to the core at the hydrogen-burning shell.

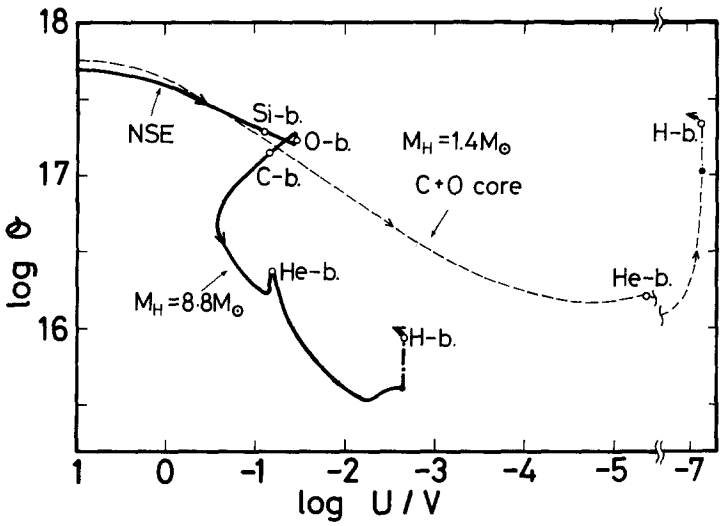

Fig. 2.4. Distribution of $\theta = P/\rho$ through the star and its relation with U/V. The solid curve is for the star of $30M_\odot$ plotted in Figure 2.2, while the dashed curve is for the intermediate mass star plotted in Figure 2.3. For these two stars the core edge corresponds to the oxygen-burning shell (O-b) and the hydrogen-burning shell (H-b), respectively, where the value of U/V takes the first local minimum.

We define the point of the first local minimum to be the core edge, which will be denoted by the subscript 1, and the region interior to it will be called the *core*. Then by definition we have

$$\Delta_1 = 0\,. \tag{2.13}$$

In many cases the core edge corresponds to the bottom of the hydrogen-rich envelope, but in Model A it does to the oxygen-burning shell as seen in Figure 2.2.

The region exterior of the core edge will be called the *envelope*. Let us consider how much mass can be contained above a shell e in the envelope. If Δ_e is positive, the mass fraction contained in the envelope Q_e and the pressure exerted at the shell e are expressed by

$$Q_e \equiv \frac{M - M_e}{M} = \left(\frac{U}{V}\right)_e \frac{1}{f(V_e, N)}\,, \tag{2.14}$$

$$P_e = f_e Q_e \frac{M_e}{4\pi r_e^2} g_e\,, \tag{2.15}$$

$$g \equiv \frac{GM_r}{r^2}\,, \tag{2.16}$$

$$f^{-1} = (N+1)\left(1 - \frac{N+1}{V}\right)^{N-3} \left(\frac{V}{N+1}\right)^{N+1} B_{(N+1)/V}(N+1, 3-N)\,,$$

$$= \sum_{k=0}^{\infty} b_k\,, \tag{2.17}$$

$$b_0 = 1,\ b_k = b_{k-1} \frac{k+3}{N+k+1} \left(\frac{N+1}{V} \right). \tag{2.18}$$

In Equation (2.17) the polytropic index N is assumed to be constant and B is the incomplete beta function (Sugimoto and Fujimoto, 1978). We call f the flatness parameter: For a flat configuration, i.e., for $H_p/r \equiv 1/V \ll 1$, it tends to $f \to 1$, while $f \ll 1$ for a spherical configuration with H_p/r of the order of unity, or more precisely, for $\Delta \ll 1$. Equation (2.17) is exact to the order of $(U/V) \ll 1$, and it converges when $(N+1)/V < 1$. If $V \gg 4$, the envelope above the shell e is flat ($f \simeq 1$) and it can contain mass fraction only of the order of $(U/V)_e$. (See Equation (2.22) for H_p.)

Let us estimate actual value of $(U/V)_1$ at the core edge for a model with relatively large θ_c/θ_1. In the preceding subsection the conditions for large value of θ_c/θ_2 were summarized. Here we assign the point 2 to the core edge 1. Then we have $V_1 \simeq 4$ so that the condition (i) is not satisfied. The condition (ii) for large $I(S_A)$ can be satisfied if the area in log U–log V plane becomes large in the region of small Δ. As seen in Equation (2.4) and in Figures 2.2 and 2.3, however, the U–V curve runs close to the line of $U/V =$ constant near the core edge with small Δ. Therefore the decrease in $(U/V)_1$ is inefficient to increase $I(S_A)$, or, in other words, the value of $(U/V)_1$ has to decrease by a large factor in order to increase $I(S_A)$ and thus θ_c/θ_1 only by a small amount. The condition (iii) is hardly satisfied either by the same reason. Then, a relatively large or even moderate value of θ_c/θ_1 (≥ 5) can be realized only by reducing the value of $(U/V)_1$ to a very small value (≤ 0.03).

If we had assigned the core edge to be the point e with $\Delta_e > 0$, the mass fraction of the envelope would have been as small as $(U/V)_e = (U/V)_1$. However, the mass contained above the core is a given quantity, which has been determined irrespectively of such situation but by the evolutionary history of the star.

How can the envelope mass be accommodated if its mass fraction exceeds $(U/V)_1$ appreciably? It can be done if the value of Δ is negative in the envelope just above the core edge. Then the U–V curve can run to the direction of increasing U/V as seen in Equation (2.4) and in Figures 2.2 and 2.3. It takes a local maximum where the value of U/V becomes of the order of mass fraction contained in the envelope and then the sign of Δ changes back to positive, i.e., the U–V curve makes a loop. Such structure corresponds to the envelope of a red giant star, in which the bulk of the envelope mass is contained in outer shells around the local maximum of U/V.

As can be understood from the discussions above, a relatively large envelope mass can be compatible with a relatively large θ_c/θ_1, only if the envelope takes a red giant structure. Here we have to discuss the implication of large θ_c/θ_1. For this purpose it is convenient to express equation of state in a generalized form as

$$\theta = \frac{P}{\rho} = \frac{k}{H} \frac{\Lambda T}{\beta \mu}. \tag{2.19}$$

Here k is the Boltzmann constant, H the atomic mass unit, μ the mean molecular weight, T the temperature, β the ratio of the gas pressure to the total pressure, and Λ

describes the effect of electron degeneracy. When electrons are strongly degenerate, we have $\Lambda T \sim \rho^{2/3}$ for non-relativistic degeneracy and $\Lambda T \sim \rho^{1/3}$ for relativistic degeneracy. Therefore, a higher central temperature, a lower temperature at the core edge and a stronger degeneracy at the center make the same effect to the stellar structure through Equation (2.11). On the other hand, a smaller β, i.e., larger radiation pressure at the core edge and a larger mean molecular weight in the underlying layers make the effect in the opposite direction.

As discussed in the preceding subsection and as seen in Figure 2.4, the value of θ_c/θ_1 cannot be larger than about 5, if the U–V curve runs in the region of positive Δ and ends at $\Delta_1 = 0$. Nevertheless a large value of $(\Lambda T)_c/(\Lambda T)_1$ is required for the core with strong electron degeneracy or with high central temperature. These two requirements are made compatible when β_1 becomes small so that the luminosity approaches the local Eddington limit corresponding to $M_1 \equiv M_r(r = r_1)$. (See Equation (4.3) for definition.)

As seen in Model B of Figure 2.4, the value of θ_c/θ can become rather large near the helium-burning shell, which is situated at the point of a $\log(V/U) = \log(V/U)_{\mathrm{He}} = 5.34$. Such value of $\theta_c/\theta_{\mathrm{He}}$ is possible because the mass fraction contained in the helium zone is as small as 4.6×10^{-6} [$\simeq (U/V)_{\mathrm{He}}$] and the value of V_{He} can be large. It is also consistent with Equation (2.11). In such model of the double (H and He) shell-burnings, the mass fraction of the helium zone is determined by the temperature or θ-distribution in the core so as to be consistent with such solution.

In case of Model A in Figures 2.2 and 2.4, the situation is different. The mass fraction of each shell with a specific nuclear fuel is determined by its preceding history of nuclear burnings, and the mass fractions are too large to be accommodated within a region of low temperature. Therefore, the U–V curve has to cross $\Delta = 0$ and make a loop near the oxygen-burning shell, for example, in order to reduce the value of θ_c/θ_1.

2.3. Single Star Approximation

The pressure at the core edge is expressed by Equation (2.15) or by

$$P_1 = \left[\frac{1}{4\pi r^2}\frac{U}{V}M_r\right]_1 g_1 . \tag{2.20}$$

This implies that the core feels the weight of the envelope only for the mass in the amount of

$$|\mathrm{d}M_r/\mathrm{d}\ln P|_1 = (U/V)_1 M_1 , \tag{2.21}$$

which is the mass contained within unit scale height of pressure

$$H_p \equiv -\mathrm{d}r/\mathrm{d}\ln P . \tag{2.22}$$

Whatever large mass is contained in the envelope, the structure of the core is, therefore, determined as if it would have the envelope of mass as small as $(U/V)_1 M_1$.

In other words, the core behaves as if it would have negligible mass in the envelope. Therefore the interior of the core is approximated to high accuracy by the interior of a single star of mass M_1. This is the single star approximation.

One may ask what is the effect exerted by the higher temperature at the core edge than at the photosphere of the single star. However, this is the same question as one why the approximation by the radiative zero boundary condition ($P = T = 0$) is valid for a single star instead of the boundary conditions at the photosphere. As discussed in many articles (Schwarzschild, 1958; Hayashi *et al.*, 1962; Nomoto and Sugimoto, 1974, for example), two solutions, which are integrated inward from different boundary conditions, become almost identical each other when the pressure is still much lower than the central pressure. This is understood also from the discussions in Section 3.

The envelope solutions are very sensitive to its initial values near the point of Δ_1, and practically envelopes of any masses can be fitted to the core at this point if other conditions such as the temperature and the density are the same. Because of such nature of the envelope solution, the envelope of a red giant can be replaced with appropriate boundary conditions at the core edge, as discussed by Hayashi *et al.* (1962) and as applied extensively by Sugimoto and his collaborators (see e.g., Sugimoto, 1970a), i.e.,

$$\Delta_1 = 0\,, \tag{2.23}$$

$$(N_1+1)_{\rm rad} = \begin{cases} V_1\,, \\ (N_1+1)_{\rm ad} \end{cases}, \tag{2.24}$$

where $(N+1)_{\rm rad}$ and $(N+1)_{\rm ad}$ are the radiative and convective polytropic index, respectively. This is the revised version of the single-star approximation with which we can compute physical quantities at the core edge as well as the energy flux (luminosity) in the envelope. Since these boundary conditions do not contain the total mass of the star at all, the core solution has nothing to do with the total mass. This is the reason why those physical quantities of red giant stars are determined only by the core mass (Hayashi *et al.*, 1962) as seen in the core-mass to luminosity relation (Paczyński, 1970) for instance.

2.4. Reason why the star becomes a red giant

The discussion in the preceding subsections gives a clear-cut answer to this fundamental question. When the core becomes of condensed type, i.e., θ_c/θ_1 becomes large, the value of $(U/V)_1$ becomes small. Nevertheless a large mass fraction in the envelope has to be accommodated. Therefore, the U–V curve makes a loop, i.e., crosses $\Delta = 0$, and runs in the region of small value of U with negative Δ. Such envelope solution of condensed type has a property that $V \to N+1$ as $r \to 0$ (Chandrasekhar, 1939; Hayashi *et al.*, 1962). When N is close to 3, the absolute value of Δ is thus very small, which makes the stellar radius very large according to Equation (2.4). Conversely, this is also the reason why the stellar radius becomes

relatively small, or is limited when a surface convection zone extends deep into the interior and reduces the value of the polytropic index.

However, such explanations are somewhat sophisticated. Though less quantitative, the following will be more intuitive and instructive.

We take the core edge as the hydrogen-burning shell. Its thermal energy should be comparable with the gravitational energy. (More exactly, $\Delta_1 \simeq 0$ or $V_1 \simeq 4$.) Because the temperature thereof must not exceed the hydrogen-burning temperature T_H, its radius must not become smaller than a certain value, i.e.,

$$r_1 = \frac{G\mu H}{k}\left(\frac{M_r\beta}{TV}\right)_1 \geqslant \frac{G\mu H}{k}\frac{M_1\beta_1}{4T_H}, \tag{2.25}$$

according to Equation (2.2).

As the star evolves, the central part of the core contracts to increase the central density and temperature. Nevertheless the size of the core hardly changes, because r_1 is almost fixed. Therefore as illustrated in Figure 2.5, the density has to decrease in the shells near the core edge, which results in the decrease in pressure. In order to sustain the envelope against the gravity with this decreased pressure, the bulk of the envelope should be pushed away to a larger radial distance where the gravitational

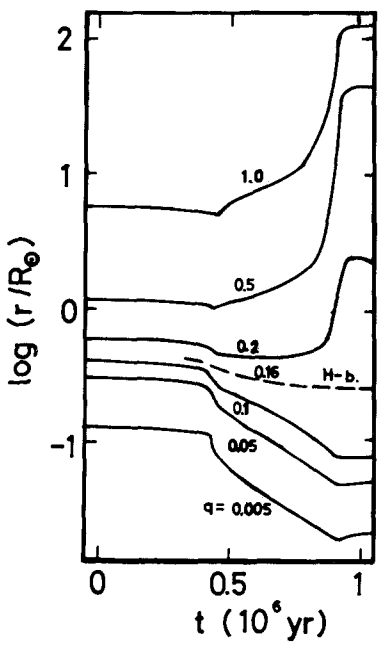

Fig. 2.5. Evolution of a star of $7M_\odot$ toward a red giant. Changes in the radial distances of different Lagrangian shells are plotted against time of evolution. (Taken from Hofmeister *et al.* (1964).) The edge of the helium core is situated at the mass fraction of $q = 0.16$ (H-b). As the core contracts, the envelope expands, keeping the hydrogen burning-shell as a node approximately.

acceleration is weaker. Thus, when the core contracts, the envelope expands keeping the hydrogen-burning shell as a node.

The explanation above is given for equilibrium configuration. However, the hydrogen shell-burning can supply necessary energy to expand the envelope. As an initial value problem it proceeds as follows. When the pressure at the hydrogen-burning shell decreases, the bottom of the envelope contracts to release more nuclear energy than to recover the photon losses. The excessive energy then expands the envelope against the gravitational attraction by the core. Then a new configuration is reached in which the envelope is more extended than in the initial configuration. In such explanation, however, we cannot understand why the new configuration should have a larger radius than the initial one. Therefore, the explanation in terms of the boundary value problem has to be supplemented as done in the main part of the present subsection.

3. Structure of the Core

Before entering into specific models of stellar evolution, we discuss the central density and temperature of the core from a standpoint of a generalized theory.

3.1. Hydrostatic equilibrium in non-dimensional form

Let us define the non-dimensional variables by

$$\begin{aligned} &r = r_0 \xi, \qquad M_r = M_o \phi, \\ &P = P_c \tilde{\omega}, \qquad \rho = \rho_c \eta. \end{aligned} \tag{3.1}$$

If we take

$$r_0^2 = \frac{1}{4\pi G} \frac{P_c}{\rho_c^2}, \tag{3.2}$$

$$M_0^2 = \frac{1}{4\pi G^3} \frac{P_c^3}{\rho_c^4}, \tag{3.3}$$

equations of hydrostatic equilibrium (2.1)–(2.3) are rewritten as

$$\begin{aligned} &U = \frac{\mathrm{d} \ln \phi}{\mathrm{d} \ln \xi} = \frac{\xi^3 \eta}{\phi}, \qquad V = -\frac{\mathrm{d} \ln \tilde{\omega}}{\mathrm{d} \ln \xi} = \frac{\phi \eta}{\xi \tilde{\omega}}, \\ &\frac{\mathrm{d} \ln \eta}{\mathrm{d} \ln \tilde{\omega}} = \frac{N}{N+1}. \end{aligned} \tag{3.4}$$

The boundary conditions at the center are

$$\phi = 0, \qquad \tilde{\omega} = 1, \qquad \eta = 1, \quad \text{at} \quad \xi = 0. \tag{3.5}$$

Therefore we can start integration from the center of the star, if N is given.

3.2. NON-DIMENSIONAL MASS

At the stellar surface or at the core edge,

$$M_1 = M_0\phi_1 \quad \text{at} \quad \xi = \xi_1 , \tag{3.6}$$

is to be satisfied. We call ϕ_1 the non-dimensional mass of the core (or the star). Let us compare the non-dimensional masses between two core solutions or stars as done in Figure 2.1. From Equations (2.4), (3.1), and (3.4), we have

$$\mathrm{d}\ln\phi = -\frac{U}{\Delta}(\mathrm{d}\ln U - \mathrm{d}\ln V) , \tag{3.7}$$

Integrating it and using Stokes' theorem we obtain

$$\int_L \mathrm{d}\ln\phi = -\int_S \frac{4U}{\Delta^2}\,\mathrm{d}\ln U\,\mathrm{d}\ln V = -\int_S \frac{4}{\Delta^2 V}\,\mathrm{d}U\,\mathrm{d}V , \tag{3.8}$$

(Sugimoto, 1964). The integrand in the right hand side of Equation (3.8) is relatively large for a relatively central region of $V \leqslant 4$. For a region of large values of V, i.e., near the core edge, it is relatively small, because its integrand $4U\Delta^{-2} \simeq 4UV^{-2}$ is small. Therefore, the non-dimensional mass is determined mainly by the solutions in the relatively central region as discussed in detail by Sugimoto (1964).

Because the relatively outer region affects only slightly, the difference in the value of ϕ_1 between a core and a single star is small as far as the structures in the central region are common to both of them. This is also the single star approximation. Therefore we may represent the core by an Emden solution of a polytrope with index N for which the value of its non-dimensional mass is equal to that of the core. The values of ϕ_1 for the polytropes are summarized in Table 3.1 (Sugimoto, 1964). The

TABLE 3.1

The values of ϕ_1 for the polytropes of index N

N	0	1.5	3.0	4.5	5.0
$\phi_1 \ldots$	4.899	10.73	16.14	22.42	25.46

values of ϕ_1 are different only by a factor of 1.50 between the polytropes of indices 1.5 and 3.0, which correspond to the adiabatic polytropic indices for gas consisting of non-relativistic and extremely relativistic particles, respectively.

3.3. RELATION BETWEEN THE CENTRAL TEMPERATURE AND DENSITY

Once the value of ϕ_1 is known, the value of P_c^3/ρ_c^4 can be computed for any (core) mass M_1 using Equations (3.3) and (3.6). If we specify the value of one more

thermodynamic variable, e.g., the central temperature T_c, the thermodynamic state at the center is fixed. Figures 3.1 and 3.2 give such relations quantitatively, where the values of $M_1 = (P_c^3/4\pi G^3 \rho_c^4)^{1/2}\, \phi_1$ are plotted against the central density ρ_c for different values of T_c. In this figure the value of ϕ_1 is approximated by its value for the polytrope with the adiabatic polytropic index corresponding to the set of T_c and ρ_c.

Its nature is explained as follows. When the density is small, the radiation pressure is dominant so that $M_1 \sim (T_c^3/\rho_c)^2$. When the equation of state is represented by ideal gas, we have $M_1 \sim (T_c^3/\rho_c)^{1/2}$. When electrons are strongly degenerate, we have $M_1 \sim \rho_c^{1/2}$ for non-relativistic case. For extremely relativistic degeneracy, M_1 approaches the constant value that is equal to the Chandrasekhar limit $M_{\rm Ch}$. Note that it takes a minimum value between the regimes of the ideal gas and the non-relativistic degeneracy. For temperatures higher than 2×10^9 K, such minimum disappears because the electrons become relativistic without passing through the regime of non-relativistic degeneracy. Their relevances to stellar evolution will be discussed in later sections.

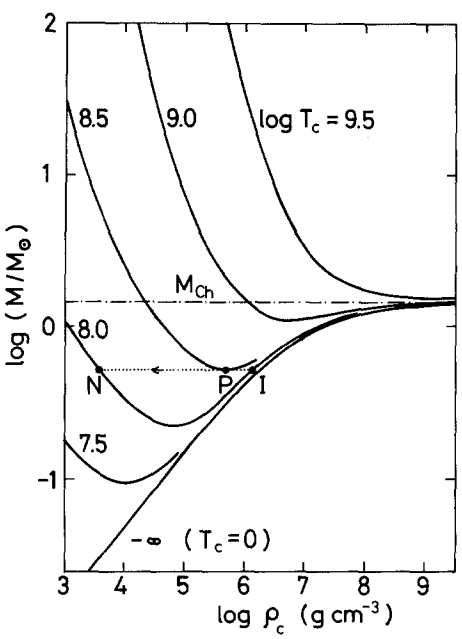

Fig. 3.1. Relation between the stellar masses or the core masses and the central densities plotted for different central temperatures. The different slopes result from different contributions in the equation of state, i.e., from the radiation pressure, ideal gas or nonrelativistic/relativistic degeneracy of electrons. Nuclear flash in the central region of a core proceeds along $I-P-N$ and the maximum central temperature is realized at the point P. (The gravitational contraction proceeds in the opposite direction.) Chemical composition is taken as carbon and oxygen with the concentrations of $X(^{12}\mathrm{C}) = X(^{16}\mathrm{O}) = 0.5$. (Taken from a book written in Japanese: D. Sugimoto, 1973, *Uchū Butsurigaku* (*Astrophysics*), p. 119, edited by C. Hayashi and S. Hayakawa, in a series of Gendai Butsurigaku no Kiso (Basis of the Modern Physics), edited by H. Yukawa, Vol. 12, Iwanami Shoten Publishers, Tokyo.)

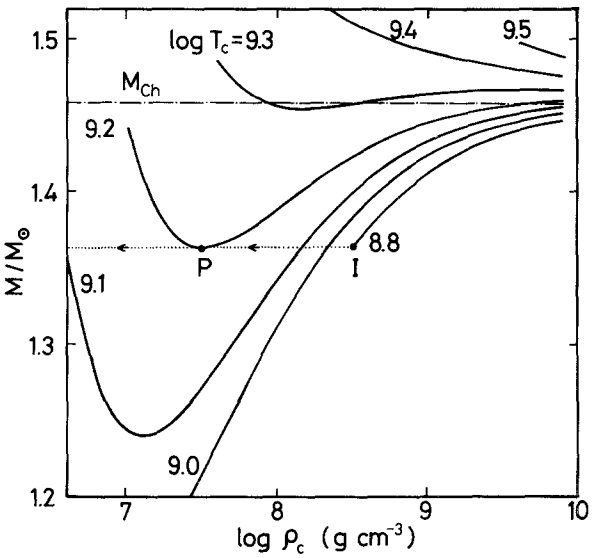

Fig. 3.2. A part of Figure 3.1 is enlarged. The local minimum in the locus of constant central temperature disappears above $T_c = 2 \times 10^9$ K.

4. Core Masses

It is important to know the relation between the initial mass of the star M_{ms} and the core mass M_1, because later evolution is determined mainly by the core mass. Moreover such core will become a real single star in a close binary system when the hydrogen-rich envelope is stripped off by mass transfer.

4.1. Mass of helium cores

Arnett (1978b) summarized the masses of the helium cores which are formed after the hydrogen burning in the core. Its mass is denoted by M_H because the hydrogen-burning shell lies at the core edge. We have added other results of computation (Alcock and Paczyński, 1978; Becker and Iben, 1979) to them. The mass fraction of the helium core M_H/M_{ms} is about $\frac{1}{4}$ for relatively small mass but $\frac{1}{3}$ for relatively large mass. Its interpolation formula is given by

$$M_H/M_{ms} \simeq 0.24 \log (M_{ms}/M_\odot), \tag{4.1}$$

for $5 < M_{ms}/M_\odot < 100$, within the error of 10%.

In the later phases of evolution the value of M_H changes by two processes: It increases by the hydrogen shell-burning and decreases by penetration of convective envelope into the helium region. The increase in M_H due to the burning is important when electrons are degenerate in the core. For the star of $M_{ms} \lesssim 2M_\odot$ the core mass grows until the helium flash is triggered. Similar growth of the carbon–oxygen core takes place in the star of $M_{ms} \lesssim 8M_\odot$ as will be discussed in Section 5.

4.2. Reduction of the Core Mass by Penetration of Convective Envelope

As the star evolves, the core contracts and the envelope expands as discussed in Section 2.4. Then the surface convection zone becomes deeper and deeper as discussed first by Hoyle and Schwarzschild (1955). As a result of it, the stellar radius becomes close to the Hayashi limit for the convective envelope in the HR diagram (Hayashi *et al.*, 1962). Such limitation to the radius of the star comes from the consistency between the photospheric condition and the interior solutions of the star, but it is understood more intuitively as the condition that the mean density of the star should be lower than that of the photosphere (denoted by the subscript ph), i.e.,

$$M > (4/3)\pi R^3 \rho_{\rm ph} \simeq (8/9)\pi R^2 \kappa_{\rm ph}^{-1}, \tag{4.2}$$

where $\kappa_{\rm ph}$ is the opacity at the photosphere (Sugimoto and Nomoto, 1974). The reason why the deep convection is consistent with a relatively small radius was discussed in Section 2.4.

As the core evolves, the density at the hydrogen-burning shell $\rho_{\rm H}$ decreases as discussed in Section 2.4. Since the temperature thereof $T_{\rm H}$ changes only a little, the specific entropy thereof $s_{\rm H}$ increases. On the other hand, the specific entropy near the photosphere $s_{\rm ph}$ is determined by the photospheric condition, i.e., by the stellar mass, radius and luminosity, and it is higher for the larger radius and the higher luminosity. When $s_{\rm H}$ becomes higher than $s_{\rm ph}$, the convection begins to penetrate into the core, if the convection in the envelope is adiabatic (Sugimoto, 1970a, b, 1971). When it is superadiabatic, there is a difference in entropy Δs (>0) between the photosphere and the bottom of the convective zone, as illustrated in Figure 4.1. Therefore, in actual case, the convective envelope penetrates into the core when $s_{\rm H}$ becomes higher than $s_{\rm ph}+\Delta s$ (Nomoto and Sugimoto, 1972; Sugimoto and Nomoto, 1974).

Therefore, the convective penetration is easier when the superadiabaticity Δs is smaller. Its amount is determined mainly by the ratio of stellar luminosity to masses,

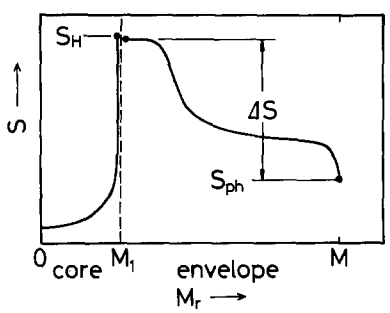

Fig. 4.1. Illustration of entropy distributions in the stellar envelope and core. In the radiative region it is increasing outward. In the convective region it is decreasing outward because of the super-adiabatic gradient. When the specific entropy at the core edge $s_{\rm H}$ becomes higher than the entropy at the photosphere $s_{\rm ph}$ plus the superadiabaticity Δs, the convective envelope penetrates into the core.

i.e., by $L/M_{\rm H}$ and L/M. They will be expressed more conveniently if we define the local Eddington's critical luminosity by

$$L_{\rm cr}(M_r) \equiv \frac{4\pi GcM_r}{\kappa} = 3.70\times 10^4 \left(\frac{1.73}{1+X}\right)\left(\frac{M_r}{M_\odot}\right) L_\odot. \tag{4.3}$$

In the extreme right hand side, the electron scattering opacity is substituted and X denotes the concentration by weight of hydrogen. Thus the superadiabaticity depends upon $L/L_{\rm cr}(M)$ and $L/L_{\rm cr}(M_{\rm H})$ though the latter is common among different stellar masses due to the core-mass to luminosity relation. Another important parameter to determine Δs is the efficiency of convective energy transport, which is represented by the ratio $\alpha \equiv l/H_p$ of mixing length of convection l to the scale height of pressure H_p for instance (Nomoto and Sugimoto, 1972). When $L/L_{\rm cr}$ is small or when α is large, the convection can transport its luminosity without producing Δs, i.e., without the superadiabatic gradient.

In actual stars the penetration of the convective envelope becomes important, if any, after the formation of the carbon–oxygen core, because $\theta_c/\theta_{\rm H}$ becomes large enough to increase $s_{\rm H}$. Because it depends on the structure of the core, the situations are classified by masses of the stars. For the stars of $0.5M_\odot \lesssim M_{ms} \lesssim 8M_\odot$ electrons become degenerate in the carbon–oxygen core which makes $\theta_c \propto \Lambda_c T_c$ large. However, for the stars of $M_{ms} \lesssim 3M_\odot$ the envelope will be ejected through the dynamical instability (Paczyński and Ziołkowski, 1968). The upper bound of the mass depends on the assumption in the mixing length theory, i.e., it ranges 3–$5M_\odot$ for $\alpha = \frac{3}{2}$–$\frac{2}{3}$, respectively (Fujimoto *et al.*, 1976b).

For the stars of mass $M_{ms} \lesssim 5M_\odot$ the convective zone does not reach the bottom of the hydrogen-rich envelope, because the mass contained in the helium zone is relatively small and because a relatively high value of $L/L_{\rm cr}(M)$ makes the envelope well superadiabatic. The upper bound of the mass depends, of course, on α and the chemical composition. According to computations by Becker and Iben (1979), the upper bound of the mass changes in the range of 3.3–$5.5M_\odot$ for the concentration of metals $Z = 0.001$–0.03 for which the concentration of helium is taken as $Y = 0.28$ and $\alpha = 1.0$.

For the stars of mass $5M_\odot \lesssim M_{ms} \lesssim 8M_\odot$, electrons become well degenerate (Λ_c large). Moreover the mass of the helium zone is large enough to be regarded as an envelope of the carbon–oxygen core. This is clearly seen in the U–V curve of Figure 4.2 which crosses $\Delta = 0$ at the helium-burning shell and makes a loop (Sugimoto, 1971). Therefore the helium zone expands as the core contracts. Such an expansion is also seen in computation of the evolution of helium star (Rose, 1969; Paczyński, 1971). As a result of expansion, the temperature at the hydrogen-rich envelope becomes so low that the hydrogen shell-burning is extinguished. In such situation, the convective envelope penetrates easily into the helium zone, because the depth of the convective zone is determined mainly by the temperature and the specific entropy thereof and has nothing to do with the mass contained in the convective envelope (Nomoto and Sugimoto, 1972).

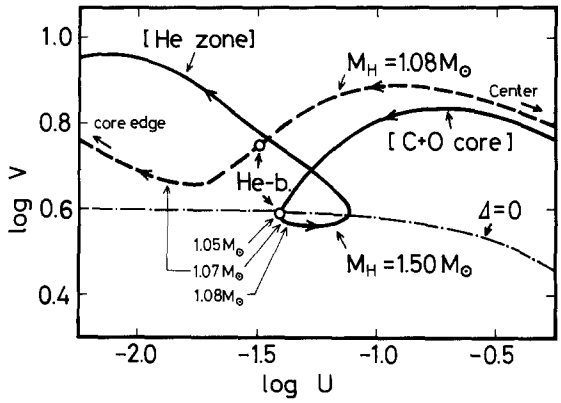

Fig. 4.2. Change in the U–V curve due to the penetration of convective envelope into the core. Case of $7M_\odot$ star with a carbon–oxygen core. The solid curve is for a stage before the convective penetration. The mass contained in the helium zone was as much as $0.45M_\odot$. Therefore, its U–V curve made a loop at the helium-burning shell and the helium zone behaved as an envelope to the carbon–oxygen core. The dashed curve is for a stage when the convective penetration has almost finished. The mass in the helium zone is now as small as $0.03M_\odot$, and it can be accommodated without making a loop in the U–V curve. (Computed by Sugimoto (1971), but was not published therein.)

In numerical computations, such penetrations were obtained by Paczyński (1970), Sugimoto (1971), and others, as seen in Figure 4.3. In particular, Becker and Iben (1979) obtained recently the results that for the star of $7M_\odot$ the value of M_H is reduced from $1.5M_\odot$ down to $0.95M_\odot$ by the penetration both with $\alpha = 0.7$ and 1.0. As seen in their results and as understood from the discussions in the earlier part of this subsection, the amount of penetration depends but only slightly upon the value of α, because $L/L_{cr}(M)$ is as small as 0.05.

As the mixing proceeds, the mass of the helium zone becomes small. Then, the loop in the U–V curve disappears as seen in Figure 4.2 and the hydrogen-shell burning is reignited, which stops the penetration. This consists also of the reason why the final value of M_H depends only slightly on α.

The upper bound of this mass range varies from $7.4M_\odot$ to $9.6M_\odot$ for $Z = 0.001$ to 0.03 ($Y = 0.28$) according to Becker and Iben (1979). Sometimes it is imagined that this upper bound would be reduced down to $5M_\odot$ if no penetration took place. From our discussions, however, the cause of the penetration is so clear that such possibility cannot be imagined.

For the stars of mass $8M_\odot \leqslant M_{ms} \leqslant 30M_\odot$, electron degeneracy is only incipient and carbon burning begins in non-degenerate condition. Near the lower bound of the mass range, such situations were computed for $12M_\odot$ star (Sugimoto, 1970b), $10M_\odot$ star (Alcock and Paczyński, 1978), 9 and $11M_\odot$ star (Becker and Iben, 1979), and $8M_\odot$ star (Barkat *et al.*, 1974). The value of θ_c/θ_H remains relatively small so that the convective envelope does not penetrate seriously. On the other hand, Weaver *et al.* (1978) computed evolution of $25M_\odot$ star and found that the penetration does not take place. Therefore the upper bound of this mass range will be set to about $30M_\odot$.

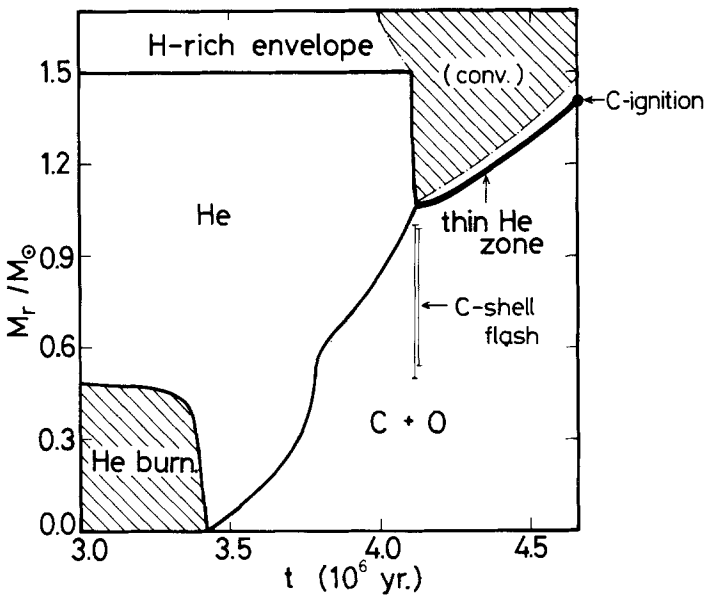

Fig. 4.3. Chemical evolution and the penetration of convective envelope into the helium zone of $7M_\odot$ star shown against the time of evolution. In this model two times of off-center carbon shell-flash took place. In the phase of the growing carbon–oxygen core the thermal pulses of helium shell-burning were suppressed artificially. (Taken from Sugimoto (1971), and Sugimoto and Nomoto (1975), and then combined into one figure.)

For the stars of mass $M_{ms} \gtrsim 30M_\odot$ the specific entropy at the core edge s_H becomes large because of the contribution of the radiation pressure. Therefore, the convective envelope penetrates into the core before the onset of carbon burning. For example, the convective penetration reduces M_H by $1.2M_\odot$ and $6.4M_\odot$ for the stars of $30M_\odot$ (Sugimoto, 1970b) and $60M_\odot$ (Nomoto, 1974), respectively, as seen in Figures 4.4 and 4.5.

From the carbon burning phase on, evolution becomes very rapid for the star more massive than $12M_\odot$, because copious neutrino loss accelerate evolution. Though θ_c/θ_1 becomes larger and larger in such phases, the convective penetration does not proceed appreciably as seen in Figures 4.4 and 4.5. The reason is as follows (Sugimoto, 1970a). In order to mix a mass element into the envelope, its specific entropy has to be raised up to the value of s_H. (Of course the difference in chemical compositions has to be taken into account.) It is realized by absorbing heat which comes from the interior of the core. Therefore the progress of the mixing or, in other words, the penetration of the convective envelope is limited by the time scale of heat transport $\tau_h(H_p)$ over unit scale height of pressure at the outer edge of the helium zone as

$$-\frac{dM_H}{dt} \lesssim \frac{\Delta M(H_p)}{\tau_h(H_p)}, \tag{4.4}$$

where $\Delta M(H_p) \equiv (U/V)M_H$ is the mass contained within unit scale height of

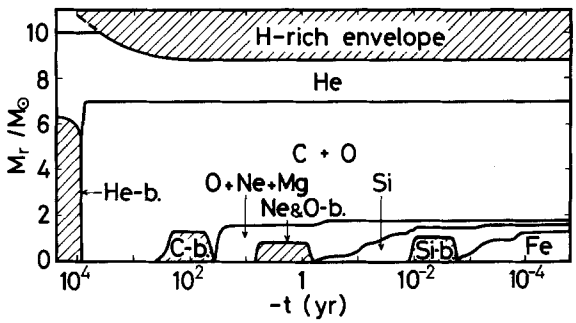

Fig. 4.4. Chemical evolution and penetration of convective envelope into the helium zone for $30M_\odot$ star. Note that the evolutionary time in the abscissa is in the logarithmic scale. When the timescale of evolution becomes short, the convective envelope has no time to penetrate any more. (Taken from Sugimoto and Nomoto (1974).)

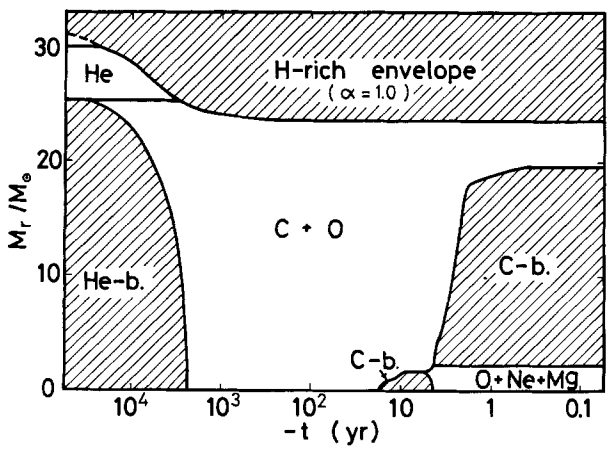

Fig. 4.5. Same as Figure 4.4 but for the star of $60M_\odot$. (Taken from Nomoto (1974).)

pressure. In numerical computations, the penetration proceeds at the speed for which the equality holds approximately in (4.4) (Sugimoto, 1970b; Fujimoto *et al.*, 1976a). From the carbon burning phase on, the timescale of evolution is short enough as compared with $\tau_h(H_p)$. Therefore we conclude that the reduction in M_H is negligible after the carbon burning phase.

5. Evolution of Intermediate Mass Stars Toward Carbon Deflagration

In Figure 5.1 we summarize the evolutions in the central temperature and density (T_c – ρ_c) diagram for the stars of different masses. In this section only the star of $M_{ms} = 7M_\odot$ is relevant. The others will be discussed in corresponding sections.

Here we discuss evolution of the growing electron-degenerate carbon–oxygen cores which were formed in the star of masses in the range of 4–$8M_\odot$. Such growth of the core will be treated in the same framework as the accreting white dwarfs.

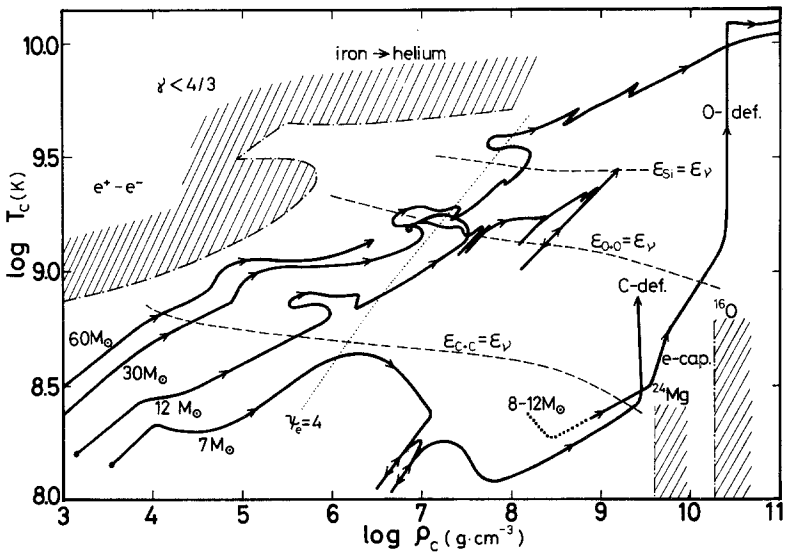

Fig. 5.1. Evolution of the stars of different masses in the central temperature and the central density diagram. The star of $7M_\odot$ is taken from Sugimoto (1971) and Sugimoto and Nomoto (1975) which evolves into the carbon deflagration supernova (Sections 5 and 6). The core corresponding to $M_{ms} = 8\text{–}12M_\odot$ is taken from Miyaji *et al.* (1979) which evolves into an electron capture supernova associated with the deflagration of oxygen (Sections 8 and 9). The star of $60M_\odot$ is taken from Nomoto (1974), $30M_\odot$ and $12M_\odot$ from Sugimoto (1970b), Sugimoto and Nomoto (1974), and Nomoto *et al.* (1979a), which evolve into a supernova triggered by the photodissociation of iron (Sections 10 and 11). In the shaded region lying in the upper-left side of the figure the star is dynamically unstable by the phase transitions as indicated in the figure. The shades in the right hand side of the figure indicate that the electron captures are important. To the right hand side of the dotted line with $\psi_e = 4$, electrons are appreciably degenerate. Also shown by dashed lines are the ignition loci for different nuclear fuels, based on updated reaction rates.

5.1. Relation between the core mass and the central density

As the electrons are strongly degenerate in the bulk of the core, its polytropic index N between the density and the pressure is determined by density and is almost independent of thermal state or the temperature in the core. Therefore the approximation discussed in Section 3.3 holds very precisely. As seen in Figure 3.1, the loci for constant temperature converge to that for zero temperature when the mass is smaller than $M_{\rm Ch}$ and the central density is high. This implies that the temperature and its distribution in the core affect only slightly to the central density. We may approximate the central density by

$$\begin{aligned} \log \rho_c &\simeq \log \rho_c(M_{\rm H}, T = 0) \\ &\simeq 6.8 + 1.2 \tan\left[1.7(M_{\rm H}/M_\odot - 0.73)\right], \end{aligned} \tag{5.1}$$

for $0.05 \lesssim M_{\rm H}/M_\odot \lesssim 1.40$ within an accuracy of 10%. The core mass $M_{\rm H}$ increases due to the hydrogen shell-burning at the rate of

$$\frac{dM_{\rm H}}{dt} = \left(\frac{dM_{\rm H}}{dt}\right)_n \equiv \frac{L_{\rm H}}{XE_{\rm H}}, \tag{5.2}$$

where L_H and E_H denote the integrated nuclear energy generation rate by the hydrogen shell-burning, and the nuclear energy release from unit mass of hydrogen ($E_H = 6.0 \times 10^{18}$ erg g^{-1}), respectively. When the helium-burning shell is close in mass to the hydrogen-burning shell, the integrated energy generation rate by helium L_{He} is related with L_H by

$$L_{He} = (E_{He}/X_e E_H) L_H , \tag{5.3}$$

in its *steady state*, or in the mean over a relatively long interval, where $E_{He} \simeq 6 \times 10^{17}$ erg g^{-1} is the energy release from unit mass of helium. Then the stellar luminosity is related by

$$L = (1 + E_{He}/X_e E_H) L_H , \tag{5.4}$$

i.e., $L \simeq 1.14 L_H$ for standard circumstances.

There is another situation for the growth of the core. It is the accretion which takes place in binary star system consisting of a white dwarf and its companion star. When the companion star overfills its critical Roche lobe, the gas will overflow from it and accrete onto the white dwarf. When some envelope is formed, the hydrogen begins to burn in the bottom of the envelope. As will be discussed in some detail in the next subsection, such accretion and subsequent nuclear burnings make a series of shell flashes. However, the core mass increases at the mean rate which is equal to the accretion rate $(dM/dt)_{acc}$, i.e.,

$$\frac{dM_H}{dt} = \left(\frac{dM}{dt}\right)_{acc} , \tag{5.5}$$

if the accretion rate is lower than $(dM_H/dt)_n$. (If mass ejection follows the shell flash, the effective accretion rate should be used.) If the accretion rate is higher than $(dM_H/dt)_n$, the accreted gas forms a red-giant like envelope, and the rate of processing is limited by the value of $(dM_H/dt)_n$ as discussed by Nomoto *et al.* (1979c).

The accreted hydrogen burns eventually into carbon and oxygen. The growth rate of the carbon–oxygen core is practically the same as dM_H/dt as far as the helium zone remains thin. Thus when dM_H/dt is given, the central density is determined as a function of time.

5.2. Evolution in the Central Temperature and Density

The timescale of heat transport is much longer than the timescale of the growth of the core mass so that the heat transport is negligible in the central region of the core. Therefore, the loss of entropy from a mass element is described by

$$\frac{kT}{\mu_i H} \frac{d \ln (T^{3/2}/\rho)}{dM_H} = -\varepsilon_\nu(\rho, T) \frac{dt}{dM_H} , \tag{5.6}$$

where μ_i and ε_ν are the mean molecular weight of ions and the neutrino loss rate, respectively. Here the specific entropy of degenerate electrons and the effect of

Coulomb interaction between ions and electrons (Brush *et al.*, 1966) are neglected though they are taken into account in detailed numerical computations.

Using Equation (5.6) together with Equation (3.6) and the core–mass to luminosity relation or the accretion rate, we obtain the evolutionary locus in the central temperature to the central denstiy ($T_c - \rho_c$) plane. Such approach was done by Arnett (1971) and Paczyński (1971) for the growing core in red giant stars, and by Ergma and Tutukov (1976) for accreting carbon–oxygen white dwarf.

5.3. Uncertainties in the Rate of Core Growth and Ignition Density

In this subsection we shall consider the growing core in red giant stars. Evolution of the core was computed for helium star of $1.45 M_\odot$ by Rose (1969) and for stars with hydrogen-rich envelope by Paczyński (1970) and Sugimoto and Nomoto (1975) for which thermal pulses of the helium burning-shell were suppressed artificially. An example of evolutionary locus is shown in $\rho_c - T_c$ diagram of Figure 5.1. Carbon burning was shown to be ignited at the central density of $\rho_c = 2 \times 10^9$ g cm^{-3}. The carbon burning in such a strongly electron degenerate core grows into a violent deflagration and the star will be totally disrupted as discussed in Section 1 and in the next section.

Anticipating to avoid the total disruption of the star, a series of efforts has been done to seek a possibility that the carbon burning is ignited at higher densities. If it were the case, beta processes and associated neutrino losses would bring the deflagrated core to reimplosion (Colgate, 1971). For this purpose the ignition density should be higher than $2 \sim 3 \times 10^{11}$ g cm^{-3} (Bruenn, 1972a; Buchler *et al.*, 1974).

As seen in Equation (5.6), the parameter which affects the ignition density is the ratio of (dM_H/dt) to the normalization factor for ε_ν. For the neutrino loss rate, old computations were based on the theory of conserved vector current (cvc). However, it is to be revised to include the effect of neutral current in weak interactions. Such neutrino loss rates were computed by Dicus (1972) on the basis of Weinberg (1967) and Salam's (1968) theory (WS). The ratio of such neutrino loss $\varepsilon_\nu^{\mathrm{ws}}$ to that by cvc theory $\varepsilon_\nu^{\mathrm{cvc}}$ depends on the Weinberg angle θ_W as

$$\varepsilon_{\mathrm{pl}\text{-}\nu}^{\mathrm{ws}} / \varepsilon_{\mathrm{pl}\text{-}\nu}^{\mathrm{cvc}} = 8 \sin^4 \theta_W + \tfrac{1}{2}, \tag{5.7}$$

for the plasma-neutrino loss. In this expression electron neutrinos and muon neutrinos are taken into account.

Recently, the existence of tau lepton was evidenced by experiment (Barbaro-Galtieri *et al.*, 1977), with which tau neutrino is associated. Because ν_τ pair is produced by the neutral current, its intensity will be the same as that for ν_μ. Therefore, Equation (5.7) is revised to

$$\varepsilon_{\mathrm{pl}\text{-}\nu}^{\mathrm{ws}} / \varepsilon_{\mathrm{pl}\text{-}\nu}^{\mathrm{cvc}} = 12 \sin^4 \theta_W - 2 \sin^2 \theta_W + \tfrac{3}{4}. \tag{5.7'}$$

For the plausible value of the Weinberg's angle (Dydak, 1979)

$$\sin^2 \theta_W = 0.230 \pm 0.015, \tag{5.8}$$

this ratio is close to unity (0.92).

Cooling due to URCA shells was also investigated for $^{23}\mathrm{Na} \rightleftarrows {}^{23}\mathrm{Ne}$ etc. However, such cooling is negligible as compared with other neutrino processes because the abundance of such odd-odd nuclei is too low (Bruenn, 1972b).

A larger uncertainty comes from the value of L_{H}. First of all, the core-mass to luminosity relation depends on the efficiency of the convective energy transport. Paczyński (1970) gave his famous relation

$$L/L_{\odot} = 59250\,(M_{\mathrm{H}}/M_{\odot} - 0.522)\,, \quad (0.6 < M_{\mathrm{H}}/M_{\odot} < 1.39)\,, \tag{5.9}$$

for $\alpha = 1$. If we assume a higher efficiency, the luminosity is higher (Uus, 1972; Sugimoto and Nomoto, 1974, 1975); for $\alpha \geq 1.5$ it is systematically more luminous by 20%.

Another uncertainty comes from effects of thermal pulses in helium shell-burning which repeat themselves more than 4000 times during the phase of its core growth (Sugimoto and Nomoto, 1975; Paczyński, 1975). The thermal pulse is sometimes called as helium shell-flash. It was found first by Schwarzchild and Härm (1965) and much discussed recently in relation to the origin of *s*-process elements.

Such thermal pulse can now be treated semi-analytically (Sugimoto and Fujimoto, 1978). It proceeds as follows (Iben, 1975; Fujimoto *et al.*, 1976a). When the helium zone is thin, the helium shell burning is unstable and makes runaway. Because nuclear energy is released at a high rate, a convection zone develops in the helium zone. However, its top does not reach the bottom of the hydrogen-rich envelope (Fujimoto, 1977). After the runaway has ceased, the convective envelope penetrates into the helium zone and mixes out or, according to Iben's (1975) terminology, dredges up a part of helium zone into the hydrogen-rich envelope.

Such thermal pulses do neither lead to any dynamical effect with a large margin nor induce total mixing of the helium zone under the standard conditions prevailing in the red giant stars. Therefore, we can regard the evolutionary sequence which is computed with the thermal pulses suppressed (Paczyński, 1970; Sugimoto and Nomoto, 1975) to be a good approximation to the mean evolution of the growing carbon–oxygen core. However, the dredging up affects the rate of the core growth.

The dredged amount is about $\frac{1}{3}$–$\frac{1}{2}$ of the helium zone (Iben, 1975; Fujimoto *et al.*, 1976a) so that the rate of the core growth is reduced by a factor of $\frac{3}{4}$–$\frac{2}{3}$. Concerning such theory of dredging-up, Paczyński (1977) raised a question about the efficiency of the convective dredging, but he did not give any recipe for a correct treatment of the problem. Therefore, we may conclude that the growth rate of the core is uncertain by a factor of 1.5.

Such range of the rate of core growth covers only a fraction of the range which will be considered in the next subsection in relation with accreting white dwarfs. Using the results in the next subsection, we can estimate that the corresponding uncertainty in the ignition density is only a factor of 1.1. As seen in Figure 5.1 and as will be discussed in the next subsection, a revision of the electron screening factor in the

nuclear reaction rate (Itoh *et al.*, 1977) changes the ignition density somewhat. When we take all of such factors into account, the ignition density in the core of a red giant star is regarded to be

$$\log \rho_c^{\text{ign}} = 9.4 \pm 0.1 , \tag{5.10}$$

against the anticipation of the reimplosion.

5.4. Evolution of Accreting Carbon–Oxygen White Dwarfs

In this subsection we consider the accreting carbon–oxygen white dwarf in a binary star system. If the accretion rate is much lower than $(\mathrm{d}M_{\mathrm{H}}/\mathrm{d}t)_n$, the growth of the core is controlled by the accretion rate, i.e., by Equation (5.5). Putting it into Equation (5.6) we see that more entropy is radiated away together with neutrinos and that the ignition density becomes higher.

Ergma and Tutukov (1976) studied such evolution for different accretion rates covering the range of 10^{-6}–$10^{-9}\, M_\odot\, \mathrm{yr}^{-1}$. These values should be compared with the standard rate of the core growth in red giant stars, i.e., $6 \times 10^{-7}\, M_\odot\, \mathrm{yr}^{-1}$ near the ignition stage. For simplicity they assumed accretion of matter with the composition of carbon plus oxygen neglecting the hydrogen and helium shell brunings of the accreted matter. Their results are reproduced in Figure 5.2.

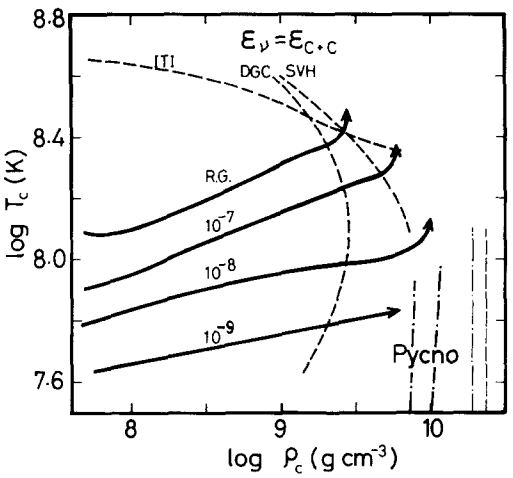

Fig. 5.2. Evolution of the electron degenerate carbon–oxygen cores in the central temperature to the central density plane. RG is the case of the core which lies deep in a red giant star (taken from Sugimoto and Nomoto (1975)). The others are the cases of accreting carbon–oxygen white dwarfs. Numbers attached to them are the accretion rates in units of $M_\odot\, \mathrm{yr}^{-1}$ (taken from Ergma and Tutukov (1976)). Dashed curves are the ignition loci along which the nuclear energy generation ε_{C+C} balances with the neutrino loss ε_ν. In computing them different enhancement factors for nuclear reactions are used as indicated by ITI (Itoh *et al.*, 1977) DGC (DeWitt *et al.*, 1973) and SVH (Salpeter and Van Horn, 1969). Ignition loci by the pycnonuclear reaction are taken from Duncan *et al.* (1976) and shown by dash–dot lines: the left and right ones correspond to the static and relaxed lattice approximations (Salpeter and Van Horn, 1969), respectively. Thin dash-dot and dashed lines indicate critical densities for electron capture on oxygen and general relativistic instability, respectively.

In Section 5.2 we noted that the evolutionary tracks in $T_c - \rho_c$ plane converge to a single track. It is right as far as we consider the carbon–oxygen cores embedded deep in a red giant. In an accreting white dwarf, however, we may imagine a quite large range for the thermal state in its initial stage when accretion commences. The white dwarf may have been cooled down, if there was enough time between the formation of the white dwarf and the onset of accretion.

In computing the rate of carbon burning, Ergma and Tutukov (1976) applied the enhancement factors due to electron screening which were computed by Salpeter and Van Horn (1969) and by DeWitt *et al.* (1973). The corresponding ignition lines, along which the nuclear energy generation rate ε_{C+C} is equal to ε_ν, are also shown in Figure 5.2. However, near the ignition points for the cases of slow accretion, the enhancement factors by both computations are greatly out of its applicability.

After their paper, the enhancement factor in a dense plasma has been recomputed (Itoh *et al.*, 1977; Alastuey and Jancovici, 1978; Itoh *et al.*, 1979), which was based on new analysis (Hansen, 1973) of Monte Carlo computation for ion-ion correlation in dense plasma. Their result is shown in the ignition line of Figure 5.2, which is applicable for the temperatures above 2.3×10^8 K. In the temperature range of $(1.5\text{–}1.0) \times 10^8$ K it is uncertain because the matter forms quantum liquid. Below 1.0×10^8 K it forms a solid, and the ignition line is drawn by equating the pycnonuclear reaction rate (Salpeter and Van Horn, 1969) with the heat capacity divided by the timescale of contraction due to accretion with critical rate (Duncan *et al.*, 1976). When the accretion rate is lower than about $10^{-8} M_\odot \text{ yr}^{-1}$, the carbon burning is ignited by the pycnonuclear reactions.

Duncan *et al.* (1976), and Canal and Schatzmann (1976) considered the limiting case where the temperature is low enough, which corresponds to the case of infinitely slow accretion and which gives an upper bound to the ignition density. The pycnonuclear reaction is ignited at $\rho_c = 0.7\text{–}1.0 \times 10^{10} \text{ g cm}^{-3}$. In the regime of pycnonuclear reaction, its temperature dependence is weaker than those for the heat diffusion and for the neutrino loss. In this sense the pycnonuclear reactions proceed steadily in balance with such heat losses. However, the central density is increasing due to the core growth and a slight increase in the density makes the energy generation dominate over the heat losses and initiates the runaway of carbon-burning.

Therefore, the density given above is the upper bound to the ignition density for any situation. It is lower than the threshold density for electron capture by ^{16}O ($E_F =$ 10.42 MeV, i.e., $\rho_{thr}(^{16}O) = 1.9 \times 10^{10} \text{ g cm}^{-3}$ for $\mu_e = 2$), lower than the critical density for the reimplosion of the core by beta processes ($\rho_{cr}^{\beta} = 3 \times 10^{10} \text{ g cm}^{-3}$, Mazurek *et al.* (1974)), and lower than the critical density for the general relativistic instability ($\rho_{cr}^{GR} = 2.3 \times 10^{10} \text{ g cm}^{-3}$; Chandrasekhar and Tooper (1964)) which is induced for the ratio of specific heats γ very close to $\frac{4}{3}$. Thus, in the event of carbon deflagration, the collapse of the core can not be anticipated as will be discussed in the next section.

6. Carbon Deflagration Supernova

When the carbon-burning is ignited, it grows into an explosive burning. Different from earlier expectations, it does not grow into a detonation wave but becomes a deflagration. However, the star will be totally disrupted.

6.1. Flash and Blocking of Heat

As is well known a nuclear burning in the central region of the electron-degenerate core is thermally unstable, and it is called a nuclear flash. Detailed numerical computation for such flash was done first by Härm and Schwarzschild (1964) for a core helium flash, and physical processes were visualized by Sugimoto (1964). When the nuclear energy generation minus energy loss by neutrinos overcomes the heat diffusion, heat is piled up in the energy generating region. It is better to express it in terms of the specific entropy s than the heat, because the former is a state variable. When the specific entropy increases in the central region, convection develops and levels the entropy distribution as illustrated in Figure 6.1.

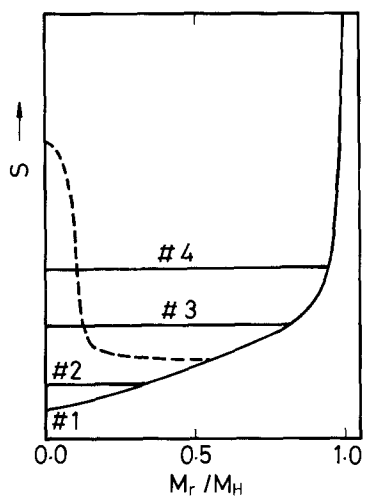

Fig. 6.1. Illustration of the change in entropy distribution during the progress of the core nuclear flash. The stage No. 1 is the stage just before the ignition. Entropy production by nuclear burning tends to make a profile as shown by the dashed curve, but the convection levels it as shown for later stages Nos. 2–4. In the event of carbon deflagration supernova, the convection is not efficient enough and such an entropy profile is realized as one drawn by the dashed curve (Section 6.3).

When the central region of the core is isentropic, i.e., its temperature gradient is adiabatic, the approximation discussed in Section 3.3 holds very precisely. Therefore, the core evolves along the line of constant core mass in Figures 3.1 and 3.2, e.g., along the line $I-P-N$ (Sugimoto, 1964). Thus the central temperature changes as shown in Figure 6.2 where the core mass is taken as a parameter (Nakada and Sugimoto, 1972). Because P_c^3/ρ_c^4 stays almost constant, the increasing specific entropy s_c implies the corresponding decrease in the central density.

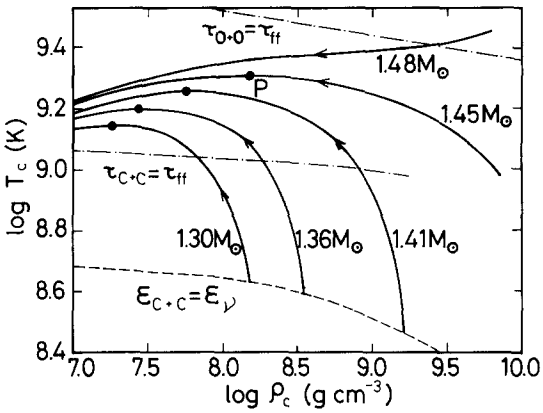

Fig. 6.2. Evolutionary loci of nuclear flash in the central region of the core. Cases with different core masses are shown. Taken mainly from Nakada and Sugimoto (1972), and was composed from Figure 3.2. This figure applies mainly to a good approximation to cores of any composition with $\mu_e = 2$. Ignition line is shown for the carbon burning by the dashed line. Evolution of the core should be dynamical above the dash-dot lines. Effects of inertia and the heat blocking are neglected in the evolutionary loci. Before reaching the point P, the carbon flash grows well into dynamical strength while the oxygen flash does not.

The central temperature takes its maximum value at the point P in Figures 3.1, 3.2, and 6.2 where the line $I-P-N$ is a tangent to a locus with a constant T_c and thus the electron degeneracy is weak (see Section 3.3). After it the central temperature decreases as electrons become non-degenerate. Such picture describes the progress of the flash very precisely as far as the convective energy transport is efficient enough to realize isentropic convective core (Sugimoto, 1964).

However, the efficiency of the convective energy transport is finite. It will be discussed conveniently in terms of the nuclear timescale for a change in temperature

$$\tau_n \equiv c_p T/\varepsilon_n\,, \tag{6.1}$$

and of the timescale of free fall

$$\tau_{ff} \equiv (24\pi G\rho)^{-1/2} \sim l/c_s\,. \tag{6.2}$$

Here c_p, c_s and l are the specific heat at constant pressure, sound velocity and the mixing length, respectively. When the ratio τ_n/τ_{ff} reaches about 0.01, heat or entropy is blocked appreciably in the central region. In our case of carbon burning, such situation takes place well before the point P as seen in Figure 6.2, where the line for $\tau_n = \tau_{ff}$ is also shown.

The blocking of heat produces a superadiabatic entropy (temperature) gradient and reduces the value of the polytropic index below its adiabatic value. This results in the decrease of the non-dimensional mass ϕ_1 as seen in Table 3.1, and thus in the increase in the temperature as can be understood from Figure 3.1 and Equations (3.3) and (3.6). In such stages, P_c = constant is a better approximation as shown by Sugimoto (1964) for cores in the helium flash. Such approximation is understood as

follows. When the heat is blocked, the strong nuclear energy generation is confined within the very central region. Since the mass contained in such superadiabatic core is small, it affects but slightly the hydrostatic equlibrium. Therefore the central pressure should remain almost constant to sustain the core.

As the nuclear energy is released, the central temperature continues to rise. Then the nuclear energy generation rate becomes so high that the dynamical effect, i.e., the effect of inertia term in the equation of hydrodynamics becomes essential. The criterion for it is $\tau_n = \tau_{ff}$ and the corresponding temperature will be denoted as deflagration temperature $T_{\rm def}$. In the limit of extremely fast energy generation, there is no time for expansion and the density remains almost constant in the central region. In such stages the energy conservation between the states before (subscript i) and after (subscript f) the nuclear deflagration gives an approximate relation as

$$u_{{\rm gas},f} + u_{{\rm rad},f} = u_{{\rm gas},i} + u_{{\rm rad},i} + E_n \,. \tag{6.3}$$

Here $u_{\rm gas}$ is the specific internal energy of the gas, and $u_{\rm rad}$ is the energy of the radiation field per volume in which unit mass of the gas is contained,

$$u_{\rm rad} \equiv aT^4/\rho, \tag{6.4}$$

and E_n is the nuclear energy release per unit mass of matter.

If we assume that electrons are degenerate for the initial state and non-degenerate for the final state, it is rewritten as

$$\frac{aT_f^4}{\rho} + \frac{3}{2}\frac{k}{H}\frac{T_f}{\mu_f} \simeq \frac{aT_i^4}{\rho} + \frac{3}{2}\frac{k}{H}\frac{T_i}{\mu_{i,i}} + E_n \,. \tag{6.5}$$

If we use $E_n = 5\times10^{17}\ {\rm erg\ g^{-1}} = 0.52\ {\rm MeV\ nucl^{-1}}$ for carbon burning, we obtain $T_f \gtrsim 8\times10^9\ {\rm K}$ for $\rho \gtrsim 1\times10^9\ {\rm g\ cm^{-3}}$. It is high enough to sustain the explosive nuclear burning, because the nuclear statistical equilibrium (NSE) is established in τ_{ff} for temperatures higher than 3×10^9 K (Truran *et al.*, 1967). According to Equation (6.5), the density as low as $(0.2\text{–}1)\times10^7\ {\rm g\ cm^{-3}}$ for $X(^{12}{\rm C}) = 0.5\text{–}1$ is compatible with such explosive burning to NSE. Therefore, our carbon burning is well explosive to a large margin.

6.2. Carbon detonation assumption

As a result of the consideration in the preceding subsection, the carbon flash grows well into an explosive burning. Then it was imagined to become a detonation and such event was named as the carbon detonation supernova (Arnett, 1968, 1969). Bruenn (1971) computed its detailed *model* assuming that the detonation wave is initiated and propagates through the core. He did not compute the propagation of the detonation wave, but he made the detonation front propagate artificially with a sound speed in the material just behind the front, i.e., changed the fuel into NSE composition shell by shell successively with a given speed. This simulated the Chapman–Jouguet detonation (CJD). Then he obtained the following results.

Before the detonation the gravitational potential energy of the core was $\Omega_0 = -3.1 \times 10^{51}$ erg, and the internal energy of gas was $U_0 = 2.6 \times 10^{51}$ erg. Thus the gravitational binding energy was as small as $E_B = -(U_0 + \Omega_0) = 5 \times 10^{50}$ erg, i.e., only a sixth of the absolute value of the gravitational potential energy. The maximum temperature attained in the course of explosion was 8.0×10^9 K, which was high enough to bring matter into NSE composition. It released nuclear energy as much as $E_n = 7.7 \times 10^{17}$ erg g^{-1} or 2.2×10^{51} erg for the whole core, of which the neutrino loss took away only 6×10^{49} erg. Therefore the available nuclear energy was as much as $4E_B$ so that the whole core was disrupted and dispersed with the kinetic energy equal to 1.6×10^{51} erg $\simeq 3E_B$.

Such model of carbon detonation supernova raised two problems. One is the shortage of the pulsar progenitors (Gunn and Ostriker, 1970; Ostriker *et al.*, 1974). If no remnant star is left after the carbon detonation, we have to assign the pulsar progenitor to more massive stars than $8M_\odot$. The other is the overproduction of the iron group elements in the Galaxy. If stars in the mass range of 4–8$M_\odot$ experience the carbon detonation and each star ejects iron group elements as much as $1.4M_\odot$, the iron group elements should have been produced by six times more than observed in the Galaxy (Ostriker *et al.*, 1974; Arnett, 1974).

Something was thought to be wrong. Then, they had to check if the assumption of the detonation was consistent. It was done as follows (Buchler *et al.*, 1971). Assume the detonation wave is initiated. Then a burning front and a preceding shock front are propagating. When the shock wave reaches a shell, the temperature of the shell is raised to T_{sh} due to the compression by the shock wave and to the entropy production at the shock front. If T_{sh} is higher than the deflagration temperature T_{def}, the shock front can detonate the shells successively and the burning front propagates just adjacent to the shock wave. Then energy generation by the detonation strengthens the shock wave.

If this is the case, the assumption of the detonation was said consistent. Buchler *et al.* (1971) made such consistency check extensively under the assumption of the Chapman–Jouguet detonation, which gives the fastest propagation and thus the weakest detonation. They obtained a result that even for the Chapman–Jouguet condition the assumption of detonation is consistent for densities higher than 1×10^7 g cm^{-3}.

6.3. Trials to Avoid the Total Disruption

Many trials have been done to seek for possibilities to avoid the total disruption of the star in the carbon detonation model. One is the carbon ignition at such higher densities that beta processes lead to reimplosion of the core. However, it seems unlikely as was discussed in Section 5.3.

Another is the convective URCA process which may take energy away with neutrino pairs (Paczyński, 1972). It is assumed that an odd-odd nucleus such as ^{23}Na captures an electron in high density region where nuclear energy is being generated and strong convection is taking place. The resultant nucleus is transported by

convection current to a region of lower density where it decay by emitting electron. Through this mechanism, neutrino pairs are produced which take away the excessive nuclear energy generation and the carbon burning would be stabilized. In order for this mechanism to work, everything has to be tuned very finely, because the convective turnover time and thus the time scales of beta processes should be much shorter than the lifetime of the stabilized carbon burning phase but no easy stabilizing mechanisms are involved. Nuclei have to capture and decay in appropriate shells. The convection should be strong enough to transport the electron-captured matter, i.e., matter with higher mean molecular weight to the region of lower mean molecular weight against the gravity. Despite that the carbon burning should not be too strong to tune everything. Iben (1978) is studying such possibility, but at present the carbon burning has not yet been regarded to be stabilized.

6.4. Spherical damping of shock wave

The consistency check discussed in Section 6.2 implies that it is consistent *if* the detonation wave has been formed. Therefore, we have to check *whether* the explosive burning grows into a detonation or not. In this relation it is important to remind us of Ōno's (1960) work concerning the shock propagation through inhomogeneous and spherical medium, i.e., through the interior of the star (Ōno *et al.*, 1961). He considered a shock wave which is continuously pushed by something like a piston. The shock strength is defined by using the pressures behind the shock front P_2 and ahead of it P_1 as

$$z \equiv P_2/P_1 \,. \tag{6.6}$$

As the shock propagates through the star, its strength changes as

$$\frac{\mathrm{d}\ln(z-1)}{\mathrm{d}\ln r} = \frac{\left[\frac{1}{N+1}+2\left(\frac{1+\lambda^2 z}{z(1+\lambda^2)}\right)^{1/2}\right]V-4\Big/\left(1+\frac{(z-1)(1-\lambda^2)}{[(1+\lambda^2)z(1+\lambda^2 z)]^{1/2}}\right)}{2-\frac{z-1}{z+\lambda^2}+2\left[\frac{1+\lambda^2 z}{z(1+\lambda^2)}\right]^{1/2}}, \tag{6.7}$$

where λ is assumed to be constant and expressed by using the ratio of specific heats $\gamma = c_p/c_v$ as

$$\lambda^2 = (\gamma-1)/(\gamma+1) \,. \tag{6.8}$$

In Equation (6.7) the numerator in the right hand side consists of two terms. According to Ōno (1960), the first term containing V describes the pressure growing of the shock and the second term describes the spherical damping. The spherical damping takes place because the area of the shock front increases. It balances with the pressure growing term at the point where

$$V = 4\Big/\left(\left\{1+\frac{(z-1)(1-\lambda^2)}{[(1+\lambda^2)z(1+\lambda^2 z)]^{1/2}}\right\}\left\{\frac{1}{N+1}+2\left[\frac{1+\lambda^2 z}{z(1+\lambda^2)}\right]^{1/2}\right\}\right) \tag{6.9}$$

holds. For the polytrope of $N=3$ with $\gamma=\frac{4}{3}$, its numerical value is $V=1.8$–2.0 for

$z = 1-\infty$. Interior to this point the shock wave is damping in its strength as it propagates. Such a damping region contains 23–27% of the core mass.

In the early phase of explosive carbon burning, the heat blocking takes place in the very central region and carbon is deflagrated in the region in which less than 0.1% of the core mass is contained. Therefore, the effect of the spherical damping is most important.

In the consistency check which was discussed in Section 6.2, the distance between the shock front and the burning front was tacitly assumed to be negligible as compared with the radius of the spherical shock front. In other words, it was treated as one-dimensional configuration in which the effect of spherical damping could never been taken into account. Now we have to check if the nuclear burning overcomes the spherical damping and the detonation wave is initiated (cf. Lee, 1972).

6.5. Carbon deflagration supernova

Ivanova *et al.* (1974) computed hydrodynamic evolution during the carbon burning without assuming a formation of detonation wave. They obtained an oscillation of the core instead of the total disruption. However, their result is strange. They did not include any mechanisms of heat transport. However, as can be read from Figures 3, 4, and 5 of their paper, i.e., from the changes in temperature, density and pressure, the specific entropy of a shell increased during the stages when neither shock appeared nor nuclear burning begins. This entropy production could be ascribed only to numerical dissipation. Their carbon burning was ignited shell by shell as a result of this spurious entropy production. The same criticism applies also to their recent work (Ivanova *et al.*, 1977a, b). Therefore the ignition was also spurious and we needed to recompute it taking account of appropriate mechanism of energy transport.

Buchler and Mazurek (1975) tried to make such a computation but they could follow only to a relatively early stage of carbon burning. As far as they computed, no detonation waves were initiated, but further computations were needed.

A little later Nomoto *et al.* (1976) published such a computation. They treated the energy transport as follows. As discussed in Section 6.1 and illustrated in Figure 6.1, the specific entropy of the burnt region becomes higher than those in the overlying layers. This implies that there is a large density inversion across the burning front and it drives the Rayleigh–Taylor instability. Then fresh fuel is taken into hot region and deflagrates. They described the propagation of such deflagration front by means of the mixing length theory of convection. They expressed the propagation velocity v_{def} as

$$v_{\mathrm{def}} = \alpha_{\mathrm{def}}[(GM_r/4r^2)\, l\Delta \ln \rho]^{1/2} . \tag{6.10}$$

Uncertainties arise from the mixing length theory itself and from applying it to a finite jump in densities $\Delta \ln \rho$ across the front. Such uncertainties were all transferred into a single parameter α_{def}.

Assuming a value of $\alpha_{\rm def}$ they computed evolution of the carbon–oxygen core from a stage well before the onset of the flash, through the heat blocking in flash, and up to the stage of explosion, which cover continuously the stages with the time scale of 10^5 years through fraction of a second. The computation of such transition stages is important because it determines how much fraction of the core is deflagrated almost simultaneously in its early stages. If only a small fraction of the core is deflagrated, the effect of the spherical damping is serious. If the carbon burning flared up in a relatively large fraction of the core, the spherical damping would be less serious.

They computed the cases for $\alpha_{\rm def} = 0.05$ and 1.0, and obtained the following results. No strong shock waves and thus no detonation waves are formed in both cases. The carbon burning front remained to be the deflagration front, i.e., it propagated with the speed less than the sound speed, i.e., $v_{\rm def} \simeq 0.01 c_s$ and $0.2 c_s$ for $\alpha_{\rm def} = 0.05$ and 1.0, respectively. Because of its relatively slow propagation, the core expanded appreciably. In the case of $\alpha_{\rm def} = 1.0$, the total energy of the core becomes positive when 20% of the core mass has been processed into NSE. In the case of $\alpha_{\rm def} = 0.05$, the core expanded more as reproduced in Figure 6.3, and the carbon burning becomes almost extinct at stage No. 6. At this stage the total energy of the core is still negative and then the core turns to contract again. In this time, however, the density is as low as $(1 \sim 1.6) \times 10^6$ g cm^{-3} at the burning front. Therefore, the heat

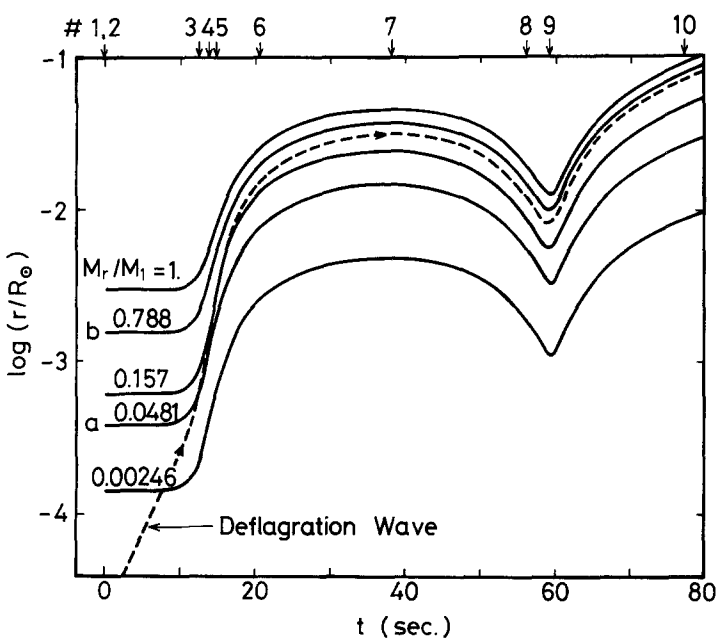

Fig. 6.3. Expansion and oscillation of Lagrangian shells in the carbon deflagration supernova for the case of $\alpha_{\rm def} = 0.05$. The deflagration front propagates as shown by dashed curve. At the stage No. 10 the expansion velocities exceed local escape velocities for all shells. (Taken from Nomoto *et al.* (1976).)

capacity of the radiation field absorbs the nuclear energy and, according to Equation (6.5), the maximum attainable temperature is as low as 2.2×10^9 K. The nuclear burning does not proceed to NSE.

However, the amount of the nuclear energy release is large enough to lift the total energy of the star positive. As a result of it the star is totally disrupted even in this case of relatively small value of $\alpha_{\rm def}$.

Though the conclusion depends on the value of $\alpha_{\rm def}$, it is almost certain that a detonation wave is not formed and that the carbon burning remains to be a deflagration. Even in the deflagration regime, the star is totally disrupted and no remnant is left. If $\alpha_{\rm def}\simeq 0.05$ is the case, the star is not totally incinerated into NSE composition, and the resultant abundance is 11% of iron group elements, 7% of elements in the range of ^{20}Ne through ^{28}Si, and 82% of the unburnt fuel (^{12}C+^{16}O). In this sense, the difficulty of the overproduction of the iron group elements is avoided but the difficulty of the shortage of pulsar progenitors still remains.

Recently, the birth rate of the pulsars is reanalyzed by Taylor and Manchester (1977) using new data of 149 pulsars. According to them, the result depends upon the average interstellar electron density $\langle n_e\rangle$, which affects the estimate of their distances. Wheeler (1978) showed that the critical stellar mass above which all star should leave neutron stars is $3M_\odot$ and $10M_\odot$ for $\langle n_e\rangle = 0.03$ and $0.02\ {\rm cm}^{-3}$, respectively. If the latter is the case, we are not necessarily short of the pulsar progenitors.

The results obtained above can be understood from the standpoint of energetics. In the case of relativistic electron degeneracy, the value of γ is close to $\frac{4}{3}$ so that the gravitational binding energy ($E_B = 5\times10^{50}$ erg) is much smaller than the absolute value of the gravitational potential energy ($-\Omega_0 = 3.1\times10^{51}$ erg) and than the internal energy ($U_0 = 2.6\times10^{51}$ erg). When the energy of the order of E_B is released, the star can be disrupted. However, the shock formation requires energies of the order of U_0. When the nuclear burning is taking place in the central region in particular, the nuclear energy release (0.5 MeV nucl^{-1} for carbon burning only and 0.3 MeV nucl^{-1} for the establishment of NSE state) should be compared with the specific internal energy in the central region ($u_{0,c}$ = 1.5 MeV nucl^{-1}). Therefore, the overpressure in the central region is only 20% of the initial pressure at the center, which is too small to overcome the spherical damping. In short the nuclear energy is large as compared with the gravitational binding energy but is small compared with the internal energy in the central region.

7. Combustion and Detonation of Helium in Accreting White Dwarfs

Type I supernovae occur in elliptical galaxies as well as in spiral and irregular galaxies. Since the star formation seems to be finished long before in the elliptical galaxies, less massive stars may be related with some of type I supernovae. In this section we will discuss a possibility that such supernovae may be related with accreting white dwarfs. This, of course, does not rule out the existence of other

classes of type I supernovae of which the progenitor is relatively massive (Arnett, 1979b). Such ones will be treated in other sections.

7.1. Accretion onto compact stars and shell flashes

Recently, accretion onto compact stars is discussed extensively. It takes place mainly in the phase of the second mass exchange in close binary systems and partly in dense gas clouds. The compact star accretes mass from its companion star which is ejecting gas as stellar wind or which is overflowing its critical Roche lobe.

Problems, which have been discussed most extensively, are nova explosion of accreting white dwarfs. When the accreted gas has formed a certain amount of hydrogen-rich envelope, a hydrogen shell-flash takes place, which grows into nova explosion depending on situations of the accretion (see e.g. Sparks *et al.*, 1977; Prialnik *et al.*, 1979; Nariai *et al.*, 1979; and references quoted therein). The amount of the gas, which accretes before the ignition of the shell flash, depends sensitively on the accretion rate, but it is in the range of $10^{-2} \sim 10^{-4} M_\odot$ (e.g. Sugimoto *et al.*, 1979).

The hydrogen burning involves two beta decays to synthesize one helium nucleus, the half lives of which are of the order of 100 s. Therefore, energy generation is relatively slow and limited to the value of $\varepsilon_H = 5.9 \times 10^{15} X_{CNO}$ erg g^{-1} s^{-1}, where X_{CNO} is the abundance of CNO elements. The energy generation is too slow to grow into a detonation. When the nuclear energy has been released as much as the gravitational energy of the hydrogen-rich envelope, the released heat makes the envelope expand and the hydrogen shell-flash is quenched. Therefore only a part of the nuclear energy can be released by the hydrogen shell-flash. Numerically, it is about 10^{46}–10^{47} erg which corresponds to the order of nova explosion.

Starrfield *et al.* (1975) considered an extreme case, in which the number of carbon nuclei is the same as protons and all protons are captured by the carbon nuclei without waiting any beta decay. Then they computed a model for massive white dwarf of $1.25 M_\odot$ having the hydrogen-rich envelope of $1.7 \times 10^{-3} M_\odot$, which corresponds to the accretion time as long as the age of the universe (Nariai and Nomoto, 1979). Even for such an extreme case, they obtained an explosion with the kinetic energy of 1×10^{47} erg, which is too weak to be considered as a supernova explosion.

Another problem is the accretion onto neutron stars. It is intended to interpret X-ray bursters. According to Joss (1978), the accreted hydrogen burns fuzzily and a helium zone is formed. Then the helium shell-flash takes place which releases energy of the order of 10^{39} erg.

However, much stronger flash and detonation are possible when the gas accretes relatively slowly onto white dwarfs and if we consider helium burning in electron degenerate conditions. Such models will be discussed in the rest of this section.

7.2. Helium detonation in accreting helium white dwarfs

In the nova event all of the accreted matter are not expelled. Therefore helium is accumulated as the hydrogen shell-flashes repeat themselves, and the mass of the

helium core grows. This core growth is assimilated by a steady accretion of helium gas onto a white dwarf. When a certain amount of helium is accumulated, helium flash is ignited.

Mazurek (1973) made hydrodynamic computation of such model. He has shown that for the helium white dwarf of mass larger than $1M_\odot$ it results in a helium detonation and the star is totally disrupted. In an old work Sugimoto (1964) considered helium flash in a relatively massive core and showed that the flash becomes dynamical if the core mass is greater than $0.7M_\odot$. These results are consistent.

In such works, however, thermal history of accretion was not computed. The initial model of the flash was approximated to be in thermal equilibrium, which assumes that the timescale of accretion is longer than the cooling time of the white dwarfs. However, the gas outflow from a binary companion is in many cases rather rapid (see e.g., Kippenhahn and Mayer-Hofmeiter, 1977; Neo *et al.*, 1977) so that we have to take account of the finiteness of the accretion rate.

Nomoto and Sugimoto (1977) followed the thermal history of accretion by numerical computation. They computed three cases for the accretion rate, i.e., $dM/dt = 4$, 2, and $1\times10^{-8}\,M_\odot\,\mathrm{yr}^{-1}$ for Cases *A*, *B*, and *C*, respectively. These accretion rates cover only a factor of 4, but as seen in Figure 7.1, Case *A*

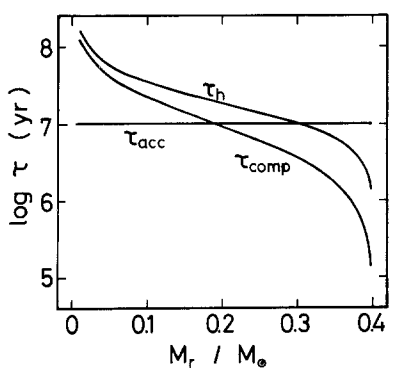

Fig. 7.1. Time scales of heat transport over unit scale height of pressure τ_h, mass accretion $\tau_{acc} \equiv \mathrm{d}t/\mathrm{d}\ln M$, and compression by accretion $\tau_{comp} \equiv \mathrm{d}t/\mathrm{d}\ln\rho$ for the accreting helium white dwarf of mass $0.4M_\odot$. The latter two are inversely proportional to the accretion rate $\mathrm{d}M/\mathrm{d}t$. Values for the case of $\mathrm{d}M/\mathrm{d}t = 4\times10^{-8}\,M_\odot\,\mathrm{yr}^{-1}$ are shown. (Taken from Nomoto and Sugimoto (1977).)

corresponds to the accretion faster than the Kelvin timescale near the bottom of the accreted layer, while Cases *B* and *C* are slow and thermally relaxed accretion. The initial model was a helium white dwarf of $0.4M_\odot$ with the central temperature of $T_c = 8\times10^6$ K.

In Case *A* a part of entropy of the accreted matter is radiated away but its appreciable fraction is retained and pushed into deep interior of the star. Therefore, the temperature is maximum in the accreted matter. When the mass of the white

dwarf reaches $0.66M_\odot$, the temperature becomes high enough to ignite helium flash in the shell of mass fraction $M_r/M_H = 0.86$. It begins as a helium flash in an electron degenerate layer, but it shifts into a shell flash in non-degenerate layer. The flashing shell moves outward in mass to $M_r/M_H = 0.90$. The maximum temperature and energy generation rate during the flash were found to be $T^{(max)} = 3.2 \times 10^8$ K and $L_{He}^{(max)} = 5.3 \times 10^{10}\, L_\odot$, which are too low to induce any dynamical effects.

In Cases *B* and *C*, on the other hand, the core is thermally well relaxed and temperature is maximum at the center of the core. The helium burning is ignited at the center when the core mass reaches 0.78 and $0.99M_\odot$ respectively. Computation was continued from the accretion phase through the flash phase up to a dynamical stage.

The sequence of events is analogous to the case of the carbon deflagration supernova except for the followings. The deflagration temperature is $T_{def} = 2.5 \times 10^8$ K. When the temperature exceeds 1.5×10^9 K, the triple-alpha reactions are almost saturated and energy is generated mainly by successive α-captures on ^{12}C, i.e., $^{12}C(\alpha, \gamma)\,^{16}O(\alpha, \gamma)\,^{20}Ne(\alpha, \gamma)\,^{24}Mg$ etc. For such situation, behavior of a wave of overpressure was computed. It was shown to grow into a detonation wave overcoming the spherical damping (Nomoto and Sugimoto, 1977).

The difference from the carbon deflagration is ascribed to the difference in the energetics. In the case of the helium burning, the central density is as low as $\log \rho = 6.85$ and the internal energy is as low as $u_{gas} = 0.13$ MeV nucl^{-1}. Since the nuclear energy generation is 0.60 MeV nucl^{-1} for helium burning and 1.5 MeV nucl^{-1} for the establishment of NSE, the overpressure due to the deflagration amounts to as much as 2.7 times the initial pressure.

In the model of Case *B*, the gravitational binding energy is $E_B = 7.5 \times 10^{49}$ erg. On the other hand, the nuclear energy of the core is $E_n = 2.3 \times 10^{51}$ erg when the helium burning proceeds to the NSE state. According to Mazurek (1973) and Nomoto and Sugimoto (1977), the star is totally disrupted and more than $0.7M_\odot$ of NSE composition is returned back to the interstellar space with the kinitic energy of about 10^{51} erg.

In the model of Case *A*, the flash was not strong enough to produce NSE elements. However, such flash in an outer shell will take place recurrently if the accretion is continuing and the core mass is kept growing. In the central region of such white dwarf appreciable amount of helium ($0.5M_\odot$ for the case *A*) is left unburnt.

However, this helium will be ignited eventually, when the mass of the white dwarf becomes close to the mass at which the white dwarf of Case *B* is ignited. Because the energetics for Case *B* suggest the NSE and the total disruption with a large margin, the situation will not be altered in the Case *A* either, even if appreciable amount of helium has been converted into carbon and oxygen by preceding shell flashes.

One may ask if it is possible to disrupt the star without producing NSE elements. Consider the case in which the accretion commences as soon as the white dwarf is formed, i.e., before the white dwarf has been cooled appreciably. Then the thermal condition is close to that of the helium core embedded deep in a red giant star, and

the helium flash is ignited at a relatively small core mass, i.e., at a relatively low density.

According to Sugimoto (1964) the heat becomes blocked and the flash grows into dynamical strength, when the core mass is greater than $0.7M_\odot$. When we take account of the relativistic effect in the equation of state of partially degenerate electrons, this limiting core mass should be revised to $0.65M_\odot$ (Nomoto and Sugimoto, 1977), which corresponds to the central density of $\rho_c^{\rm ign} = 4\times10^6$ g cm^{-3} at the stage of ignition.

On the other hand, we estimate the lower bound of the density above which the detonated material becomes NSE composition. According to Equation (6.5), the final temperature of $T_f \gtrsim 3\times10^9$ K requires the density $\rho_c^{\rm def}$ at the deflagration stage higher than $\rho_{\rm NSE} = 2\times10^6$ g cm^{-3}. Once the helium flash becomes dynamical, therefore, the helium white dwarf will be incinerated into the NSE composition in most cases, though $\rho_c^{\rm def}$ is somewhat lower than $\rho_c^{\rm ign}$.

7.3. Strong Helium Shell Flash in Accreting Carbon–Oxygen White Dwarfs

Let us consider the case where the accreting white dwarf is composed of carbon plus oxygen. The accreted gas is processed by the hydrogen shell-burning and then forms a helium shell surrounding the carbon–oxygen core. When a certain mass of helium has been accumulated, helium shell-flash is ignited. It proceeds in the same way as the thermal pulses which take place in the phase of growing carbon–oxygen core of the intermediate mass stars and which were discussed in Section 5.3.

However, in the case of accreting white dwarf, there are wide varieties in the accretion rates and in the initial conditions. When the white dwarf has been cooled down to a lower temperature before the onset of mass accretion, or when the accretion is slower, the entropy of the accreted matter is well transported away and more mass of helium can be accumulated before the ignition of the helium shell-flash. According to the generalized theory of shell flash (Sugimoto and Fujimoto, 1978), the maximum energy generation by the helium shell-burning is given by

$$\log L_{\rm He}^{(\max)}/L_\odot = 8.1 + 4.9(\log P_{\rm He} - 20) - 0.6(\log P_{\rm He} - 20)^2 + \\ + 10.5\log(M_{WD}/M_\odot) + 5.0\log(1 - M_{WD}/1.6M_\odot)\,. \tag{7.1}$$

Here M_{WD} is the mass of the white dwarf and $P_{\rm He}$ is the pressure of the helium burning-shell at the onset stage of the flash. The latter is expressed by means of Equations (2.20) and an interpolation formula for the radius of the core as

$$\frac{P_{\rm He}}{10^{20}\ \text{dyn cm}^{-2}} = 38\left(\frac{\Delta M_{\rm He}}{M_\odot}\right)\left(\frac{M_{WD}}{M_\odot}\right)\left(1 - \frac{M_{WD}}{1.6M_\odot}\right)^{-4}, \tag{7.2}$$

where $\Delta M_{\rm He}$ is the mass of the helium zone contained above the burning shell. These

equations give the maximum energy generation rate as high as $L_{\rm He}^{(\max)} = 7 \times 10^{13}\, L_\odot$ for $\Delta M_{\rm He} = 0.043 M_\odot$ and $M_{WD} = 1.077 M_\odot$, for example.

Numerical computation by Fujimoto and Sugimoto (1979) gives a following model. A carbon–oxygen white dwarf of $1.077 M_\odot$ was cooled for 9.6×10^7 years after its formation. Then, the helium gas began to accrete at the rate of $3.16 \times 10^{-8}\, M_\odot\, {\rm yr}^{-1}$. After 2.7×10^6 years the helium shell-flash is ignited when the helium zone of $0.097 M_\odot$ is formed. The maximum energy generation rate is found to be as high as $L_{\rm He}^{(\max)} = 8.4 \times 10^{15}\, L_\odot$. At this stage the helium-burning shell has been shifted to $\Delta M_{\rm He} = 0.043 M_\odot$.

At the stage of the maximum energy generation, the ratio of the timescales τ_{ff}/τ_n, which were defined by Equations (6.1) and (6.2), amounts to as much as 5. Therefore the helium burning would have been well detonative, if the inertia term had been included into their computation. The density at this stage is $5 \times 10^5\, {\rm g\, cm}^{-3}$ which is lower than the critical density $\rho_{\rm NSE} = 2 \times 10^6\, {\rm g\, cm}^{-3}$ for the incineration to NSE composition.

They computed also a case of slower accretion with the rate of $3.16 \times 10^{-9}\, M_\odot\, {\rm yr}^{-1}$. When the helium zone of $\Delta M_{\rm He} = 0.29 M_\odot$ is formed, the helium burning is ignited at the density of $2 \times 10^7\, {\rm g\, cm}^{-3}$. Though they did not follow the flash to its peak, the helium zone of this model would have been incinerated well into NSE composition. It is interesting to note that the nuclear energy available in such detonation is 3×10^{51} erg for $\Delta M_{\rm He} = 0.1 M_\odot$ which is well of the order of the energy of type I supernova. In this sense such models will deserve well of further studies.

8. Evolution Toward Electron-Degenerate Oxygen Core

In this section we discuss the mass range of 8–$12 M_\odot$, for which the carbon burning proceeds under non-degenerate conditions but electrons become degenerate in the oxygen core. Its supernova explosion will be triggered by electron captures as will be discussed in the next section.

8.1. Evolution near the upper mass limit of $12 M_\odot$

Numerical studies on evolution are scarce for this mass range, because its evolution is rather complicated after the carbon-burning phase.

Sugimoto (1970b), and Nomoto *et al.* (1979a) studied evolution of a helium core of $3 M_\odot$ up to the presupernova stage. Its chemical evolution, evolutionary track in the central temperature-density diagram and a U–V curve of a presupernova stage are shown in Figures 8.1, 5.1, and 8.2, respectively. Here the *core* implies that its edge was fitted to the boundary conditions (2.23) and (2.24) at the bottom of the hydrogen-rich envelope. This model approximates the core embedded in the star of $M_{ms} = 12 M_\odot$ according to Equation (4.1). When the carbon is exhausted in the non-degenerate core, a oxygen core of mass $0.7 M_\odot$ is formed. Then the carbon burning shifts to the shell burning, which grows to the values as strong as $L_{\rm C+C} = 1 \times 10^6$–$2 \times 10^7\, L_\odot$ at the stages with the central temperatures of $\log T_c = 8.94$–9.12,

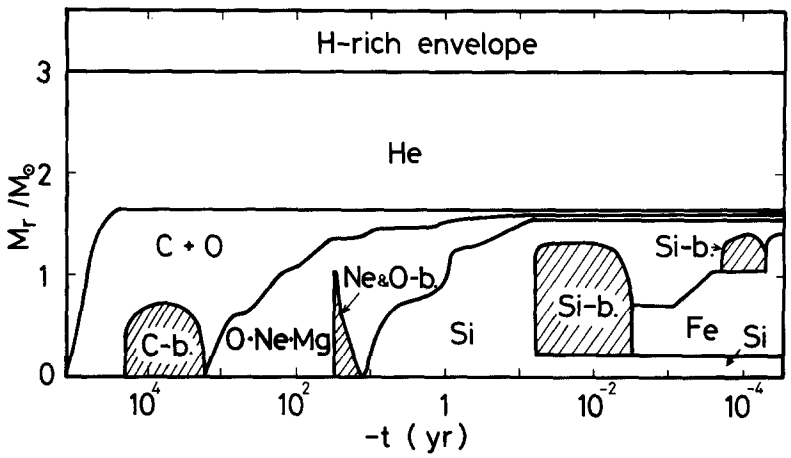

Fig. 8.1. Chemical evolution of the star of about $12M_\odot$ (Sugimoto, 1970b; Nomoto *et al.*, 1979a). A part of the hydrogen-rich envelope is omitted from figure. Note that the evolutionary time is in logarithmic scale.

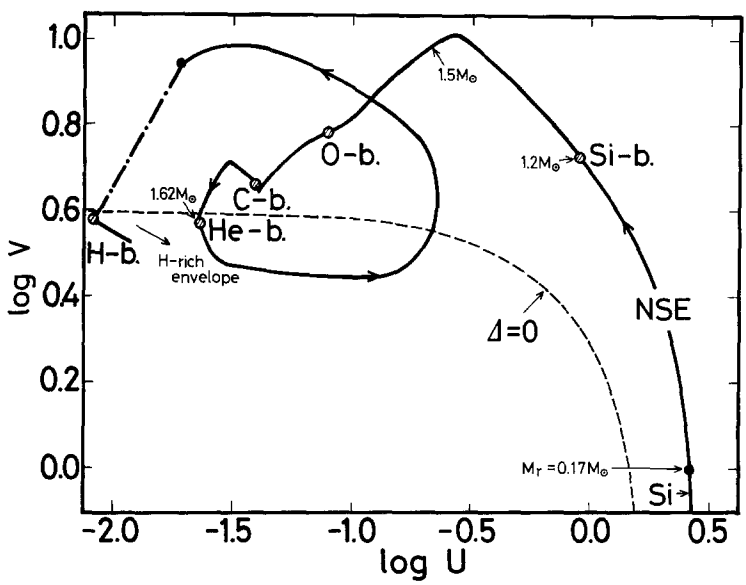

Fig. 8.2. U–V curve of the star of about $12M_\odot$. Hydrogen-rich envelope is omitted from figure. It crosses the locus of $\Delta = 0$ at the helium-burning shell and makes a loop. Therefore, the region interior to it is the core as defined in Section 2.2. Other notations are the same as in Figure 2.2.

respectively. The neutrino losses are $L_\nu = 2\times10^6$–$6\times10^7\ L_\odot$ for the corresponding stages, i.e., larger than L_{C+C}. Therefore the energy for neutrino loss is supplied mainly by the gravitational contraction.

Because of the carbon shell-burning, the oxygen core grows up to $1.38M_\odot$ and the electrons become somewhat degenerate in the central region. The degree of degeneracy is conveniently expressed by the value of ψ_e, which is the chemical

protential $\tilde{\mu}_e$ of an electron without the rest mass in units of kT, i.e.,

$$\psi_e = \tilde{\mu}_e / kT. \tag{8.1}$$

The maximum value of ψ_e attained during the growing oxygen core was $\psi_{e,c} = 7.3$ at the stage of $\log \rho_c = 7.486$ and $\log T_c = 9.122$. This degeneracy is moderate but is not strong enough to consider the core as an electron degenerate core. Such results can be understood if we look into the U–V curve of stellar structure in Figure 8.2. It crosses the locus of $\Delta = 0$ at the helium-burning shell and makes a loop there. Consequently, core edge as defined in Section 2.2 lies at the helium-burning shell and the core mass is $1.62 M_\odot$. This is somewhat larger than the Chandrasekhar limit so that the degree of electron degeneracy does not become too strong.

In this model the core was composed of neon, oxygen, and magnesium. At the stage of $\log \rho_c = 7.3$, neon began to burn as a weak flash. The rate of neon burning reached $4 \times 10^{10}\, L_\odot$ at its maximum. After this weak flash neon and oxygen burnings took place under non-degenerate conditions.

In view of these results the helium core of $3M_\odot$, i.e., the main-sequence mass of $M_{ms} = 12 M_\odot$ is a limiting mass below which electrons become degenerate in the oxygen core.

8.2. Evolution near the lower mass limit of $8M_\odot$

According to the discussions in Section 4.2, the critical mass, above which the carbon–oxygen core is non-degenerate, lies within $8M_\odot \pm 1M_\odot$ depending on chemical compositions. Barkat *et al.* (1974) paid and wanted to draw attentions to the lack of studies in the mass range of $8M_\odot$–$12M_\odot$, and they computed evolution of the star of $8M_\odot$. However, their description in their Letter to the Editors (Barkat *et al.*, 1974) was only sketchy, but we can draw Figure 8.3 from their letter.

In their model the carbon burning took place in the core under non-electron-degenerate condition. Therefore the surface convective zone did not penetrate into the core as discussed in Section 4.2. After the carbon-burning phase, the structure of the core is rather complicated, because the carbon shell-burning (stage No. 2 in Figure 8.3), off-center ignition of oxygen burning (No. 3) etc. complicate the chemical evolution of the core. Anyway they followed evolution until the stage No. 4 at which the central temperature and density reached $T_c = 4.5 \times 10^8$ K and $\rho_c = 8.5 \times 10^9$ g cm^{-3}.

Though the chemical evolution depicted in Figure 8.3 seems very complicated, it can be interpreted easily as far as the qualitative nature is concerned. The convection in the carbon shell-burning (No. 2) is due to the high rate of energy generation which is necessary to supply the energy lost by neutrino emission. When the carbon-shell burning decays, the effective mass of the oxygen core grows almost suddenly. Therefore oxygen is ignited (No. 3) in an outer shell, as in the case A of rapidly accreting helium white dwarf which was discussed in Section 7.2. When carbon is almost exhausted, the growth of the core mass becomes to be controlled by the rate of the helium shell-burning. Evolution becomes relatively slow because the neutrino

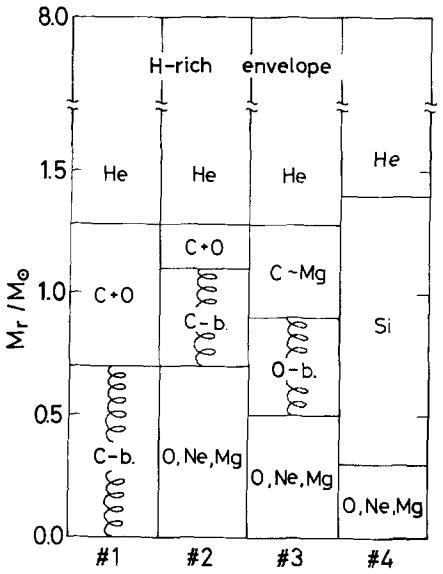

Fig. 8.3. Chemical evolution of $8M_\odot$ star read out of a paper by Barkat *et al.* (1974). Four different stages are shown. Regions with spiral coils are in convective equilibrium.

loss is negligible from the helium-burning shell. However, it is about $E_H X_e / E_{He} \simeq 7$ times more rapid than the growth of the carbon–oxygen core in a red giant star.

Therefore things left are just to construct numerical models. The importance of this mass range was stressed by Barkat *et al.* (1974) five years ago. However, such numerical works have not been accomplished. The reason seems to be related with the fact that we have not done much work concerning supernova explosion triggered by electron capture. However, it is now available as will be discussed in the next section.

8.3. Oxygen flash

Before entering into detailed processes of electron capture supernova it is instructive to discuss the oxygen flash from a standpoint of the generalized theory as discussed in Section 3.3. We see in Figure 3.2 that a line with constant central temperature has a minimum if it is lower than $\log T_c = 9.3$. The maximum temperature, that can be assigned to the core of the Chandrasekhar's limiting mass, is close to this value as also seen in Figure 6.2. Because this value is higher than the oxygen burning temperature, there exists the oxygen flash. However, the maximum temperature attained is only $\log T_c = 9.3$. As can be seen from Figures 3.2 and 6.2 the corresponding central density is $\log \rho_c = 8.2$. The nuclear energy generation rate is as low as $\varepsilon_{O+O} = 5 \times 10^{14}$ erg g^{-1} s^{-1}, or $L_{O+O} = 9 \times 10^{12} L_\odot$, and the condition for the heat blocking is not satisfied with a large margin as seen also in Figure 6.2.

This result implies that the oxygen flash is a relatively weak as compared with the carbon deflagration. (Note that Figures 3.1 and 3.2 are almost determined only by

the mean molecular weight of electrons but that the temperatures necessary for deflagration are different very much among different kinds of nuclear fuels.) For a strong deflagration of oxygen, some mechanisms are necessary which make the central temperature higher than the value referred above as will be discussed in the next section.

9. Supernova Explosion Triggered by Electron Captures

Until recent days this type of supernova was paid only a little attention, probably because this lies between the two major types of supernovae, the deflagration of carbon cores and the collapse of iron cores. Because of such situation there are relatively small number of works and yet unclear understanding of physical concepts. In this section we criticize them and give a clear picture together with a recent modeling by Miyaji *et al.* (1979).

9.1. Effects of electron capture on stellar structure

Stellar evolution in the central temperature – the central density diagram are usually drawn in a plane like Figure 5.1. In its shaded region, the value of the adiabatic exponent γ, i.e., the ratio of the specific heats, is smaller than $\frac{4}{3}$, and the star is dynamically unstable. Such region is usually said to consist of three parts corresponding to three types of phase changes, i.e., (i) Photodissociation of nuclei or NSE state, (ii) electron pairs in equilibrium with the radiation field, and (iii) electron capture-beta decay equilibrium.

In the former two cases the reaction time is much shorter than the dynamical time scale of stellar collapse/explosion, and the mass element can be regarded as a closed system as far as the local thermodynamic equilibrium (LTE) is concerned. In other words, the thermodynamic change can always be regarded to be quasi-static as compared with the recovery of LTE. It guarantees the validity of the concept of the adiabatic exponent γ.

On the contrary, γ is not a good concept in the case of the electron capture. In the first place, neutrinos escape from the system, i.e., the local mass element is an open system. Secondly, the timescales of electron capture and beta decay are, at the fastest, comparable with and/or longer than the relevant timescale of quasi-static or dynamical evolution of the star. Therefore, the electron captures do not become even in detailed balance with beta decay, as illustrated by Sugimoto (1970c) and as will be discussed later in this section. Therefore, the concept of γ, which premised the establishment of LTE, breaks down. One might think that neutrino energy tends to vanish when temperature is zero and the Fermi energy of electron is just equal to the threshold energy of the electron capture. In such case, however, the reaction time is infinitely long. When we consider the adiabatic exponent for a change with the dynamical time scale, we should compute the value of γ with the beta processes frozen.

Therefore, it is better to treat the electron captures in the same way as the nuclear reactions, i.e., as a slow process through which chemical composition changes with releasing or absorbing subatomic energy. Here we note that the nuclear reactions in the stars are also understood to be the process approaching very slowly to NSE.

In many works electron capture is described in terms of the rate of electron capture λ_{ec} and the neutrino loss rate $\langle E_\nu \rangle \lambda_{ec}$ (e.g., Hansen, 1968), where $\langle E_\nu \rangle$ is the mean energy of an emitted neutrino. However, these two rates do not contain enough information. As shown in Figure 9.1 we have to add information of the energy

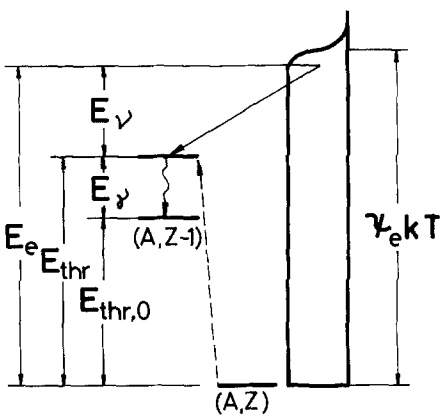

Fig. 9.1. Energies relevant to electron capture. An electron with E_e is captured on the parent nucleus of (A, Z) to an excited state of the daughter nucleus $(A, Z-1)$. This is the case where the transition between ground states is highly forbidden because of their spin-parities. A neutrino with E_ν and then a gamma ray with E_γ are emitted. The distribution function of electrons, whose chemical potential is $\psi_e kT$, suffers from a distortion.

difference between the ground states of the daughter and the parent nuclei $E_{\mathrm{thr},0}$ and the energy of the associated gamma ray emission E_γ if any. If an electron is captured on an excited state of the daughter nucleus, they will be, for simplicity, treated separately as if they were different kinds of nuclei in the following formulation.

If we denote the mean energy of the captured electrons by $\langle E_e \rangle$, these quantities are related by

$$\langle E_e \rangle = E_{\mathrm{thr},0} + \langle E_\nu \rangle + E_\gamma \,. \tag{9.1}$$

From the standpoint of stellar structure, only the sum of $E_{\mathrm{thr},0} + \langle E_\nu \rangle$ is important, and it is not relevant how much it is shared between them. In other words, we need to know only $\langle E_e \rangle$ and E_γ, i.e., the energy of electron which is lost from the system and the energy of the gamma ray which is returned to the system. Such presentation is urged in further computations of electron capture rates.

Though the energy in a mass element dies away into a neutrino and the subatomic energy, the change in the temperature is a quite different matter, when the mass

element lies within the star. In order to separate the effect of the energy loss from the gravothermal effect, it is better to discuss it in terms of the specific entropy rather than the temperature. If the system is adiabatic except for neutrino escape the laws of thermodynamics give the change in the entropy of matter as

$$kT\frac{\mathrm{d}(N_e\sigma_e)}{\mathrm{d}t}+T\frac{\mathrm{d}s_i}{\mathrm{d}t}=[E_{\mathrm{thr},0}+\langle E_\nu\rangle-\psi_e kT]\frac{\mathrm{d}N_e}{\mathrm{d}t}$$

$$=[\langle E_e\rangle-\psi_e kT-E_\gamma]\frac{\mathrm{d}N_e}{\mathrm{d}t}, \tag{9.2}$$

where N_e is the number of electrons in unit mass of matter, σ_e is the entropy of electrons per one electron in units of k, and s_i the specific entropy of ions. This equation expresses the entropy production due to the electron capture as an irreversible process. Since $\mathrm{d}N_e/\mathrm{d}t$ is negative, entropy is produced when the gamma ray is emitted (Rudzskii and Seidov, 1974; Bisnovatyi–Kogan *et al.*, 1974), and when $\langle E_e\rangle$ is smaller than $\psi_e kT$. The latter is the entropy production due to the distortion in the Fermi-Dirac distribution function and resultant down scattering of electron in momentum space (Bisnovatyi-Kogan and Seidov, 1970; Sugimoto, 1970c; Nakazawa *et al.*, 1970).

The threshold energy for the electron capture is given by

$$E_{\mathrm{thr}}=E_{\mathrm{thr},0}+E_\gamma\,. \tag{9.3}$$

When the density is low and the corresponding chemical potential $\psi_e kT$ is lower than E_{thr} the energy of the captured electron $\langle E_e\rangle$ is higher than $\psi_e kT$ and the term $\langle E_e\rangle-\psi_e kT$ plays a role to reduce the entropy. In such case, however, the electron captures proceed very slowly. In practically interesting cases, $\psi_e kT$ is much higher than E_{thr} and the electron captures proceed rapidly. In the limit of $\psi_e kT \gg E_{\mathrm{thr}}$, $\langle E_e\rangle$ tends to $(\frac{5}{6})\,\psi_e kT$ so that the entropy production is appreciably large (Nakazawa *et al.*, 1970). When $\psi_e kT$ is moderately large, both of the distortion of the distribution function and the gamma-ray emission are important to increase the entropy of matter.

As another result of the electron capture, the pressure decreases because the number of electrons decreases. It is followed by the gravitational contraction of the star. All of these effects raise the temperature of the matter, though the electron capture itself is an energy absorbing process. For application to the stellar structure equation, we have to add in- and outcome of other energies and it is conveniently formulated as

$$\frac{\mathrm{d}L_r}{\mathrm{d}M_r}=\varepsilon_n-\varepsilon_\nu^{(D)}-T\frac{\mathrm{d}s_i}{\mathrm{d}t}-kT\frac{\mathrm{d}(N_e\sigma_e)}{\mathrm{d}t}+\varepsilon_{ec}\,, \tag{9.4}$$

where $\varepsilon_\nu^{(D)}$ is the neutrino loss rate excluding the nuetrinos from the electron

captures and where the energy rate by the electron capture is defined by

$$\varepsilon_{ec} = [\psi_e kT - \langle E_e \rangle + E_\gamma] \left(-\frac{dN_e}{dt} \right)$$

$$= [\psi_e kT - E_{\text{thr},0} - \langle E_\nu \rangle] \left(-\frac{dN_e}{dt} \right). \tag{9.5}$$

According to the discussions above, ε_{ec} can be both negative and positive. It is negative, if any, only in the early stages of a phase with electron captures when the Fermi energy of electron is low and the electron capture is very slow. In most of its phase ε_{ec} is positive. The temperature rise due to the electron captures and associated contraction of the core were computed by Sugimoto (1970c) but he treated only the cores somewhat more massive than the Chandrasekhar's limiting mass.

9.2. Decrease of the Chandrasekhar's Limiting Mass due to Electron Capture

The Chandrasekhar's limiting mass is expressed as

$$M_{\text{Ch}} = 1.46(Y_e/0.5)^2 M_\odot, \tag{9.6}$$

where Y_e is the mole number of electrons in one gram of matter,

$$Y_e = N_e/N_A, \tag{9.7}$$

with N_A being the Avogadro number. When the electron captures proceed, Y_e decreases and correspondingly Chandrasekhar's limiting mass decreases. It may be reduced even below the core mass if the core mass is smaller than yet close to the initial value of M_{Ch}. Then, as seen in Figure 3.1, there are no solutions with vanishing temperature any more, and the core will begin to collapse.

Finzi and Wolf (1967) proposed such evolution as a cause of type I supernova. The presupernova star is a white dwarf which contains ^{24}Mg as much as 10% by mass. It captures electron when the density is higher than 3.2×10^9 g cm^{-3}. They showed that the white dwarfs of mass between 1.396 and $1.400 M_\odot$ will begin such collapse in 10^{10} and 10^6 years, respectively. However, they did not make detailed computation for the evolutionary processes associated with the electron captures.

9.3. Model of Electron Capture Supernova

Bisnovatyi-Kogan and Seidov (1970), Nakazawa (1973), Rudzskii and Seidov (1974), and Basko and Imshennik (1975) discussed the thermal balance as expressed by Equation (9.4) in the iron core or in the white dwarf for the case of $\psi_e kT \gg E_\gamma$ and $E_{\text{thr},0}$, but they did not compute the stellar structure. Sugimoto (1970c) computed the stellar structure together with Equation (9.4), but he neglected E_γ and, moreover, his treatment of electron capture was too rough. So we need a much

refined model. Recently, such computation has been done by Miyaji *et al.* (1979). We summarize some of their important results.

For the initial model they constructed a white dwarf of mass $M_1 = 1.2M_\odot$ which consists of ^{16}O, ^{20}Ne, and ^{24}Mg. Their concentrations by weight were assumed to be $X(^{16}O) = 0.35$, $X(^{20}Ne) = 0.55$ and $X(^{24}Mg) = 0.10$, which were the composition left after the carbon burning in the helium star of $4M_\odot$ (Arnett, 1973b). This white dwarf will approximate the O–Ne–Mg core embedded in the star of mass $M_{ms} = 8$–$12M_\odot$. Therefore, the mass of the helium core should be in the range of 2–$3M_\odot$. The growth of the O–Ne–Mg core by helium shell-burning was assimilated by accretion of the gas with the same composition at the rate of

$$\frac{dM_1}{dt} = 4 \times 10^{-6} M_1 \text{ yr}^{-1}. \tag{9.8}$$

The evolution of the core proceeds through the following phases. In Figure 9.2 the energy generations/losses and the timescales involved are shown against the

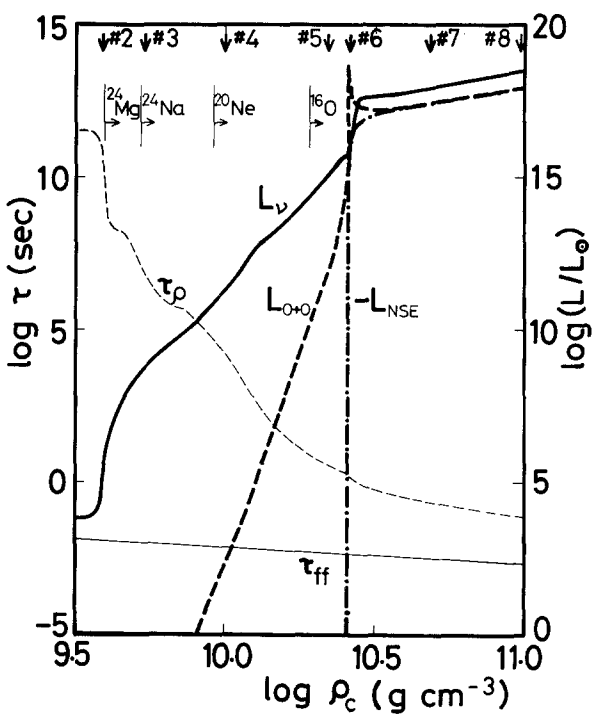

Fig. 9.2. Evolution of oxygen core leading to a supernova collapse which is triggered by electron capture. The central density increases as the evolution proceeds. The timescales of contraction $\tau_\rho \equiv dt/d \ln \rho_c$ and of free fall τ_{ff} are shown. The energy rates are also shown for the loss by neutrinos L_ν, the energy generation by oxygen burning L_{O+O}, and the energy absorption by dissociation of nuclei into lighter ones $-L_{NSE}$ in the NSE core. Threshold densities against electron capture for different nuclei are also shown. (Taken from Miyaji *et al.* (1979).)

increasing central density. Evolutionary changes in the central density and temperature are shown in Figure 5.1.

(1) *Growth of the core*: As the core mass grows the central density increases with the timescale as long as 10^4 yr.

(2) *Electron capture on* ^{24}Mg: It commences when ρ_c reached 4×10^9 g cm^{-3} (No. 2 in Figure 9.2). The resultant ^{24}Na captures also an electron after the stage of $\rho_c = 5\times10^9$ g cm^{-3} (No. 3). The central part of the core is heated mainly by the associated gamma-rays. Temperature rises and a convective core appears as shown in Figure 9.3. It extends eventually to $M_r = 0.6M_\odot$ and prevents ^{24}Mg from being

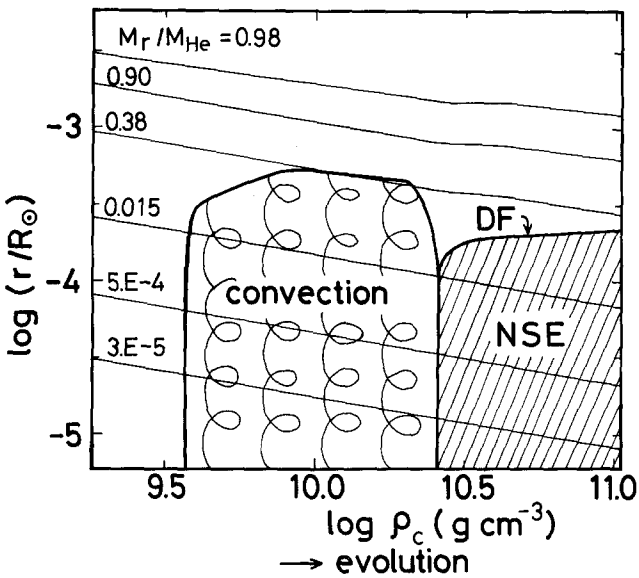

Fig. 9.3. Quasi-static through quasi-dynamic contraction of the oxygen core which is shown in Figure 9.2. Thin lines are Lagrangian shells to which attached are their mass fractions. Their contractions are shown by plotting their radial distance r against the increasing central density. Development of the convective core and propagation of the deflagration front (DF) are also shown. Behind the deflagration front a core is left with NSE composition. (Taken from Nomoto *et al.* (1979b).)

exhausted in the central region. The mole number of electrons Y_e decreases in the entire convective core, i.e., over a relatively large portion of the core. It results in appreciable decrease in $M_{\rm Ch}$ as discussed in the preceding subsection, and the contraction of the core is accelerated.

(3) *Electron capture on* ^{20}Ne: Beyond the stage of $\rho_c = 9\times10^9$ g cm^{-3} (No. 4), ^{20}Ne captures electron and the resultant ^{20}F captures another electron immediately. The Chandrasekhar limit at this stage seems to be almost equal to the core mass. The contraction becomes faster and faster as seen in Figure 9.2.

(4) *Ignition of oxygen burning*: When ρ_c reaches 2.5×10^{10} g cm^{-3} (No. 6), the oxygen burning is ignited. It grows into a deflagration and the fuel is processed into

NSE composition. However, the nuclear energy release is 0.4 MeV nucl^{-1} which is only 4% of the internal energy $u = 10$ MeV nucl^{-1}.

(5) *Competition between the oxygen deflagration and the electron captures*: The deflagration is so weak that its front does not propagate by itself but that it is almost standing in Eulerian coordinate (Figure 9.3). In other words, it does not propagate by the heat transport, but each shell is ignited consecutively as it is compressed to the density of about 2.5×10^9 g cm^{-3} by the quasi-dynamic collapse. It does not grow into a detonation either. Aftet the deflagration the matter is processed into NSE composition as shown in Figure 9.3. Though energy is generated near the deflagration front at the rate of L_{O+O} as seen in Figure 9.2, almost the same energy is absorbed in the NSE core at the rate of $-L_{NSE}$, because nuclei are dissolved into lighter ones. Between the stages with $\rho_c = 2.5 \times 10^{10}$ and 1×10^{11} g cm^{-3}, the gravitational binding energy of the core increased by 3×10^{50} erg. This amount of energy was carried away with neutrinos which were generated by electron captures in the NSE core.

Though their computation was stopped at the stage with $\rho_c = 1 \times 10^{11}$ g cm^{-3}, the quasi-dynamic collapse will continue further because of the following reasons. First of all the total energy is decreasing, i.e., the gravitational binding energy is increasing. Secondly, the Chandrasekhar limit seems to have already been reduced below the core mass. Thirdly, the central density has already exceeded the critical density $\rho_{cr}^{GR} = 2.3 \times 10^{10}$ g cm^{-3} beyond which the star enters into the regime of general relativistic instability (Chandrasekhar and Tooper, 1964). We have seen that the oxygen burning does not win over the electron capture. The main reason has been in the energetics.

9.4. Production of Neutron Stars

Since Miyaji *et al.* (1979) stopped their computation at the stage with $\rho_c = 1 \times 10^{11}$ g cm^{-3}, it is not certain whether the quasi-dynamic collapse results in the formation of a neutron star or a black hole. However, further evolution of the core will be similar to the collapse of $1.4 M_\odot$ iron core which was computed by Arnett (1977b). It will make a bounce when the central density reaches around the nuclear density (see Section 11.4).

However, only the bounce does not always guarantee the formation of a neutron star, because the overlying layers continue to fall onto the bounced core as will be discussed in Section 11.6. Nevertheless in our O–Ne–Mg core, it does not seem necessary to worry about it. The mass of the core is smaller than the limiting mass of the neutron star, the mass contained in the carbon–oxygen zone is negligible, the mass of the helium zone is likely to be small because of the penetration of a convective envelope in the preceding stages, and the gravitational binding energy of the hydrogen-rich envelope is negligible. In order to reach a definite conclusion, however, further computations are necessary not only for the collapsing stages but also for the presupernova evolution.

9.5. Formation of O–Ne–Mg white dwarf and quiet supernova

When the star of mass in the range of $8–12M_\odot$ is a primary star in a close binary system, it will evolve as follows (Nomoto *et al.*, 1979b). After the first mass exchange, it leaves a helium star of mass $2–3M_\odot$. Since the carbon burning takes place in the non-degenerate condition, the helium envelope does not expand to a red-giant size. In the resultant O–Ne–Mg core, electrons become degenerate. During the stages when the core mass grows by the carbon shell-burning, the timescale of evolution is so short that the helium envelope will not expand appreciably. After the carbon zone becomes thin in mass, the growth of the core is controlled by the helium shell-burning. Now the evolution is relatively slow so that its evolution is similar to that of $2M_\odot$ helium star having the carbon–oxygen core which was studied by Paczyński (1971). The helium zone will expand to a red giant size and it overflows the Roche lobe. Then the star will cool down to leave an O–Ne–Mg white dwarf.

When the companion star evolves to fill its Roche lobe, the mass begins to accrete onto the O–Ne–Mg white dwarf. Evolution of this accreting white dwarf is essentially the same as those discussed in this section. Therefore, the white dwarf collapses to form a neutron star. This event will be associated, if any, only with a very small amount of mass ejection. In this sense this is a quiet supernova to produce the neutron star. There will be only a slight sling shot and the binary orbit will remain almost circular, even if the companion star is less massive. Such quiet supernova seems to be required in interpreting the origin of some X-ray binaries (cf. van den Heuvel, 1977).

10. Evolution of Massive Stars Toward Presupernova Stage

In this section we will discuss the evolutions toward the formation of iron core for the stars of masses in the range of $12–100M_\odot$ and the formation of oxygen core for the stars more massive than $100M_\odot$. From the standpoint of presupernova models, main concerns are the values of masses of the iron core or the oxygen core which are formed during the course of evolution.

10.1. Summary of existing computations

Recently some numbers of computations are available which extend well up to stages of presupernovae as summarized in Table 10.1. In earlier computations, the hydrogen-rich envelope and even some other layers were neglected. This was a single star approximation which was discussed in Section 2. Such approximations are specified in the second column of Table 10.1 by indicating the composition of their outermost layer (envelope). Here, *star* indicates that the specified layer was fitted to the outer boundary conditions of a single star, while *core* does that it was fitted to the boundary conditions (2.23) and (2.24) at the core edge. The mass of the carbon–oxygen star, for example, is listed in the column of $M_{\rm He}$, since the surface of the carbon–oxygen star would correspond to the bottom of the helium zone if it were taken into computation.

TABLE 10.1

Summary of presupernova structure*

Approximation	$M_{ms}/M_\odot$	$M_H/M_\odot$	$M_{He}/M_\odot$	$M_C/M_\odot$	$M_O/M_\odot$	$M_{Si}/M_\odot$
R . . . O star . . .	(25–30)			2	1.5	1.4
	(50)			4	1.7	1.4
	(>70)			10	2.8	2.2
I . . . C+O star . . .	(15.6)		2.6	2.0	1.8	1.4
	(24)		5	2.1	1.6	1.0
	(35)		10	2.5	2.3	1.8
	(>70)		30	9.6	3.7	3.0
SN . . . He core . . .	(12)	3	1.6	1.6	1.5	1.2
	(30)	10	6.9	1.9	1.7	1.4
A . . . He star . . .	(14)	4	1.8	–	1.5	1.4
	(19)	6	3.4	1.8	1.7	1.4
	(24)	8	4.9	1.8	1.6	1.3
	(33)	12	8.5	2.4	2.0	1.6
	(40)	16	12	2.7	2.4	–
	(70)	32	24	7.6	3.4	2.2
W . . . H star . . .	15	4.5	2.6	1.9	1.6	1.4
	25	9.5	7.0	2.7	1.9	1.6

* *Note*:
R: Rakavy *et al.* (1967).
I: Ikeuchi *et al.* (1971, 1972).
SN: Sugimoto (1970b), Nomoto *et al.* (1979a).
A: Arnett (1973b, 1977a, 1978a).
W: Weaver *et al.* (1978).

The corresponding masses of the main-sequence stars are also listed and enclosed with parenthesis. In modern computations the initial model is chosen to be a main-sequence star (Weaver *et al.*, 1978) which is specified as H-star in Table 10.1.

Examples of chemical evolutions of the stars with $M_{ms} = 12$, 30, and $60 M_\odot$ (Sugimoto, 1970b; Nomoto *et al.*, 1979a; Nomoto, 1974) are shown in Figures 8.1, 4.4, and 4,5, respectively. For many models they are complicated because of many shell burnings in convective equilibrium. Therefore we listed in Table 10.1 only the masses of the oxygen core M_C, the silicon core M_O and the iron core M_{Si}, which are taken from the last stage of each computation. We notice that the iron-core masses depend but slightly on M_{ms}, and they are close to $1.4 M_\odot$. This value of mass is close to the Chandrasekhar limit for a star with $Y_e = 0.5$ ($\mu_e = 2$), but exceeds this limit for pure ^{56}Fe ($Y_e = 0.464$) which is $1.26 M_\odot$.

10.2. Effect of neutrino loss and mass of the iron core

When the temperature of the star exceeds 5×10^8 K, the effect of neutrino loss by direct interaction between electrons and neutrinos becomes essential in determining thermal state of the stellar interior. Neutrinos take away the specific entropy of

matter with them. Then the central region of the star becomes almost isothermal when there is no nuclear energy generation therein. Evolutionary changes in the central temperature and density are drawn in Figure 5.1.

When the core mass is greater than the Chandrasekhar limit, the central temperature increases as the specific entropy is extracted from the central region of the star and the gravitational contraction follows it. On the contrary, the higher temperature results in the higher neutrino loss rate so that the neutrino loss works as a thermostat. Structure and evolution of such a cooled core are described as follows. Because of the weak temperature gradient in the core, the polytropic index between the pressure and the temperature

$$n+1 = \mathrm{d}\ln P/\mathrm{d}\ln T, \tag{10.1}$$

becomes large. It is reflected to a large polytropic index N between the density and the pressure which was defined by Equation (2.3). When gas is the ideal gas, these two polytropic indices are identical. When N becomes large in the core, the non-dimensional mass of the core ϕ_1, which was defined by Equation (3.6), becomes large as seen in Table 2.1. If we take such effect into account, the ordinate of Figure 3.1 should read as $M^* = M(\phi_{1,\mathrm{ad}}/\phi_1)$, where $\phi_{1,\mathrm{ad}}$ is its value corresponding to the adiabatic polytropic index N_{ad} at the center of the polytrope. A thermal state of a star with a larger ϕ_1 corresponds to a star with a smaller mass M^*. Then the central temperature can stay relatively low despite the low entropy. This is the reason why the evolutionary loci in Figure 5.1 become less steep after the carbon-burning phase.

Around and after the silicon-burning phase, however, the situation becomes quite different. Because of high central densities, the chemical potential of electrons becomes well relativistic even when the electron degeneracy is only incipient. Then the polytropic index N, which determines the stellar structure, becomes different very much from the polytropic index n, and the value of N becomes close to 3. For example, the state with $\log \rho = 8.032$ and $\log T = 9.375$ corresponds to $\psi_e = 7$ and $\tilde{\mu}_e = \psi_e kT = 2.8 m_e c^2$, where m_e is the electron rest mass, and N varies only between 2.7 and 3.3 corresponding to the range between the adiabatic and the isothermal ($n = \infty$) temperature gradients.

When the value of N becomes relatively close to N_{ad}, Figure 3.1 becomes applicable again with M^* nearly equal to M. Then the core cannot be sustained against the gravity and it begins to contract. The central temperature tends to rise up to the value which corresponds to the entropy in the central region. However, such a large difference in θ (see Equation (2.7)) between the center and the helium-burning shell $\theta_c/\theta_{\mathrm{He}}$ cannot be accommodated in a single ($\Delta \geqslant 0$) core solution as discussed in Section 2.2. Then the U–V curve should make a loop at the oxygen-burning shell to shift the core edge ($\Delta_1 = 0$) from the helium-burning shell to the oxygen-burning shell as discussed in Section 2.2 and as seen in Figure 2.2.

As an initial value problem, this shift of the core edge is accomplished as follows. The oxygen-burning shell contracts together with the central region of the core. Then the rate of the oxygen shell-burning $\varepsilon_{\mathrm{O+O}}$ becomes larger than the neutrino loss rate

ε_ν. This shell burning is unstable, makes an oxygen shell-flash and adds much entropy. It changes characteristics of the U–V curve to make a loop near the flashing shell. This is the same change as seen in the hydrogen shell-flash model of nova explosion (Nariai *et al.*, 1979). (When M_{ms} is as small as $12M_\odot$, the mass contained between the oxygen-burning shell and the helium-burning shell is small, i.e., $M_{\rm He} \simeq M_{\rm O}$ (Figure 8.1) so that the helium-burning shell remains to be the core edge (Figure 8.2).)

When such shift of the core is accomplished, the silicon core of mass $M_{\rm O}$ can now be regarded to be the core in the sense as defined in Section 2. As discussed above the polytropic index N in the central region is now close to $N_{\rm ad}$ and the relations in Figure 3.1 hold more closely. Therefore, the core mass has to be close to the value corresponding to the silicon-burning temperature $T_{\rm Si} \simeq 3 \times 10^9$ K and the central density higher than 1×10^8 g cm^{-3}, i.e., close to the Chandrasekhar limit. This is the reason why the masses of the silicon cores $M_{\rm O}$ depend weakly on the main-sequence masses M_{ms} as seen in Table 10.1.

Further evolution is determined mainly by these silicon-core masses. Therefore the resultant masses of the iron cores $M_{\rm Si}$ should lie in the range of 1.4–$1.6M_\odot$ for the stars of $M_{ms} = 12$–$100M_\odot$ as seen in Table 10.1. In the iron core the central density is higher and the relativistic effect is stronger than in the silicon core. Therefore, the discussions, which were given for the silicon core, hold better for the iron core, though the core edge should be taken as the oxygen-burning shell even for the iron core.

10.3. Silicon flash

Arnett (1977a) discussed silicon flashes in helium stars of masses in the range of 4–$8M_\odot$. Such silicon flashes were also encountered in other numerical computations (Ikeuchi *et al.*, 1971, 1972; Nomoto *et al.*, 1979a). As discussed in Section 8.3, the oxygen flash is the last flash to take place because the curve for the temperature corresponding to the silicon burning ($T_{\rm Si} \simeq 3 \times 10^9$ K) does not have a minimum in Figure 3.2. However, it is only under the assumption that ϕ_1 is close to $\phi_{1,\rm ad}$.

As discussed in the preceding subsection, ϕ_1 becomes rather close to $\phi_{1,\rm ad}$ in the silicon core, but ϕ_1 is still somewhat larger than $\phi_{1,\rm ad}$. When the silicon burning begins, a convective core appears and the effective polytropic index decreases. Then ϕ_1 approaches to $\phi_{1,\rm ad}$, and the central temperature and density shift from the values corresponding to M^* to one corresponding to somewhat larger mass M in Figure 3.1, which makes the central temperature increase. This increase in the central temperature overweighs its decrease due to the addition of entropy by the silicon burning and the resultant expansion of the core. Thus the silicon flash is driven by a quite different mechanism from one driving the helium, carbon, or oxygen flash.

In the case of $M_{ms} = 12M_\odot$ star, the silicon burning is ignited in an outer shell of $M_r = 0.18M_\odot$ as seen in Figure 8.1. An iron zone is formed which lies above the small silicon core. However the central temperature continues to rise and, after all, the silicon burning is ignited at the center of this small silicon core as seen in Figure 5.1.

Though numerical computation was stopped at this ignition stage, an iron core would be formed which extended from the center to $M_r = 1.4M_\odot$.

10.4. Pressure distribution in the core

The most important structural parameters in the presupernova models are the pressure distribution in the core, because the propagation of a shock wave is determined primarily by it (Section 6.4). In Figure 10.1 the pressure distributions at

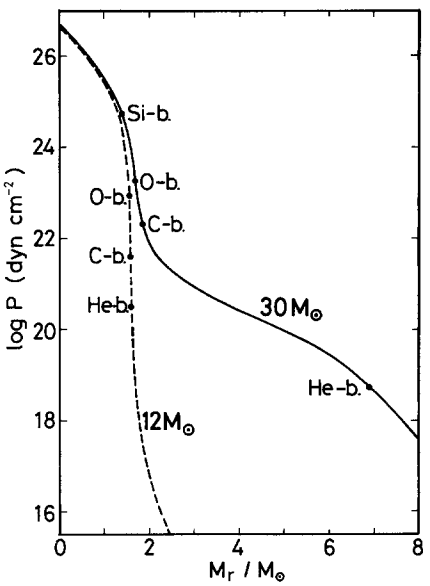

Fig. 10.1. Pressure distributions at the presupernova stages for the stars of $30M_\odot$ and $12M_\odot$ plotted against the Lagrangian mass coordinate M_r. Region of shell burning is shown by filled circle. The pressure gradient $|\mathrm{d} \ln P/\mathrm{d} \ln M_r| = U/V$ is steepest at the oxygen-burning shell and helium-burning shell for the star of $30M_\odot$ and $12M_\odot$, respectively. (Taken from Nomoto *et al.* (1979a).)

the presupernova stages are shown for the stars of $30M_\odot$ and $12M_\odot$ against the Lagrangian mass coordinate (Sugimoto and Nomoto, 1974; Nomoto *et al.*, 1979a). Arnett (1978a) published similar curves for the density distributions. As anticipated from the discussion in the preceding section, the pressure drops sharply near the core edge, i.e., near the transition region between the silicon zone and the oxygen zone.

When we compare the pressure distributions for different masses, they are almost the same as far as the regions within the core, i.e., interior to $M_r = M_O$, are concerned, because the core masses are almost the same for the two models and because the polytropic indices N in the cores are almost the same due to the relativistic degeneracy (Section 10.2). They can be well approximated by the polytropes of $N = 3$.

The pressure at the oxygen-burning shell is $P_O = 2 \times 10^{23}$ dyn cm^{-2} for $30M_\odot$ star, which is only 0.03% of the pressure at the center. The mass contained in unit scale height of pressure is also as small as about $0.06M_\odot$ at the oxygen-burning shell. Thus the core edge at M_O feels only this amount of weight as discussed in Section 2.3. Therefore, when we investigate the collapse of the iron core, its initial model can be well approximated consistently by a single star or even by the polytrope of $N = 3$ with $M = M_O$. However, it has to contain the silicon zone within M_O, though it is thin in mass. According to computations of the gravitational collapse due to the photodissociation of iron nuclei (Arnett, 1977b; Nomoto *et al.*, 1979a), the silicon shell-burning is ignited in a relatively early stage of the collapse where the central density is about 3×10^9 g cm^{-3} and the contraction is still relatively slow. Then, the core edge shifts again to the silicon-burning shell at $M_r = M_{Si} = 1.38M_\odot$ for the star of $M_{ms} = 30M_\odot$ (Nomoto *et al.*, 1979a), for instance, and its U–V curve makes a small loop there. After this stage, the collapsing core is well approximated by a single star with $M = M_{Si}$, if we do not intend to compute nuclear processes in the silicon zone. If we intend to do so, the single star of mass M_O with the silicon zone is recommended for the initial model.

10.5. Oxygen core of very massive stars

In the carbon burning phase the neutrino loss is appreciable but is not so strong as to cool down the central regions of very massive stars. Therefore, the mass of the oxygen core M_C is rather large (Arnett, 1978a). Because the corresponding specific entropy in the central region is high, electron-positron pairs appear and make the adiabatic exponent γ smaller than $\frac{4}{3}$ as can be imagined from the model of $M_{ms} = 60M_\odot$ in Figure 5.1. Then the core becomes dynamically unstable and begins to collapse as will be discussed in Section 11.7. Such evolution takes place in the star of M_{ms} greater than $100M_\odot$ (Arnett, 1973a). (See also Section 12.1.)

11. Gravitational Collapse Triggered by Photodissociation of Iron Nuclei

Different from presupernova models and from deflagration-type supernovae, physics involved in the gravitational collapse are much less enlightened. Difficulties come from several sides. First of all the equation of state at high densities is still uncertain. Secondly, the neutrino transport in the transition densities between transparent and opaque stages is too complicated. Thirdly, the overall hydrodynamics is poorly understood even though there are some numerical computations available. Moreover, a slight change in an input parameter makes sometimes a large difference in the hydrodynamical results. Therefore, when a parameter involved in the physical processes is to be changed, it is very difficult to foresee its effect to overall hydrodynamics, bouncing of the core, shock generation, mass ejection and so on. For example, it used to be thought that the general relativistic effect and the softness of the equation of state help the *collapse* into a black hole. Recently they are thought to

help *explosion* as will be discussed in Section 11.4. (These two statements are not necessarily contradictory, because the *explosion* is a different matter from the *bouncing* of the core.) Of course some explanation is given for it, but a quantitative understanding seems still remote.

Therefore, discussions in this section are limited to summarize recent trends of studies. Nevertheless, they seem to be in progress toward final understanding of the problem, and, recently, it seems hopeful to succeed in constructing theoretical models in which neutron stars are formed after the gravitational collapse consistently with known basic physical processes.

11.1. Energetics of supernova explosion

Different from deflagration-type supernovae, the photodissociation of iron is an endothermic reaction. Despite that the mass ejection has to occur. The energy of the ejected matter is denoted by $E_{ej} > 0$ in which included are thermal and kinetic energies of the ejected portion of the envelope and of an outer part of the core if any. On the other hand, a remnant star should be formed whose total energy, i.e., the thermal plus gravitational energies, is denoted by E_{rem}. If we denote the total energy of the presupernova by $E_{tot} < 0$, these are related by

$$E_{rem} = E_{tot} - Q_{nuc} - Q_{loss} - E_{ej} , \tag{11.1}$$

where $Q_{nuc} > 0$ is the energy absorbed into the subatomic energy through the photodissociation and electron captures, and where $Q_{loss} > 0$ is the energy emitted as the radiation, the neutrinos and the gravitational wave. Since E_{tot} is negative, E_{rem} is negative and its absolute value has to be large, i.e., the remnant has to lie deep in the gravitational potential well. This implies that the energy released by the gravitational contraction/collapse should be transferred to the ejected envelope with some efficiency.

11.2. Neutrino deposition

As a mechanism of this transfer Colgate and White (1966) was the first to propose the neutrino deposition. It assumed that the neutrinos emitted from the core stop and deposit energy in a mantle of the core and then blow it off. However, this mechanism was not shown to operate with the conserved vector current theory of weak interaction, when more detailed neutrino opacity and the effect of general relativity were taken into computation (Wilson, 1971).

As discussed in Section 1, the situation seemed to have changed when the existence of the neutral current in the weak interaction was proven experimentally. Because of it the neutrinos are scattered by nuclei coherently (Freedman, 1974), and the mean free path of the neutrino becomes of the order of the size of neutron star when the density becomes higher than 1×10^{12} g cm^{-3} (see e.g., Arnett, 1979a). It was anticipated that the neutrinos emitted from the core stop in the mantle where nuclei are still left undissolved.

The neutrino deposition is conveniently described in terms of the local Eddington's critical neutrino luminosity which is expressed as

$$L_{\nu,\,\mathrm{cr}}(M_r) = 4\pi cGM_r/\kappa_\nu\,, \tag{11.2}$$

with κ_ν being the neutrino opacity. In order to blow the mantle off, the neutrino luminosity has to be higher than $L_{\nu,\,\mathrm{cr}}(M_r)$ in the mantle, i.e., $L_\nu > L_{\nu,\,\mathrm{cr}}$ (mantle). On the other hand, L_ν has to be lower than $L_{\nu,\,\mathrm{cr}}(M_r)$ in the core, i.e., $L_\nu < L_{\nu,\,\mathrm{cr}}$ (core). These conditions require a high κ_ν in the mantle while a relatively low κ_ν in the core. They would be compatible if the mass number of nuclei were large enough in the mantle and the nuclei were dissolved in the core.

However, the quantitative studies do not allow such situations. The neutrino luminosity of $L_{\nu,\,\mathrm{cr}}$ (mantle) $\simeq 10^{54}\,\mathrm{erg\,s^{-1}}$ is required (see, e.g., Freedman *et al.*, 1977), while only $1\times10^{52}\,\mathrm{erg\,s^{-1}}$ (Nadyezhin, 1977; Arnett, 1977b) of L_ν is emitted from the iron cores of masses 1.4–$2M_\odot$. Wilson (1978) obtained much higher value of L_ν (core) $\simeq 8\times10^{53}\,\mathrm{erg\,s^{-1}}$, but did not find any explosion for standard models. Thus, the neutrino opacity is so high in the core that the neutrinos are trapped in the core rather than are deposited in the mantle.

11.3. Neutrino trapping in the core

The neutrino of lower energy has a smaller scattering cross section. When the neutrino (optical) depth is of the order of unity, the lower energy neutrinos in momentum space escape more easily than those close to the neutrino Fermi surface. It distorts the distribution function of neutrinos, and then the new Fermi–Dirac distribution function has to be reestablished through the down-scattering in momentum space. This is a process leading to new thermal equilibrium, with which associated is the entropy production. Though this is a complicated neutrino transfer problem, it is taken into recent computations under some approximations (see e.g. Bruenn *et al.*, 1978).

However, such complication arises only for densities below $1\times10^{12}\,\mathrm{g\,cm^{-3}}$. Above this density, neutrinos can be considered as trapped in the core (Arnett, 1977b). For this trapping, the following mechanism of positive feed back operates (Sato, 1975). When some neutrinos are trapped and its Fermi energy becomes appreciable, the electron captures on nuclei, i.e., the neutronizations are suppressed. Because the proton to neutron ratio does not decrease too much, the neutron drip and/or the melting of nuclei are prevented, and the nuclei keep their mass number at a high value. Such nuclei help to keep the neutrino opacity at a relatively high value by their coherent scattering, which helps still more the neutrino trapping, and prevents still more the electron capture from reducing the lepton number.

Thus the problem is to find how much neutrinos escape and/or how much lepton number is reduced during the phase before the neutrinos can be regarded as trapped. Such problem is answered by computing the neutrino transfer just mentioned above together with the collapse of the core. The results are, for example, $Y_e \simeq 0.2$ and $Y_\nu \simeq 6\times10^{-2}$ for the core of mass $1.4M_\odot$, which was formed in the helium star of

$8M_\odot$ (Arnett, 1977b). Here Y_ν is the mole number of neutrinos contained in one gram of matter. These quantities should be compared with the values $Y_e \simeq 0.01$ and $Y_\nu = 0$ for which the effect of the neutrino trapping was not taken into account (Arnett, 1977b).

11.4. Core bounce and shock propagation

As a result of the neutrino trapping, the pressure exerted by leptons becomes appreciably large. Moreover, the lepton gas is extremely relativistic and its adiabatic exponent γ is very close to $\frac{4}{3}$. This affects the equation of state appreciably, especially for the density range between 1×10^{12} and $3\times10^{13}\,\mathrm{g\,cm^{-3}}$ (Arnett, 1979a). As another effect of the neutrino trapping, further thermodynamic change can be regarded to be adiabatic in the core. This makes the hydrodynamics of collapse much less complicated. Van Riper (1978, 1979) studied such adiabatic collapse of $1.4M_\odot$ iron core in the frameworks of both Newtonian gravity and of the general theory of relativity. He replaced the equation of state with a simple adiabatic relation. He assigned the adiabatic exponent γ to appropriate values in an outer and in an inner part of the core, and then he joined them continuously inbetween. This is not a modelling but a numerical experiment. However, it leads to a relatively clear understanding of the problem as will be discussed below.

Recent computations for collapsing core in the framework of Newtonian gravity showed that the core bounces at relatively low densities in the range of 10^{13}–$10^{14}\,\mathrm{g\,cm^{-3}}$ (Wilson, 1978). However, Van Riper (1979) has shown that such low density bounce may not take place in the case of general relativistic treatment and that the collapse will proceed to nuclear densities. Van Riper (1978) continued his adiabatic equation of state with $\gamma = 1.33$ into the regimes of cold catalyzed matter under different assumptions, and he found that the bounce of the core takes place at the neutron-star density. After the bounce, a reflecting shock was found to develop. It was stronger as the amplitude of the bounce was larger, i.e., as the bounce took place at higher densities and the bounced layer came back to a higher level. This amplitude is larger when the equation of state is softer in the sense that the *effective* adiabatic index $\gamma_{\mathrm{eff}} = \gamma - 2.6P_c/\rho_c c^2$ (Chandrasekhar, 1964) is smaller due to the general relativistic effect. Such dependence on γ was also seen in Newtonian case (Van Riper, 1978). The reason why such a soft equation of state results in a stronger explosion was discussed by Arnett (1979a).

Van Riper and Arnett (1978) extended them still to include equations of state which seem to be more realistic, and they computed collapses for different masses. When they used the equation of state by Pandharipande (1971) with hyperons, for example, they obtained the explosion at nuclear densities for cores of masses smaller than $1.93M_\odot$ though not for masses larger than $1.94M_\odot$. Thus the critical mass which discriminates between the explosion and the continued collapse is $1.94M_\odot$ for this equation of state. However, it is to be noticed that the critical mass depends much on the choice of the equation of state. The reflected shock is stronger and the energies of

ejection is larger for the core mass below but closer to this critical mass. This is due to the stronger softening effect in γ_{eff}.

Though uncertainties are still involved in the equation of state in the bouncing core, it is hopeful that the cores of masses around 1.4–$1.9 M_\odot$ make explosion even within the regime of spherical collapse of the star.

11.5. Mass ejection

In numerical models of the collapse and the following explosion, only the iron core or at most iron core plus silicon zones are taken into computation. In many models, mass ejection resulted when the shock wave propagated through the outer layers of such stars. Though the amount of the ejected mass M_{ej} changes very much depending on the initial conditions and the assumptions on physical data, it lies in the range of 0–$0.14 M_\odot$ (Van Riper, 1979). From the standpoint of the shock propagation more important is the pressure P_{ej} of the initial model at the point where the mass of the overlying layers is equal to M_{ej}. For the polytrope of $N = 3$ having the central density of $\rho_c = 1 \times 10^9$ g cm^{-3} and temperature of $T_c = 5 \times 10^9$ K, which corresponds to a pre-supernova model of $30 M_\odot$ (Sugimoto and Nomoto, 1974; Nomoto *et al.*, 1979a), the ejected masses of $M_{\text{ej}} = 10^{-3}$, 10^{-2}, and 10^{-1} M correspond to $P_{\text{ej}} = 8 \times 10^{21}$, 1×10^{23}, and 3×10^{24} dyn cm^{-2} respectively. As seen in Figure 10.1, these pressures correspond to those for carbon, oxygen, and silicon zone, respectively. Therefore, the outer layers than those will be ejected, if the corresponding mass ejection resulted in the computation of collapsing iron star. When the shock propagates through these shells, nuclear deflagration will take place (Ohyama, 1963), which is related both with the formation of elements and with the energetics of explosion. They are, however, still open questions.

What happens when no bouncing takes place and thus no reflected shock is generated either? The outer shells of nuclear fuel will collapse and their temperatures will increase by the adiabatic compression. Then they will be ignited and suffer from explosive nuclear burning.

Barkat *et al.* (1975) studied a similar problem for several cases where a weak shock is generated by the bouncing at the nuclear density. In most cases the shock is so weak that it passes the silicon zone without igniting it. Then the silicon zone continues to collapse and is compressed. Finally it is ignited, but then the gravitational potential energy of the silicon zone is already larger than the available nuclear energy so that the collapse cannot be reversed back into an explosion. What happens in the outer layers, i.e., in oxygen, carbon, and helium zones? In the helium zone, in particular, the nuclear energy will not be smaller than the gravitational potential energy at the time of the collapse and the ignition, as can be estimated from its value of the specific entropy. In this sense it seems to deserve further investigations.

If electrons are strongly degenerate in outer shells, the nuclear fuels can be ignited only by adding a relatively small amount of extra energy so that even a partial neutrino deposition may be able to set a fire (*ignitatia*) to a carbon-oxygen zone (Gershtein *et al.*, 1975; Chechetkin *et al.*, 1979). However, such electron-degenerate

shells should have been formed in a star which will end up as an electron capture supernova, as discussed in Sections 8 and 9. Such incendiarism will trigger the explosion of the corresponding mass range if the nuclear bounce is not the case.

11.6. Formation of black holes

If the nuclear bounce does not take place, the core will continue to collapse until a trapped surface is formed. This direct formation of a black hole is the case when the core mass lies between the maximum mass of hot neutron stars and $2.5M_\odot$ (Van Riper and Arnett, 1978).

If the equation of state for the nuclear matter gives high enough pressure, even a core in this mass range will make a bounce and the direct formation of a black hole will not take place. However, if the outer layers, i.e., the silicon, oxygen and carbon layers, are not ejected as discussed in the preceding subsection, they will continue to accrete the bounced core. Then the core will collapse eventually, when its mass exceeds the critical mass for the neutron stars. If the outer layers are ejected by explosion, a hot neutron star will be left as a result of the bounce. However, the neutron star will cool down afterwards and eventually collapse into a black hole, because the core mass is larger than the maximum mass of the cold neutron stars (Van Riper and Arnett, 1978).

If the core mass is greater than $2.5M_\odot$ it makes a bounce by thermal pressure (Van Riper and Arnett, 1978), i.e., at the density lower than the nuclear. However, such bounce will be led to a collapse again (Van Riper, 1979) as the bounced core exceeds the limiting mass of the cold neutron star.

In short, the star of large M_{ms} collapses into a black hole in its final stage of evolution. However, the value of mass which discriminates its fate between a neutron star and a black hole is still uncertain. In order to fix it further studies are necessary on the equation of state at high densities as well as quasistatic evolution and hydrodynamic collapse of the stars.

11.7. Electron-pair instability in the massive oxygen core

The collapse triggered by electron-positron pair formation was computed by Barkat *et al.* (1967) and Fraley (1968) for the oxygen stars of masses 40–$60M_\odot$, and by Arnett (1973a) for the helium stars of 64 and $100M_\odot$. Such stars become dynamically unstable when the central temperature reaches $(1.5\text{–}2.2)\times 10^9$ K and the adiabatic exponent becomes smaller than $\frac{4}{3}$. As the collapse continues, the central density increases and then the center of the star gets out of the region with $\gamma < \frac{4}{3}$. The stability is recovered and the collapse is halted. At this stage the central temperature is 3.2×10^9 K and the oxygen burning is rapid enough to make the star explode.

In the case of relatively less massive stars the total energy of the star remains negative so that a part of the stellar core is left as a remnant. For example, the helium star of $64M_\odot$ leaves a silicon star of $2.2M_\odot$ after explosion (Arnett, 1973a). This silicon star will evolve further in the same way as those which were formed deep

interior of the stars, i.e., the star will proceed to the formation of the iron core and then to its collapse.

In the case of relatively massive stars, i e., in the case of the oxygen core (star) of masses 50–$60M_\odot$, on the other hand, a sufficient amount of nuclear energy is released by the explosive oxygen burning and the star is disrupted completely.

The cases of supermassive oxygen stars of 10^3 and $10^4\ M_\odot$ were computed by Wheeler (1977). The stars are so massive that the collapse is not halted despite the explosive oxygen burning. The star proceeds further to enter another unstable region, i.e., to the photodissociation of silicon and iron nuclei. After all, the stars of such high mass become black holes.

12. Summary and Observational Accounts

In Section 1 the overall pictures of supernova explosions were summarized in the historical point of view. In the present section we will summarize the present-day pictures and the discussions given in the preceding sections from the observational point of view.

12.1. Single stars

(1) $4M_\odot \lesssim M_{ms} \lesssim 8M_\odot$: In the stars of this mass range an electron-degenerate carbon–oxygen core is formed (Section 6). It evolves to become the carbon deflagration supernova (Section 7). The deflagration wave propagates at a speed of $v_{\rm def}$ by the convective energy transport across the deflagration front, though $v_{\rm def}$ itself is difficult to determine (Section 6.5). A part of the core material is processed into the iron-peak elements. The star disrupts itself completely and no remnant is left.

The abundance in the ejected matter and the energy of explosion depend upon the assumption on $v_{\rm def}$. As the deflagration is faster, more iron-peak elements are produced and thus more energy is released as summarized in Table 12.1 (Nomoto *et al.*, 1976). If the slow deflagration is the case, the difficulty of overproduction of the iron-peak elements can be avoided.

(2) $8M_\odot \lesssim M_{ms} \lesssim 12M_\odot$: In the stars of this mass range, an electron-degenerate O–Ne–Mg core is formed (Section 8). Electron captures on ^{24}Mg and ^{20}Ne trigger the collapse of this core, and then oxygen is deflagrated. The collapse overcomes the oxygen deflagration (Section 9.3). The core material is processed into NSE elements

TABLE 12.1

Energy of explosion and nuclear products of carbon deflagration supernova

	Energy	M(C+O)	M(Ne−Si)	M(Fe)
$\alpha_{\rm def} = 0.05\ldots$	5.0×10^{49} erg	$1.03M_\odot$	$0.22M_\odot$	$0.15M_\odot$
$\alpha_{\rm def} = 1.0\ \ldots$	1.33×10^{51} erg	$0.10M_\odot$	$0.28M_\odot$	$1.02M_\odot$

through the oxygen-deflagration front. It is likely that the collapsing core becomes a neutron star, because the extended thin outer layers and the envelope surrounding the collapsing core are easily blown off by the passage of a shock wave (Section 9.4). Since the carbon–oxygen zone and the helium zone may be thin, the ejected matter will contain a relatively small amount of silicon or the iron-peak elements.

(3) $12M_\odot \lesssim M_{ms} \lesssim 100M_\odot$: In the stars of this mass range an iron core is formed whose mass is about $1.4M_\odot$ irrespective of its main-sequence mass (Section 10.2). The core collapses due to photodissociation of iron nuclei. Such a star has much masses in the silicon through carbon zones (Section 10.1). When the star explodes and leaves a neutron star (Section 11.4), these zones of heavy elements must be ejected (Section 11.5). The yields from these massive stars were discussed in great detail by Arnett (1978b). If M_{ms} is greater than a critical mass, the star will collapse into a black hole. However, the value of the critical mass is uncertain (Section 11.6).

(4) $M_{ms} \gtrsim 100M_\odot$: When a massive core is formed in the stars of this mass range (Section 10.5), it becomes dynamically unstable due to the phase change of electron-positron pair creations. It collapses and then explodes by the explosive oxygen burning, unless the star is not too massive (Section 11.7). Products of the explosive oxygen burning will be ejected.

However, the stars more massive than $60M_\odot$ suffer from pulsational instability which is excited by the nuclear energy generation (ε-mechanism) (Schwarzschild and Härm, 1959). Such star will lose a rather large fraction of its mass before the formation of a helium core, though its details are uncertain (Appenzeller, 1970; Ziebarth, 1970; Talbot, 1971a, b). Even if such massive stars survive the hydrogen-burning phase without losing their masses, the penetration of the convective envelope will reduce their core masses in later phases (Section 4.2). Therefore, such a massive oxygen core may be a ghost.

All the stars described in this subsection have hydrogen-rich envelopes of red-giant sizes. Therefore, their supernova explosion will be observed as type II (see, e. g., Oke and Searle, 1974).

12.2. Helium stars and type-I supernovae

In typical type I supernovae, hydrogen-emission lines are absent, which implies that the abundance of hydrogen should be vanishingly low (see, e.g., Lasher, 1975; Wheeler, 1978). Nevertheless their presupernova stars are required to have such a large radius as $10^3 R_\odot$ in order to interpret their optical characteristics of type I (Lasher, 1975). The helium stars of masses in the ranges of $1.5–2M_\odot$ and $2–3M_\odot$ can meet these two conditions for type I, because they have strongly electron-degenerate C–O core and O–Ne–Mg core, respectively (Sections 4.2, 8, and 9.5). Such helium stars may be formed in some close binary systems. They explode as the carbon deflagration supernovae (Section 6.5) or as the supernovae triggered by electron captures (Section 9.3). These supernovae yield some amount of ^{56}Ni, which decay through $^{56}\text{Ni} \rightarrow {}^{56}\text{Co} \rightarrow {}^{56}\text{Fe}$ and will supply energy required to explain light curves of type I supernovae (see, e.g., Arnett, 1979b).

12.3. Accreting white dwarfs

In some close binary systems, one of the component star is a white dwarf. Mass accretion onto such a white dwarf triggers various types of unstable nuclear burning in its interior. When the accretion rate is relatively rapid, the nuclear burning is relatively weak and it may be just a weak flash or may result only in nova explosion. When the accretion is relatively slow, on the contrary, and when some conditions are met, such nuclear burning grows into a supernova explosion (Sections 5.4, 7, and 9.5).

(1) *Detonation in helium white dwarf*: When a certain amount of hydrogen-rich gas is accreted, the hydrogen shell-flash is triggered. A part of the accreted gas will be ejected back to space, but another part is processed into helium and accretes onto the helium core of the white dwarf. As a result of many cycles of the accretion and the shell-flash, the mass of the helium core grows appreciably (Section 7.1). Then, the helium burning is ignited. If it is ignited in the central region of the core with mass larger than $0.65M_{\odot}$, the white dwarf explodes as a helium detonation supernova. The star is disrupted completely and the ejected matter consists, in most cases, of the iron-peak elements (Section 7.2).

(2) *Strong helium shell-flashes in carbon-oxygen white dwarfs*: When the star is a carbon–oxygen white dwarf, the accreted gas will form a helium zone surrounding the C–O core. When the mass of the helium zone grows up to 0.1–$0.4M_{\odot}$ depending upon the accretion rate, the mass of the carbon–oxygen core and so on, the helium shell-flash is triggered. It will grow into another type of the helium detonation super-nova. The matter in the helium zone is processed into the α-process elements which are not in NSE, or into the iron-peak elements depending on the density at the ignition. Such elements will be ejected into space and a carbon-oxygen white dwarf will be left as a remnant star (Section 7.3). Numerical models of such an explosive case are only preliminary and await further studies.

(3) *Carbon deflagration in the carbon–oxygen white dwarfs*: When the accretion is relatively rapid, the helium shell-flash does not grow into the explosion but just processes helium into carbon. After many cycles of the helium shell-flashes, the mass of the carbon–oxygen core grows close to the Chandrasekhar limit (Section 5.4). Then the carbon burning is ignited and it results in the carbon deflagration supernova (Section 6.5). Its fate will be the same as the usual carbon deflagration supernova, which was discussed in Section 6, i.e., even in the case of the ignition at the highest densities, it seems very difficult that the deflagrated core should make a reimplosion thereafter by beta processes (Section 5.4).

(4) *Quiet supernovae and O–Ne–Mg white dwarfs*: White dwarf having O–Ne–Mg core may be formed from a star of mass 8–$12M_{\odot}$ as a result of mass exchange in a close binary system. When this white dwarf accretes matter from its companion star, many cycles of various shell flashes take place and eventually its O–Ne–Mg core grows close to the Chandrasekhar limit (Section 9.5). When the central density becomes high enough, the electrons are captured on ^{24}Mg and ^{20}Ne, and the quasi-dynamic collapse of the core is triggered (Section 9.3). It proceeds in the same

way as the ordinary electron capture supernova which were discussed in Section 12.1. In this case, however, the ejected mass is very small, for example, of the order of 10^{-1}–$10^{-2}\,M_\odot$, since the star has only a very thin hydrogen-rich envelope in mass. Thus the sling effect on the companion star is avoided, even when the mass of the companion star is very small. Such a supernova may be called a quiet supernova, which may be required to interpret some X-ray binaries.

The supernova explosions of white dwarfs, which are discussed in (1)–(3) above, may be related with type I supernovae in elliptical galaxies, because the ages of their progenitors should be very old (Whelan and Iben, 1973). Because these supernova explosions are of deflagration/detonation type, appreciable amount of iron-peak elements will be ejected into space except for some cases of helium shell-detonation at low ignition densities. However, it is an open question whether the overproduction of iron-peak elements is serious or not in this interpretation of type I supernovae. The frequency of such supernova explosions is difficult to estimate, because they depend upon the situations in binary systems, i.e., upon accretion rates and ages since the formation of the white dwarf. This question is related also with a problem of galactic wind, which may eject heavy elements from the galaxy (Arnett, 1979b).

In the presupernova stages of these white dwarfs they may be chemically peculiar and rich in carbon and the *s*-process elements, because of the following reasons. When the accretion is relatively rapid, the relatively weak helium shell-flashes recur many times. During the flash a convetive shell developes in the helium zone. It reaches the bottom of the hydrogen-rich envelope, and mixes protons down into the helium zone, because an entropy barrier is low in the case of thin hydrogen-rich envelope (Fujimoto, 1977). Then the *s*-process elements are synthesized and brought up to the stellar surface (Sugimoto *et al.*, 1977). In this sense it is an interesting suggestion that the type I supernovae are statistically related with the hydrogen-deficient carbon stars (Wheeler, 1978).

13. Future Problems

Even within the framework of spherical single stars there still remain many problems awaiting further investigation. Concerning the hydrostatic presupernova evolution, they are evolution of the stars in the range of $M_{ms} = 8$–$12 M_\odot$. For these stars, the shell flashes and associated convection make their chemical evolution complicated (Section 8). However, they affect very much the element synthesis, because the number of such stars are appreciably large. For more massive stars silicon shell-flash may change somewhat the mass of the iron core (Section 10), which affect rather sensitively the supernova collapse through the iron core mass (Sections 11.4 and 11.5). Structures in the regions with steep pressure gradiant and with different compositions require further detailed study, because they are important in determining the shells and their chemical compositions which are to be ejected in the event of explosion (Section 10.2). For the mass range around and below $8M_\odot$ the

penetration of the convective envelope has to be elaborated because it affects somewhat the upper mass limit for the carbon deflagration supernova (Section 4.2). However, it requires more elaborate theory of convective heat transport in the stellar interior.

More uncertainties exist in the supernova explosions themselves. One might still seek a possibility that the carbon burning in the degenerate core should be stablilized (Section 6.3). It is also uncertain what are the appropriate treatments of convection and of the propagation of the carbon deflagration front. They affect the element synthesis sensitively in this type of supernova (Section 12.1). In the electron capture supernovae we need to start with detailed models of presupernovae and include detailed network of electron captures on ^{23}Na, ^{28}Si, etc, photo-dissociation of daughter nuclei and subsequent captures of neutrons (Sections 8 and 9). Moreover, the computation should be extended to the stages of nuclear densities in order to see if a neutron star is actually formed (Section 9.4). For the collapse which is triggered by the photodissociation of iron nuclei, uncertainties in the equation of state at high densities reflected directly to the uncertainties in the discrimination of its fate between a neutron star and a black hole formation (Section 11). Moreover, a clear-cut understanding of the hydrodynamics of the collapse is badly needed.

The next and relatively easy step of investigations is to apply the present theories of spherical stars to the evolution of the stars in binary systems, where a variety of different conditions are realized in determining the evolution of the core (Section 7). Evolution in such conditions can be understood relatively easily if we have good understanding of the physics involved in the stellar structure. As shown in Sections 2 through 4, discussions in the phase plane, i.e., in the U–V plane help it very much. Though one may think it somewhat old fashioned, it can uncover even the inaccuracies which may be hidden in a huge pile of numerical results. As the numerical computations become more and more sophisticated, such an approach becomes more indispensable because any inconsistencies are possible to be hidden more easily behind the complications.

If we do not want to enter into fine details, however, the global nature of the stellar evolution and supernova explosion may be regarded to be understood as far as the spherical stars are concerned. Therefore, their natural extensions are to include non-spherical effects such as the effects of rotation and magnetic field, and non-spherical explosion of the star. In some cases such effects may be more important than the existing uncertainties in the regime of the spherical star. Unfortunately, however, such nonspherical effects can, in many instances, be treated quantitatively only under rough approximations in mathematical treatment. On the contrary, the spherical star can be treated rather rigorously as far as the mathematical treatment is concerned, though the spherical symmetry itself is a strong restriction or approximation to the physics. Therefore, these studies should be complementary to each other. However, the non-spherical stars are out of the scope of the present review.

Acknowledgments

The authors are indebted directly or indirectly to many astrophysicists for conversations concerning the topics involved in the present paper. In this connection one of the authors (D.S.) thanks the Japan Society for the Promotion of Science and Yamada Science Foundation which sponsored his travel to USSR in 1976 and to North America in 1979, respectively. This research is supported in part by the Scientific Research Fund of the Ministry of Education, Science and Culture (464080 and 274062).

Appendix: Notations

Listed are symbols which are used frequently or have generalized significance. Numbers quoted in parentheses denote the equation number in which the symbol is defined explicitly or implicitly, or used primarily.

A	mass number of atomic nucleus.
$B_\nu(a, b)$	incomplete beta function.
c_p	specific heat at constant pressure.
c_s	sound velocity.
c(sub)	center of the star.
$\langle E_e \rangle$	mean energy of an electron captured by nucleus.
E_n	nuclear energy release from unit mass of the nuclear fuel specified by n.
$E_{\rm thr}$	threshold energy (9.3).
$E_{\rm thr,0}$	energy difference between the ground states of daughter nucleus and parent nucleus (9.1).
E_γ	energy of gamma ray emitted from daughter nucleus (9.1).
$\langle E_\nu \rangle$	mean energy of a neutrino emitted by electron capture (9.1).
f	flatness parameter (2.17).
g	local gravitational acceleration (2.16).
H	atomic mass unit.
H_p	scale height of pressure (2.22).
H (sub)	hydrogen-burning shell.
k	Boltzmann constant.
l	mixing length of convection.
$L_{\rm cr}(M_r)$	local Eddington's critical luminosity (4.3).
L_n	integrated nuclear energy generation rate by nuclear fuel specified by n.
L_ν	neutrino luminosity.
$L_{\nu,\rm cr}(M_r)$	local Eddington's critical neutrino luminosity (11.2).
M	(current) mass of a star.
$M_{\rm C}$	core mass contained interior to the carbon-burning shell.
$M_{\rm Ch}$	Chandrasekhar's limiting mass (9.6).
$M_{\rm H}$	core mass contained interior to the hydrogen-burning shell.
$M_{\rm He}$	core mass contained interior to the helium-burning shell.
M_{ms}	mass of a star at its zero-age min-sequence.
$M_{\rm O}$	core mass contained interior to the oxygen-burning shell.
M_r	mass contained interior to a shell at r.
$M_{\rm Si}$	core mass contained interior to the silicon-burning shell.
M_{WD}	mass of white dwarf (7.1).
M_0	normalization factor to the non-dimensional mass (3.3).
M_1	core mass (3.6).
N	polytropic index between pressure and density (2.3).

n	polytropic index between pressure and temperature (10.1).
N_A	Avogadro number.
N_{ad}	adiabatic polytropic index.
N_e	number of electrons in unit mass of matter.
NSE	nuclear statistical equilibrium.
P	pressure.
ph (sub)	photosphere.
Q_e	mass fraction of the envelope exterior of the shell e (2.14).
R	stellar radius.
r	radial distance of a shell.
r_0	normalization factor to the non-dimensional radius (3.2).
s	specific entropy.
s_i	specific entropy of ions.
T	temperature.
U	homology invariant defined by (2.1).
u_{gas}	specific internal energy of gas.
u_{rad}	energy of the radiation field per volume in which unit mass of gas is contained (6.4).
V	homology invariant defined by (2.2).
v_{def}	velocity of deflagration front (6.10).
X	concentration by weight of hydrogen.
Y	concentration by weight of helium.
Y_e	mole number of electrons in one gram of matter (9.7).
Y_ν	mole number of neutrinos in one gram of matter.
Z	concentration by weight of the elements other than hydrogen and helium.
z	shock strength (6.6).
1 (sub)	usually denotes the core edge (2.13).
α	ratio of the mixing length to the scale height of pressure (l/H_p).
β	ratio of gas pressure to the total pressure.
γ	ratio of the specific heats.
Δ	locus of singularity in U–V plane (2.5).
$\Delta M(H_p)$	mass contained within unit scale height of pressure (4.4).
ε_{ec}	energy rate by electron captures (9.5).
ε_n	nuclear energy generation rate by the nuclear fuel specified by n.
ε_ν	neutrino loss rate.
$\varepsilon_\nu^{(D)}$	neutrino loss rate excluding the neutrinos from the electron captures (9.4).
η	non-dimensional density (3.1).
θ	P/ρ, not the non-dimensional temperature (2.7).
θ_W	Weinberg's angle (5.8).
κ	opacity
κ_ν	neutrino opacity (11.2).
Λ	describes the effect of electron degeneracy in equation of state (2.19).
λ_{ec}	rate of electron capture.
μ	mean molecular weight.
μ_e	mean molecular weight of electrons.
$\tilde{\mu}_e$	chemical potential of an electron excluding the rest mass (8.1).
μ_i	mean molecular weight of ions.
ξ	non-dimensional radius (3.1).
$\tilde{\omega}$	non-dimensional pressure (3.1).
ρ	matter density.
ρ_{cr}^{GR}	critical density above which the general relativistic instability sets in.
ρ_{cr}^{β}	critical density for reimplosion of the core by beta processes (Section 5).
ρ_{ign}	density at the ignition.
ρ_{NSE}	density above which the deflagrated matter results in NSE composition.
σ_e	non-dimensional entropy of electron per one electron in units of k(9.2).
τ_{ff}	timescale of free fall (6.2).
$\tau_h(H_p)$	timescale of heat transport over unit scale height of pressure (4.4).

τ_n nuclear timescale for a change in temperature (6.1).
ϕ non-dimensional mass (3.1).
ψ_e chemical potential of an electron in units of kT (8.1).

References

Alcock, C. and Paczyński, B.: 1978, *Astrophys. J.* **223**, 244.
Alastuey, A. and Jancovici, B.: 1978, *Astrophys. J.* **226**, 1034.
Appenzeller, I.: 1970, *Astron. Astrophys.* **9**, 216.
Arnett, W. D.: 1967, *Can. J. Phys.* **45**, 1621.
Arnett, W. D.: 1968, *Nature* **219**, 1344.
Arnett, W. D.: 1969, *Astrophys. Space Sci.* **5**, 180.
Arnett, W. D.: 1971, *Astrophys. J.* **169**, 113.
Arnett, W. D.: 1973a, in D. N. Schramm and W. D. Arnett (eds.), *Explosive Nucleosynthesis*, Univ. of Texas Press, Austin.
Arnett, W. D.: 1973b, *Astrophys. J.* **179**, 249.
Arnett, W. D.: 1974, *Astrophys. J.* **191**, 727.
Arnett, W. D.: 1977a, *Astrophys. J. Suppl.* **35**, 145.
Arnett, W. D.: 1977b, *Astrophys. J.* **218**, 815.
Arnett, W. D.: 1978a, in R. Giacconi and R. Ruffini (eds.), *Physics and Astrophysics of Neutron Stars and Black Holes*, North-Holland Publ. Co., Amsterdam, p. 356.
Arnett, W. D.: 1978b, *Astrophys. J.* **219**, 1008.
Arnett, W. D.: 1979a, *Ninth Texas Symposium on Relativistic Astrophysics, Annals N.Y. Acad. Sci.*, in press.
Arnett, W. D.: 1979b, *Astrophys. J.* **230**, L37.
Barbaro-Galtieri, A., Kwan, B. P., Litke, A. M., Dorfan, J. M., Ely, R., Feldman, G. J., Feller, J. M., Fong, A., Gobbi, B., Hanson, G., Jaros, J. A., Lecomte, P., Lüke, D., Madaras, R. J., Martin, J. F., Mast, T. S., Miller, D. H., Parker, S. I., Perl, M. L., Peruzzi, I., Piccolo, M., Pun, T. P., Rapidis, P. A., Ronan, M. T., Ross, R. R., Sadoulet, B., Trippe, T. G., Vuillemin, V., and Yount, D. E.: 1977, *Phys. Rev. Letters* **39**, 1058.
Barkat, Z., Rakavy, G., and Sack, N.: 1967, *Phys. Rev. Letters* **18**, 379.
Barkat, Z., Reiss, Y., and Rakavy, G.: 1974, *Astrophys. J.* **193**, L21.
Barkat, Z., Rakavy, G., Reiss, Y., and Wilson, J. R.: 1975, *Astrophys. J.* **196**, 633.
Basko, M. M. and Imshennik, V. S.: 1975, *Astron. Zh.* **52**, 469; English translation: 1976, *Sov. Astron.* **19**, 286.
Becker, S. A. and Iben, Jr., I.: 1979, *Astrophys. J.* **232**, 831.
Benvenuti, A., Cheng, D. C., Cline, D., Ford, W. T., Imaly, R., Ling, T. Y., Mann, A. K., Messing, F., Piccioni, P. L., Pilcher, J., and Reeder, D. D. L.: 1974, *Phys. Rev. Letters* **32**, 880.
Bisnovatyi-Kogan, G. S. and Seidov, A. F.: 1970, *Astron. Zh.* **47**, 139; English translation: 1970, *Soviet Astron.* **14**, 113.
Bisnovatyi-Kogan, G. S., Rudzskii, M. A., and Seidov, Z. F.: 1974, *Zh. Eksp. Teor. Fiz.* **67**, 1621; English translation: 1975, *Soviet Phys.-JETP* **40**, 806.
Bruenn, S. W.: 1971, *Astrophys. J.* **168**, 203.
Bruenn, S. W.: 1972a, *Astrophys. J. Suppl. No. 207*, **24**, 283.
Bruenn, S. W., 1972b, *Astrophys. J.* **177**, 459.
Bruenn, S. W., Arnett, W. D., and Schramm, D. N.: 1977, *Astrophys. J.* **213**, 213.
Bruenn, S. W., Buchler, F. R., and Yueh, W. R.: 1978, *Astrophys. Space Sci.* **59**, 261.
Brush, S. G., Sahlin, H. L., and Teller, E.: 1966, *J. Chem. Phys.* **45**, 210.
Buchler, J.-R. and Mazurek, T. J.: 1975, *Mém. Soc. Roy. Sci. Liège, 6e sér.* **VIII**, 435.
Buchler, J.-R., Wheeler, J. C., and Barkat, Z.: 1971, *Astrophys. J.* **167**, 465.
Buchler, J.-R., Mazurek, T. J., and Truran, J. W.: 1974, *Comm. Astron. Astrophys.* **6**, 45.
Canal, R. and Schatzman, E.: 1976, *Astron. Astrophys.* **46**, 229.
Chandrasekhar, S.: 1939, *An Introduction to the Study of Stellar Structure*, The University of Chicago Press, Chicago, 1939, and Dover Publications, New York, 1957.
Chandrasekhar, S.: 1964, *Astrophys. J.* **140**, 417.

Chandrasekhar, S. and Tooper, R. F.: 1964, *Astrophys. J.* **139**, 1396.
Chechetkin, V. M., Gershtein, S. S., Imshennik, V. S., Ivanova, L. N., and Khlopov, M. Yu.: 1979, *Astrophys. Space Sci.*, (submitted).
Colgate, S. A.: 1971, *Astrophys. J.* **163**, 221.
Colgate, S. A. and White, R. H.: 1966, *Astrophys. J.* **143**, 626.
Danziger, I. J. and Renzini, A. (ed.): 1978, *Proceedings of the First Workshop on the Advanced School of Astronomy, «E. Majorana» Center for Scientific Culture, Erice, Italy, Memorie della Società Astronomica Italiana* **49**.
DeWitt, H. E., Graboske, H. C., and Cooper, M. S.: 1973, *Astrophys. J.* **181**, 439.
Dicus, D. A.: 1972, *Phys. Rev.* **D6**, 941.
Duncan, M. J., Mazurek, T. J., Snell, R. L., and Wheeler, J. C.: 1976, *Astrophys. Letters* **17**, 19.
Dydak, F.: 1979, EPS High Energy Physics Conference (CERN).
Ergma, E. V. and Tutukov, A. V.: 1976, *Acta Astron.* **26**, 69.
Finzi, A. and Wolf, R. A.: 1967, *Astrophys. J.* **150**, 115.
Freedman, D. Z.: 1974, *Phys. Rev.* **D9**, 1389.
Freedman, D. Z., Schramm, D. N., and Tubbs, D. L.: 1977, *Ann. Rev. Nucl. Sci.* **27**, 167.
Fraley, G. S.: 1968, *Astrophys. Space Sci.* **2**, 96.
Fujimoto, M. Y.: 1977, *Publ. Astron. Soc. Japan.* **29**, 331.
Fujimoto, M. Y. and Sugimoto, D.: 1979, in H. M. Van Horn and V. Weidemann (eds.), 'White Dwarfs and Variable Degenerate Stars', *IAU Colloq.* **53**, in press.
Fujimoto, M. Y., Nomoto, K., and Sugimoto, D.: 1976a, *Publ. Astron. Soc. Japan* **28**, 89.
Fujimoto, M. Y., Nomoto, K., and Sugimoto, D.: 1976b, *Astrophys. Space Sci.* **45**, 71.
Gershtein, S. S., Imshennik, V. S., Nadyozhin, D. K., Folomeshkin, V. N., Khlopov, M. Yu, Chechetkin, V. M., and Éramzhyan, R. A.: 1975, *Zh. Eksp. Teor. Fiz.* **69**, 1473; English translation: 1976, *Soviet Phys. JETP* **42**, 751.
Giacconi, R. and Ruffini, R.: 1978, *Physics and Astrophysics of Neutron Stars and Black Holes*, North-Holland Publishing Co., Amsterdam.
Gunn, J. E. and Ostriker, J. P.: 1970, *Astrophys. J.* **160**, 979.
Hansen, C. J.: 1968, *Astrophys. Space Sci.* **1**, 499.
Hansen, J. P.: 1973, *Phys. Rev.* **A8**, 3069.
Härm, R. and Schwarzschild, M.: 1964, *Astrophys. J.* **139**, 594.
Hasert, F. J., Kabe, S., Krenz, W., Von Krogh, J., Lanske, D., Morfin, J., Schultze, K., Weerts, H., Bertrand-Coremans, G. H., Sacton, J., Van Doninck, W., Vilain, P., Camerini, U., Cundy, D. C., Baldi, R., Danilchenko, I., Fry, W. F., Haidt, D., Natali, S., Musset, P., Osculati, B., Palmer, R., Pattison, J. B. M., Perkins, D. H., Pullia, A., Rousset, A., Venus, W., Wachsmuth, H., Brisson, V., Degrange, B., Haguenauer, M., Kluberg, L., Nguyen-Khac, U., Petiau, P., Belotti, E., Bonetti, S., Cavalli, D., Conta, C., Fiorini, E., Rollier, M., Aubert, B., Blum, D., Chounet, L. M., Heusse, P., Lagarrigue, A., Lutz, A. M., Orkin-Lecourtois, A., Vialle, J. P., Bullock, F. W., Esten, M. J., Jones, T. W., McKenzie, J., Michette, A. G., Myatt, G., and Scott, W. G.: 1973, *Phys. Letters* **463**, 138.
Hayashi, C., Hōshi, R., and Sugimoto, D.: 1962, *Prog. Theor. Phys. Kyoto Suppl.* **22**, 1.
Hofmeister, E., Kippenhahn, R., and Weigert, A.: 1964, *Z. Astrophys.* **59**, 242.
Hoyle, F. and Fowler, W. A.: 1960, *Astrophys. J.* **132**, 565.
Hoyle, F. and Schwarzschild, M.: 1955, *Astrophys. J. Suppl.* **2**, 1.
Iben, I., Jr.: 1975, *Astrophys. J.* **196**, 525.
Iben, I., Jr.: 1978, *Astrophys. J.* **226**, 996.
Ikeuchi, S., Nakazawa, K., Murai, T., Hōshi, R., and Hayashi, C.: 1971, *Prog. Theor. Phys. Kyoto* **46**, 1713.
Ikeuchi, S., Nakazawa, K., Murai, T., Hōshi, R., and Hayashi, C.: 1972, *Prog. Theor. Phys. Kyoto* **48**, 1890.
Itoh, N., Totsuji, H., and Ichimaru, S.: 1977, *Astrophys. J.* **218**, 477: Errata 1978, *Astrophys. J.* **220**, 742.
Itoh, N., Totsuji, H., Ichimaru, S., and DeWitt, H. E.: 1979, *Astrophys. J.* **234**, in press.
Ivanova, L. N., Imshennik, V. S., and Chechetkin, V. M.: 1974, *Astrophys. Space Sci.* **31**, 497.
Ivanova, L. N., Imshennik, V. S., and Chechetkin, V. M.: 1977a, *Astron. Zh.* **54**, 661; English translation: *Soviet Astron.* **21**, 374.
Ivanova, L. N., Imshennik, V. S., and Chechetkin, V. M.: 1977b, *Astron. Zh.* **54**, 1009; English translation: *Soviet Astron.* **21**, 571.

Joss, P. C.: 1978, *Astrophys. J.* **225**, L123.
Kippenhahn, R. and Meyer-Hofmeister, E.: 1977, *Astron. Astrophys.* **54**, 539.
Lasher, G.: 1975, *Astrophys. J.* **201**, 194.
Lee, J. H.: 1972, *Astronaut. Acta* **17**, 455.
Mazurek, T. J.: 1973, *Astrophys. Space Sci.* **23**, 365.
Mazurek, T. J., Truran, J. W., and Cameron, A. G. W.: 1974, *Astrophys. Space Sci.* **27**, 261.
Miyaji, S., Nomoto, K., Yokoi, K., and Sugimoto, D.: 1979, *Proceedings 16th International Cosmic Ray Conference, Kyoto* **2**, 13; *Publ. Astron. Soc. Japan* (submitted).
Nadyezhin, D. K.: 1977, *Astrophys. Space Sci.* **51**, 283.
Nakada, Y. and Sugimoto, D., 1972, *Publ. Astron. Soc. Japan* **24**, 139.
Nakazawa, K.: 1973, *Prog. Theor. Phys. Kyoto* **49**, 1932.
Nakazawa, K., Murai, T., Hōshi, R., and Hayashi, C.: 1970, *Prog. Theor. Phys. Kyoto* **44**, 829.
Nariai, K. and Nomoto, K.: 1979, in H. M. Van Horn and V. Weidemann (eds.), 'White Dwarfs and Variable Degenerate Stars', *IAU Colloq.* **53**, in press.
Nariai, K., Nomoto, K., and Sugimoto, D.: 1979, *Publ. Astron. Soc. Japan*, (submitted).
Neo, S., Miyaji, S., Nomoto, K., and Sugimoto, D.: 1977, *Publ. Astron. Soc. Japan* **29**, 249.
Nomoto, K.: 1974, *Prog. Theor. Phys. Kyoto* **52**, 453.
Nomoto, K. and Sugimoto, D.: 1972, *Prog. Theor. Phys. Kyoto* **48**, 46.
Nomoto, K. and Sugimoto, D.: 1974, *Publ. Astron. Soc. Japan* **26**, 129.
Nomoto, K. and Sugimoto, D.: 1977, *Publ. Astron. Soc. Japan* **29**, 765.
Nomoto, K., Sugimoto, D., and Neo, S.: 1976, *Astrophys. Space Sci.* **39**, L37.
Nomoto, K., Kamiya, Y., Yokoi, K., and Miyaji, S.: 1979a, in preparation.
Nomoto, K., Miyaji, S., Yokoi, K., and Sugimoto, D.: 1979b, in H. M. Van Horn and V. Weidemann (eds.), 'White Dwarfs and Variable Degenerate Stars', *IAU Colloq.* **53**, in press.
Nomoto, K., Nariai, K., and Sugimoto, D.: 1979c, *Publ. Astron. Soc. Japan* **31**, 287.
Ohyama, N.: 1963, *Prog. Theor. Phys. Kyoto* **30**, 170.
Oke, J. B. and Searle, L.: 1974, *Ann. Rev. Astron. Astrophys.* **12**, 315.
Ōno, Y.: 1960, *Prog. Theor. Phys. Kyoto* **24**, 825.
Ōno, Y., Sakashita, S., and Ohyama, N.: 1961, *Prog. Theor. Phys. Kyoto, Suppl.* **20**, 85.
Oppenheimer, J. R. and Snyder, H.: 1939, *Phys. Rev.* **56**, 455.
Oppenheimer, J. R. and Volkoff, G. M.: 1939, *Phys. Rev.* **55**, 374.
Ostriker, J. P., Richstone, D. O., and Thuan, T. X.: 1974, *Astrophys. J. Letters* **188**, L87.
Pandharipande, V.: 1971, *Nucl. Phys.* **A178**, 123.
Paczyński, B.: 1970, *Acta Astron.* **20**, 47.
Paczyński, B.: 1971, *Acta Astron.* **21**, 271.
Paczyński, B.: 1972, *Astrophys. Letters* **11**, 53.
Paczyński, B.: 1975, *Astrophys. J.* **202**, 558.
Paczyński, B.: 1977, *Astrophys. J.* **214**, 812.
Paczyński, B. and Ziołkowski, J.: 1968, *Acta Astron.* **18**, 255.
Prialnik, D., Shara, M. M., and Shaviv, G.: 1979, *Astron. Astrophys.* **72**, 192.
Rakavy, G., Shaviv, G., and Zinamon, Z.: 1976, *Astrophys. J.* **150**, 131.
Rose, W. K.: 196 , *Astrophys. J.* **155**, 491.
Rudzskii, M. A. and Seidov, Z. F.: 1974, *Astron. Zh.* **51**, 936; English translation: 1975, *Soviet Astron.* **18**, 551.
Salam, A.: 1968, in N. Svartholm *Elementary Particle Theory*, Almquist and Forlag, Stockholm, p. 367.
Salpeter, E. E. and Van Horn, H. M.: 1969, *Astrophys. J.* **155**, 183.
Sato, K.: 1975, *Prog. Theor. Phys.* **54**, 1325.
Schramm, D. N. (ed.): 1977, *Supernovae*, D. Reidel Publ. Co., Dordrecht, Holland.
Schwarzschild, M.: 1958, *Structure and Evolution of the Stars*, Princeton University Press, Princeton.
Schwarzschild, M. and Härm, R.: 1959, *Astrophys. J.* **129**, 637.
Schwarzschild, M. and Härm, R.: 1965, *Astrophys. J.* **142**, 855.
Sparks, W. M., Starrfield, S., and Truran, J. W.: 1977, in M. Freidjung (ed.), *Novae and Related Stars*, D. Reidel Publ. Co., Dordrecht, Holland, p. 189.
Starrfield, S., Truran, J. W., and Sparks, W. M.: 1975, *Astrophys. J. Letters* **198**, L113.
Sugimoto, D.: 1964, *Prog. Theor. Phys. Kyoto* **32**, 703.
Sugimoto, D.: 1970a, *Prog. Theor. Phys. Kyoto* **44**, 375.

Sugimoto, D.: 1970b, *Prog. Theor. Phys. Kyoto* **44**, 599.
Sugimoto, D.: 1970c, *Astrophys. J.* **161**, 1069.
Sugimoto, D.: 1971, *Prog. Theor. Phys. Kyoto* **45**, 761.
Sugimoto, D. and Nomoto, K.: 1974, in R. J. Tayler (ed.), 'Late Stages of Stellar Evolution', *IAU Symp.* **66**, 105.
Sugimoto, D. and Nomoto, K.: 1975, *Publ. Astron. Soc. Japan* **27**, 197.
Sugimoto, D. and Fujimoto, M. Y.: 1978, *Publ. Astron. Soc. Japan* **30**, 467.
Sugimoto, D., Fujimoto, M. Y., Nariai, K., and Nomoto, K.: 1977, in Y. Terzian (ed.), 'Planetary Nebulae', *IAU Symp.* **76**, 208.
Sugimoto, D., Fugimoto, M. Y., Nariai, K., and Nomoto, K.: 1979, in H. M. Van Horn and V. Weidemann (eds.), 'White Dwarfs and Variable Degenerate Stars', *IAU Colloq.* **53**, in press.
Talbot, R. J., Jr: 1971a, *Astrophys. J.* **163**, 17.
Talbot, R. J., Jr: 1971b, Astrophys. J. **165**, 121.
Taylor, J. H. and Manchester, R. N.: 1977, *Astrophys. J.* **215**, 885.
Truran, J. W., Arnett, W. D., and Cameron, A. G. W.: 1967, *Canadian J. Phys.* **45**, 2315.
Uus, U.: 1972, *Nauch. Inform. Acad. Nauk SSSR* **23**, 85.
van den Heuvel, E. P. J.: 1977, *Ann. N.Y. Acad. Sci.* **302**, 14.
Van Riper, K. A.: 1978, *Astrophys. J.* **221**, 304.
Van Riper, K. A.: 1979, *Astrophys. J.* **232**, 558.
Van Riper, K. A. and Arnett, W. D.: 1978, *Astrophys. J. Letters* **225**, L129.
Weaver, T. A., Zimmerman, B., and Wooseley, S. E.: 1978, *Astrophys. J.* **225**, 1021.
Weinberg, S.: 1967, *Phys. Rev. Letters* **19**, 1264.
Wheeler, J. C.: 1977, *Astrophys. Space Sci.* **50**, 125.
Wheeler, J. C.: 1978, *Memorie della Società Astronomica Italiana* **49**, 349.
Whelan, J. and Iben, I., Jr.: 1973, *Astrophys. J.* **186**, 1007.
Wilson, J. R.: 1971, *Astrophys. J.* **163**, 209.
Wilson, J. R.: 1978, R. Giacconi and R. Ruffini (eds.), *Physics and Astrophysics of Neutron Stars and Black Holes*, North-Holland Publ. Co., Amsterdam, p. 676.
Ziebarth, K.: 1970, *Astrophys. J.* **162**, 947.